MAGNETIZATION AND SUSCEPTIBILITY OF AuMn AND AuFe

By

JING-CHENG LIU

A dissertation submitted to the Graduate Faculty in Physics in partial fulfillment of the requirements for the degree of Doctor of Philosophy, The City University of New York.

1975

This manuscript has been read and accepted for the Graduate Faculty in Physics in satisfaction of the dissertation requirement for the degree of Doctor of Philosophy.

May 12, 1975
date

Frederick W. Smith
Chairman of Examining Committee

May 16, 1975
date

Myriam P. Sarachik
Executive Officer

Professor Frank Martino

Professor Myriam P. Sarachik

Professor Narkis Tzoar

Professor Fred J. Cadieu

Professor Thomas Kitchens

The City University of New York

ACKNOWLEDGEMENTS

The author would like to acknowledge the efforts of his mentor Professor Frederick W. Smith and Professor Myriam P. Sarachik. Their guidance, assistance, discussions, and enthusiastic support were most valuable and were greatly appreciated.

Further, the author wishes to acknowledge many valuable discussions and assistance in various aspects of the experimental work which were forthcoming from Dr. James Haddad, especially for allowing the author to use his ever-reliable experimental apparatus.

The author would like to thank Dr. Robert W. Houghton, Dr. Randy Caton, Dr. Jerold Touger, and Mr. B. W. Kasell, for their assistance in making samples and for helpful discussions. The entire staff of the City College machine shop assisted in the construction and maintenance of the experimental apparatus.

Finally, the author would like to express special thanks to his wife Kuo-peing for the typing of this thesis, and for her patience and endurance during the years of work on which it is based.

Abstract

MAGNETIZATION AND SUSCEPTIBILITY OF AuMn AND AuFe

By

Jing-cheng Liu

Adviser: Professor Frederick W. Smith

We have measured the initial susceptibility χ and magnetization M of series of dilute AuMn and AuFe alloys in magnetic fields up to 50 kG over the temperature range 1.2 to 100K. The Mn concentrations in the AuMn alloys are from 50 to 2000 ppm and the Fe concentrations in the AuFe alloys are from 18 to 6050 ppm. From the magnetization measurements, the value of V_o, i.e., the strength of the Ruderman-Kittel-Kasuya-Yosida (RKKY) interaction $V(r) = (V_o \cos 2k_F r)/r^3$, is determined. For AuMn we obtain $V_o = (2.4 \pm 0.3) \times 10^{-37}$ erg cm^3, almost independent of concentration of Mn. Our results for χ and M for AuMn obey quite well the scaling laws predicted for magnetic impurities which interact via the RKKY interaction, i.e., $\chi(n,T) = F_1(T/n)$ and $M(n,T,H)/n = F_2(T/n,H/n)$. For the spin per Mn atom, it is found that $S = 2.25 \pm 0.1$, assuming $g = 2$. For the AuFe alloys, the value of V_o is found to decrease from $V_o = 11.9 \times 10^{-36}$ erg cm^3 at n = 42 ppm Fe to 1.03×10^{-36} erg cm^3 at 6050 ppm Fe, the highest Fe concentration studied. We suggest that the decrease is due

to self-damping of the RKKY oscillations. We have proposed modified scaling laws for χ and M which take the variation of V_o and spin S into account, i.e., $\chi V_o/S(S+1) = F_1(T/nV_o)$ and $M(n,T,H)/ng\mu_B S = F_2(T/nV_o, H/nV_o)$. Our measured results for AuFe obey these modified scaling laws very well. The spin per Fe atom is also found to be dependent on n, with a value of 1.23 ± 0.07 for 42 ppm Fe increasing to 1.55 ± 0.06 for 6050 ppm Fe. The decrease of V_o with increasing Fe concentration can account for the observed deviation from scaling law behavior in several recent studies of AuFe in which a constant V_o has been implicitly assumed.

TABLE OF CONTENTS

LIST OF TABLES

LIST OF FIGURES

I. INTRODUCTION

Dilute alloys of 3d transition metal impurities in metallic hosts have been of considerable interest both theoretically and experimentally for the past twenty years. The magnetic and transport properties [1-4] of such alloys have been observed to be dependent on both temperature and impurity concentration. The interaction responsible for such effects in the s - d interaction between the localized moment of the impurities and the conduction electrons of the metal. Both single impurity effects (Kondo effect)[1-4] and effects due to the indirect impurity -impurity interaction via the Ruderman-Kittel-Kasuya-Yosida (RKKY)[5-7] potential have as their origin the s-d interaction. The characteristic energy of each effect determines which effect will be dominant in a particular alloy. The characteristic energy of single impurity effects is $k_B T_K$ where T_K is the Kondo temperature, while for impurity-impurity effects the characteristic energy is nV_o, where n is the concentration of magnetic impurities and V_o is the strength of the RKKY interaction $V(r) = (V_o \cos 2k_F r)/r^3$. If $k_B T_K > nV_o$, single impurity effects will dominate, if $k_B T_K < nV_o$, impurity-impurity effects will dominate, and if $k_B T_K \sim nV_o$ both effects will co-exist. Obviously, the determination of V_o and T_K for a given alloy system is of great importance.

The goals of this investigation are to determine V_o for both AuMn and AuFe, and to study the magnetic properties of both alloy systems. By investigating a series of alloys of increasing concentration n, we would expect to see the magnetic properties of the alloys shift from the single impurity limit to the indirect impurity-impurity interaction (RKKY) limit as n increases.

When $k_B T_K > nV_o$, single impurity effects will dominate, and theoretical calculations predict that experimentally measured quantities such as magnetic susceptibility, magnetization, resistivity and heat capacity per unit concentration will be universal functions of T/T_K.[4] When $k_B T_K < nV_o$, the RKKY interaction will dominate, and it is predicted that the above mentioned quantities will follow scaling laws [8,9] with scaling parameter n, e.g., $\chi(T,n) = F_1(T/n)$ and $M(H,T,n)/n = F_2(H/n,T/n)$, where F_1 and F_2 are some universal functions.

At high temperatures; i.e., when $k_B T \gg nV_o$, Larkin et al.[10] have predicted that $\chi = ng^2\mu_B{}^2 S(S+1)/3(k_B T+\theta_s)$ where S is the spin, $\theta_s = C_s nV_o$, and C_s is a constant of order of unity. In addition, for $g\mu_B H \gg k_B T$ and nV_o, they predict that

$$M = nS\mu_B g \left[1-2(2S + 1)nV_o/3g\mu_B H \right] .$$

At low temperatures or high concentrations, i.e.,

when $k_B T \ll nV_o$, the alloys are in the "spin glass" state.[11] The dilute impurities then are strongly correlated in clusters due to short-range order but without long-range order present; i.e., the clusters are disconnected. As $T \rightarrow 0$ it is predicted that $\chi = 2ng^2 S(S+1)\mu_B/3\pi\Delta$[12] where Δ is the width of the molecular field probability distribution $P(H) = \Delta/\pi(\Delta^2 + H^2)$.[13]

Alloys of AuMn and AuFe have been studied extensively in the past. Loram, Whall and Ford [14] measured the resistivity of very dilute AuMn alloys and they determined that the Kondo temperature of AuMn was of the order of 10^{-13} K. The susceptibility and magnetization of AuMn alloys with concentrations of Mn of 1 at. % and 2 at. % were measured by Lutes and Schmit.[15] They observed low temperature susceptibility maxima at temperatures T_o approximately proportional to the concentration of Mn and T_o/n is 4K/at. % Mn. Above the maxima, they observed that the alloy susceptibility followed a Curie-Weiss law.

Lutes and Schmit also measured the susceptibility and magnetization of AuFe alloys of Fe concentrations 0.5 at.% and 1 at. %. They concluded that the properties of AuFe are similar to those of AuMn except that T_o/n = 8K/at. % Fe, where T_o is the temperature of the susceptibility maximum. Loram, Grassie and Swallow [16] have measured the magnetization of AuFe alloys of 0.002, 0.005, and 0.01 at.

% Fe. They determined that S = 1.29 and T_K = (0.10±0.1)K and that the magnetization can be expressed as a Brillouin function with spin S and a modified g-factor dependent on temperature, applied magnetic field and T_K. Tholence and Tournier [17] have studied the magnetization of dilute AuFe alloys and found that the properties of the alloys are characteristic of the RKKY interaction for concentrations higher than 0.1 at. % Fe. At very low concentrations and low temperatures; i.e., n < 0.01 at. % Fe and T = 0.05 K, from the measurements of initial susceptibility, they concluded that there is good evidence in favor of a spin-compensated state in AuFe.[18] The excess specific heat of AuFe alloys has been studied by Dreyfus et al.[19] Souletie and Tournier [9] have analyzed this data and shown that it is in fair agreement with a scaling law of f(T/n). Cannella and Mydosh [20] have found a sharp cusplike peak in the low field A-C susceptibility at a magnetic ordering temperature T_o. Their analysis indicates the existence of small regions of short-range ferromagnetic order which undergo long-range interactions as the temperature is lowered. Borg and Kitchens [21] have measured the magnetization of AuFe alloys with concentrations in the range from 0.05 ⩽ Fe ⩽ 17 at. %. They found that the alloys behave mictomagnetically;[22] i.e., they exhibit magnetic effects due to spin orientations frozen at low tempera-

tures but without long-range magnetic order present. They found no evidence for pure ferromagnetism in the concentration range studied. Mydosh et al.[23] have measured the electrical resistivity of AuFe alloys in the spin glass (0.5 - 8 at. % Fe), mictomagnetic (8 - 15 at. %) and ferromagnetic ($n > 15$ at. % Fe) regimes. Tholence and Tournier [24] have also defined the concentration range in which a dilute alloy behaves as a spin glass. They contend that the susceptibility of a spin glass contains one reversible part χ_r with a sharp peak at a temperature $T_o \propto n$.

In this investigation, the results of the susceptibility and magnetization measurements of series of AuMn and AuFe alloys with different concentrations are presented. The magnetic properties of the alloys will be studied and values of V_o will be deduced from the magnetization measurements. The data will be compared with existing theoretical predictions.

In section II, a brief outline of the theories related to the magnetic impurity problem is given, including: single impurity effects (Kondo effect), the RKKY potential, the derivation of scaling laws, spin glass behavior and self-damping [25] of the RKKY interaction.

In section III, descriptions of sample preparation, concentration determination, experimental apparatus and experiment procedures are given.

Section IV is devoted to data analysis of AuMn and AuFe alloys, including the susceptibility, Curie - Weiss fits, magnetization, determination of V_o, scaling law fitting etc. In section V, we will present a discussion of our results, including comparisons with existing theories and other experiments.

Section VI is the conclusion of this investigation, including suggestions for future work.

II. THEORY

A. Brief review of the dilute magnetic impurity problem.

When small amounts of transition metal impurities are dissolved in non-magnetic metals, it is often found that the magnetic and transport properties of the alloys become strongly temperature-dependent. This temperature-dependent behavior is attributed to the presence of localized magnetic moments on the impurity atoms. There are several good review articles on the subject of localized magnetic moments.[1-4,26,27] I will therefore only attempt to present the major theoretical developments in the magnetic impurity problem.

Friedel [28] contributed most to the understanding of the problem of the localized magnetic moment by presenting the phenomenclogical concept of the virtual bound state. It was pointed out that when a 3-d transition metal atom is present in a metal, the d-orbital electrons would retain much of their localized character even when their energy levels were within the conduction band of the host material. The effect of the interaction between the d-electrons and the conduction electrons is just to broaden and shift the energy level of the d-electron from its unperturbed value. The d-electron could not be bound permanently in this virtual state since its energy is the same as that of a conduction electron, but, nevertheless,

most of its wavefunction would be localized near to the impurity.

The localized magnetic moment problem can also be treated as a scattering problem. In this approach, the metal is described by free electrons, and an impurity, within the Hartree or Hartree-Fock method, creates a self-consistent spherical potential V(r) which is almost deep enough to have bound d states. The potential V(r) creates a virtual bound state, which is resonant with the d component of the conduction electron wave function and which is localized near the impurity site.

The presence of a net magnetic moment on an impurity is the result of including exchange energy in the potential V(r); i.e., when the up-spin electron state and down-spin electron state are separated in energy. A net magnetic moment will occur in those cases where the number of spin-up electrons exceeds the number of spin-down electrons.

P. W. Anderson [29] put all these ideas on a more quantitative basis and did a self-consistent Hartree-Fock calculation on a simple model Hamiltonian

$$H = H_{band} + H_{sd} + H_d$$

where

$$H_{band} = \sum_{k\sigma} \varepsilon_k n_{k\sigma}$$

$$H_d = \sum_d \left(E_d n_{d\sigma} + U n_{d\uparrow} n_{d\downarrow} \right)$$

$$H_{sd} = \sum_{k\sigma} V_{dk} \left(C^+_{k\sigma} C_{d\sigma} + C^+_{d\sigma} C_{k\sigma} \right)$$

H_{band} and H_d are the Hamiltonians for the conduction band electrons and the d electrons respectively, and H_{sd} represents the s-d mixing interaction. U is the Coulomb exchange integral between d electrons. V_{dk} is the s-d mixing potential. Also, $n_{k\sigma} = C^{+}_{k\sigma} C_{k\sigma}$ and $n_{d\sigma} = C^{+}_{d\sigma} C_{d\sigma}$ are the occupation number operators. $C^{+}_{d\sigma}$ and $C_{d\sigma}$ are the creation and destruction operators with subscripts d denoting d electron, k for conduction electron, σ for spin.

By solving this Hamiltonian self-consistently, Anderson derived a condition for the formation of a localized moment by using the Hartree-Fock approximation. The condition is $U/\Delta \gg 1$, where Δ is the width of the virtual level, defined by $\Delta = \pi \langle |V_{dk}|^2 \rangle_{av} \rho(E_d)$, $\rho(E_d)$ is the host density of states at the d state energy.

Recently, Hirst [30] proposed a different but natural approach to the localized magnetic moment problem. He used the ionic many-electron state of the impurity as a zero-order eigenstate which interacts weakly with the conduction electrons. The model Hamiltonian has a form $H = H_{ion} + H_{cond} + H_I$, where H_{ion} describes the localized electrons interacting with each other and with any fixed external field, and H_{cond} describes the conduction electrons moving independently in the fixed external field. $H_{ion} + H_{cond}$ is the zero-order Hamiltonian with the energy associated with the screening of impurity charge included. H_I gives

the interaction between local and conduction electrons; i.e. exchange coupling and several types of mixing terms which convert local into conduction electron or vice versa. Using this Hamiltonian and a restricted Hartree-Fock calculation, Hirst concluded that whenever the inter-configurational excitation energy is not small compared to v.b.s. width, the impurity retains an ionic-type structure, even though this structure may be masked by Kondo-condensation phenomena. The Hirst model explains naturally the different effective widths of the magnetic and non-magnetic local state and predicts successfully the properties of rare-earth impurities in metals.

B. Single impurity effect (Kondo effect).

J. Kondo [31] used an s-d exchange model Hamiltonian, and assuming that the local moment exists, considered only the interaction between the conduction electrons and the d electrons of the impurity; i.e.,

$$H_{ex} = -J\ \vec{S}\cdot\vec{s} \qquad J < 0,$$

where J is the strength of the exchange interaction, $\vec{S}$ is the local moment spin and $\vec{s}$ is the conduction electron spin. By doing the perturbation calculation in the second order Born-approximation, Kondo has shown that the impurity resistivity $\rho = n\rho_m \left[1 + N(0)J\ln(kT/D) + \cdots \right]$ where ρ_m is the first Born scattering term and N(0) is the density

of states in a flat band of width 2D. The experimental results in a variety of alloy systems do show a logarithmic increase in resistivity with decreasing temperature over a broad temperature range in agreement with Kondo's theory. Calculations of other physical properties also arrived at a similar logarithmic temperature dependence.[32,33] The Kondo perturbation calculation will break down at the Kondo temperature T_K ,

where $$T_K = D \exp\{-|J| N(0)\}^{-1}.$$

Subsequent theoretical[34-37] studies have suggested that the break-down of the perturbation theory is associated with the formation of a spin-compensated singlet ground state. The transition to the spin-compensated state is characterized by a decrease in entropy and magnetic moment of the impurity system as well as by peak in the thermoelectric power and an increase in resistivity. Theory also predicts that experimental observed quantities, such as magnetization and magnetic susceptibility per impurity will be universal functions of T/T_K.

C. RKKY interaction.

Zener[38] proposed a model of transition metals in which the d electrons are localized at the atomic sites and the s electrons are itinerant over the entire crystal. In this model the s-d interaction creates a polarization

of the conduction electrons. A similar problem of the hyperfine interaction between conduction electrons and nuclear spins in a metal has been investigated by Frohlich and Nabarro.[39] Ruderman and Kittel [5] carried through a second order perturbation calculation and explained the anomalous broadening of the nuclear magnetic resonance absorption line in metals. Kasuya [6] and Yosida [7] did similar calculations but with a different order of integration over the electron coordinates.

The RKKY interaction for the case of nuclear spins will be derived first. The conduction electrons can be expressed as Bloch functions,

$$\psi_{kS}(\chi) = e^{ik\cdot\chi}\, u_{kS}(\chi) = \varphi_k(\chi)\,|S\rangle$$

where $|S\rangle$ is the spin index and denotes $\uparrow$ or $\downarrow$ for S_z.

For the hyperfine contact interaction between a nucleus at R_n and an electron, the Hamiltonian has the form [40,41]

$$H = \sum_i A(\chi_i - R_n)\, S_i \cdot I_n$$

where $A(\chi_i - R_n)$ is proportional to a delta function, χ_i is the position of electron i, and I_n is the nuclear spin at position R_n.

In the language of second quantization, the electron field operator is

$$\psi(\chi) = \sum_{kS} C_{kS}\, \varphi_{kS}(\chi) \qquad \psi^+(\chi) = \sum_{kS} C^+_{kS}\, \varphi^*_{kS}(\chi)$$

where C_{ks}, C^{+}_{ks} are fermion annihilation and creation operators.

Then the Hamiltonian will have the form

$$H = \sum_{kk'} \left[\int d^3x \, \varphi^{*}_{k's'}(x) A(x-R_n) S \cdot I_n \varphi_{ks}(x) \right] C^{+}_{k's'} C_{ks}$$

$$= \frac{1}{2} \sum_{kk'} e^{i(k-k')\cdot R_n} J(k',k) \left[I_n^{+} C^{+}_{k'\downarrow} C_{k\uparrow} + I_n^{-} C^{+}_{k'\uparrow} C_{k\downarrow} + I_n^{z} \left(C^{+}_{k'\uparrow} C_{k\uparrow} - C^{+}_{k'\downarrow} C_{k\downarrow} \right) \right]$$

where $J(k'k) = \int d^3x \, \varphi^{*}_{k'}(x) A(x) \varphi_k(x)$

If $A(x) = J\,\delta(x)$, then $J(k'k) = J$ is a constant.

In the Born approximation, the wavefunctions to first order in J are, with $R_n = 0$,

$$|k\uparrow\rangle = |k\uparrow\rangle_0 + \sum_{k's}{}' |k's\rangle_0 \frac{\langle k's|H|k\uparrow\rangle}{\varepsilon_k - \varepsilon_{k'}}$$

$$= |k\uparrow\rangle_0 + \sum_{k'}{}' \frac{m^{*}J}{k^2-k'^2} \left(I_n^{+} |k'\downarrow\rangle_0 + I_n^{z} |k'\uparrow\rangle_0 \right)$$

$$|k\downarrow\rangle = |k\downarrow\rangle_0 + \sum_{k'}{}' \frac{m^{*}J}{k^2-k'^2} \left(I_n^{-} |k'\uparrow\rangle_0 - I_n^{z} |k'\downarrow\rangle_0 \right)$$

where $\varepsilon_k \propto k^2$ has been assumed. m* is the effective mass of the electron. After summation over k', one obtains 7,40,41

$$|k\uparrow\rangle = |k\uparrow\rangle_0 + \frac{m^{*}J \cos kr}{4\pi r} \left(I_n^{+} |\downarrow\rangle + I_n^{z} |\uparrow\rangle \right)$$

and for the corresponding electron density one obtains

$$\rho(k\uparrow) = 1 + \frac{m^{*}J \cos kr}{2\pi r} \cos kx \, I_n^{z}$$

$$\rho(k\downarrow) = 1 - \frac{m^{*}J \cos kr}{2\pi r} \cos kx \, I_n^{z}$$

After the summation of k over the ground state Fermi sea, one obtains

$$\rho(\uparrow) = -\frac{k_F^3}{6\pi^2}\left[1 - \frac{3m^* J I_n^z k_F}{\pi} F(2k_F r)\right]$$

where $$F(x) = \frac{x\cos x - \sin x}{x^4}$$

If the electron concentration is 2n, (n for each spin direction), then the net polarization at large distances will be

$$\rho(\downarrow) - \rho(\uparrow) = n\left[1 - \frac{9n}{\varepsilon_F}\pi J F(2k_F r) I_n^z\right] - n\left[1 + \frac{9n}{\varepsilon_F}\pi J F(2k_F r) I_n^z\right]$$

$$= -\frac{18 n^2 \pi J}{\varepsilon_F} I_n^z F(2k_F r)$$

$$\cong -\frac{9\pi n^2}{4\varepsilon_F} J I_n^z \frac{\cos 2k_F r}{(k_F r)^3}$$

Now suppose a second nuclear moment I_m is added at the lattice point R_m at distance r from R_n. The nucleus at m will be perturbed by the conduction electron spin polarization created by the nucleus at n. Thereby the two nuclei interact by means of the indirect interaction between their two moments, via the conduction electrons.

The second-order interaction between two nuclear spins is given by the Hamiltonian H"

where $$H'' = \sum_{k,k'}{}' \frac{\langle ks|H|k's'\rangle\langle k's'|H|ks\rangle}{\varepsilon_k - \varepsilon_{k'}}$$

After performing similar integrations and summing over spin states,

$$H''(x) = I_n \cdot I_m \frac{4J^2 m^* k_F^4}{(2\pi)^3} F(2k_F r)$$

Now for the case of the indirect interaction between localized ionic moments, the Hamiltonian H" (x) will have the form

$$H''(\chi) \propto J^2 S_n \cdot S_m F(2k_F r)$$

This interaction decreases like r^{-3} for large r and oscillates with the period $(2k_F)^{-1}$.

The RKKY interaction can then be expressed as a potential V(r) between two ionic spins at r_i and r_j; i.e.,

$$V(r) = V_0 \frac{\cos 2k_F r_{ij}}{r_{ij}^3} \quad ; \quad k_F r_{ij} \gg 1 \ , \ r_{ij} = |r_i - r_j|$$

where $$V_0 = \left(\frac{3n}{N}\right)^2 \frac{2\pi}{\epsilon_F} J^2(0) (2k_F)^{-3}$$

N is the total number of lattice points and 2n is the number of conduction electrons.

D. Spin glass and scaling laws.

Blandin [8] observed that a dilute alloy with concentration n may be used to represent an alloy of concentration n', provided that the unit of measurement of distance is changed; i.e., if $r \longrightarrow r'$ then $n \longrightarrow n'$ where $nr^3 = n'r'^3$. Note that the same number of particles exists in the new volume. Now, since nr^3 is a concentration-independent parameter, the molecular field can be expressed a as

$$\frac{H_i}{n} = A \sum_{i \neq j} \mu_j \frac{\cos(2k_F r_{ij} + \phi)}{n r_{ij}^3}$$

where A is some coefficient with arbitrary dimension, μ_j

is the magnetic moment at j, and Φ is some arbitrary phase angle. Souletie and Tournier [9] have shown by using this molecular field that the probability distribution function P(H) for the molecular field has the property that

$$n\,P(H) = f\left(\frac{H}{n}\right)$$

where f is a universal function independent of concentration. For P(H,T,h) at a temperature T and in an external field h

$$n\,P(H,T,h) = g\left(\frac{H}{n},\frac{T}{n},\frac{h}{n}\right)$$

where g is a universal function independent of concentration. By using these properties of the probability density distribution, it can be shown that [9]

the energy $\quad E = n^2 \eta\left(\frac{T}{n};\frac{h}{n}\right)$

the specific heat $\quad \Delta C_p(T,h) = n\Gamma\left(\frac{T}{n},\frac{h}{n}\right)$

the magnetization $\quad M(\mathbf{h},T) = n\,F_1\left(\frac{h}{n},\frac{T}{n}\right)$

the initial susceptibility $\quad \chi(T,0) = F_2\left(\frac{T}{n},\,0\right)$

where η, Γ, F_1 and F_2 are all universal functions. Now $\Delta C_p/n$, M/n, and χ should each follow a scaling law with scaling parameters T/n and H/n for each alloy system.

We define "spin glass" as an alloy whose transport, magnetic, and thermal properties obey the above scaling laws.

At high temperature and low concentration; i.e., $k_B T > nV_o$, Larkin et al.[10] have used a virial expansion of the free energy in a power series of the concentration of impurities n to study the effect of the RKKY potential on the thermodynamic functions of dilute magnetic alloys.

The RKKY potential, $V(r) = V_o \cos 2k_F r/r^3$, will influence the thermodynamic functions if $V(r) \gtrsim k_B T$. Therefore the volume in which the RKKY interaction is important is inversely proportional to temperature. At high temperature or low concentration, the probability of finding two impurities in such a volume is small and the free energy can be obtained by a power series expansion in the concentration n. Larkin et al. predict for $k_B T \gg nV_o$ that

$$\chi = ng^2\mu_B{}^2 S(S+1)/3(k_B T + \theta_s)$$

where $\theta_s = C_s nV_o$ and C_s is a constant of order unity. In a high magnetic field; i.e., $g\,\mu_B H \gg k_B T$, $g\,\mu_B H \gg nV_o$, they predict that

$$M = g\,\mu_B S\, n \left[1 - \frac{2(2S+1)nV_o}{3g\,\mu_B H} \right]$$

In the low temperature and high concentration region, ($k_B T \ll nV_o$), a dilute magnetic alloy such as CuMn will have a specific heat linear in temperature and independent of concentration and a magnetic suscepibility which approaches a value at T = 0 which is independent of n.[42] In this region, the impurity spins are strongly correlated

with each other but without long range magnetic order. Anderson's [11] physical explanation is that since the structure of the alloy is irregular, the impurities will form many individually disconnected clusters. At low temperature, each cluster will go through a transition temperature and all impurity spins in this cluster will be aligned. Each cluster has its own transition temperature, and there is no sharp transition, and no long range order.

Marshall [43] and Klein, and Brout [13] used a model of independent spins in a random local field with a distribution function $P(H) = \Delta / \pi (H^2 + \Delta^2)$, where Δ is the width of the distribution, to investigate the low T behavior of a dilute magnetic alloy. At $T = 0$, the susceptibility is predicted to be[12]

$$\chi = \frac{2ng^2 S\,(S+1)\,\mu_B}{3\,\pi\,\Delta}$$

and specific heat $C \propto T$. They also predict that T_0, the temperature of the susceptibility maximum, is proportional to the impurity concentration.

E. Self-damping of the RKKY interaction.

Heeger, Klein, and Tu [45] have pointed out that if a dilute magnetic alloy is made less periodic by adding some non-magnetic scattering centers, then the RKKY oscillation will be damped by a factor $e^{-r/\ell}$ where ℓ is the mean free path of the conduction electrons. In a

dilute magnetic alloy, the effect may be divided into damping due to the magnetic impurities which also generate the RKKY interaction (self-damping) and damping due to the resistivity of the host. Walstedt and Walker [25] have discussed the effect of damping on the line broadening of the nuclear resonance line shape of CuMn alloys. The self-damping of the RKKY interaction will cause a narrowing of the undamped RKKY-broadened line. The line-narrowing effect is predicted to increase initially as $n^{2/3}$ and to become appreciable for magnetic impurity resistivity of the order of a few $\mu\Omega$/at. % impurity at $n \sim 1$ at. %. Their result can be expressed in terms of an effective concentration-dependent RKKY interaction strength V_o by $V_o(n) = V_o(0) \exp\left[-1.61 (\rho n)^{2/3} \sigma_{sp} Z\right]$, where $V_o(0)$ is the undamped RKKY strength, ρ is the density of sites available to the impurities, σ_{sp} is the effective scattering cross section, and Z is the number of conduction electrons per atom.

III. EXPERIMENT APPARATUS AND PROCEDURE

A. Sample preparation.

1. AuFe.

A series of AuFe alloys was prepared with Fe concentrations n in the range from 18 to 6050 parts per million (ppm). Nine alloys were prepared, with nominal concentrations of 10, 20, 50, 100, 200, 500, 1000, 2000 and 6000 ppm.

The alloys were prepared from 99.999 % Asarco Au nugget and 99.999 % Uminco Fe rod by melting the constituents in an argon atmosphere arc furnace with a water cooled hearth. All materials were cleaned before melting and annealing. The polycrystalline samples, with masses of 0.5 to 2 grams, were annealed under vacuum for 24 hrs at 900 C and quenched in ice brine. All samples were kept at liquid nitrogen temperature prior to measurement. Drawings of the arc furnace and annealing apparatus, along with further procedures of sample preparation, are carefully detailed in the thesis of R. Caton.[46]

A master sample of AuFe with 0.87 atomic % Fe was prepared first. Starting from this master alloy, AuFe samples of 6000 ppm, 2000 ppm and 1000 ppm Fe were made by melting appropriate amounts of Au with slices of the master alloy. Fe samples with 500 ppm, 200 ppm and 100 ppm were made from the 1000 ppm AuFe sample. Lastly, 50

ppm, 20 ppm and 10 ppm Fe samples were made from the 100 ppm sample. All above mentioned concentrations of Fe were nominal concentrations.

2. AuMn.

A series of AuMn alloys was prepared with Mn concentrations n in the range from 50 to 2000 ppm Mn. Six alloys were prepared, with nominal concentrations of 50, 100, 200, 500, 1000 and 2000 ppm Mn.

The alloys were prepared from 99.999 % Asarco Au nugget and 99.99 % Johnson Matthey Mn flakes.

A master alloy of 2000 ppm Mn in Au was prepared first by melting in an arc furnace appropriate amounts of Au and Mn. The rest of the samples were made by using slices of the master alloy and additional amounts of pure Au.

3. Determination of impurity concentrations.

The concentrations of Fe in the AuFe alloys were determined by measuring the residual resistance ratios, $\rho = R(4.2)/[R(273) - R(4.2)]$, of the samples used, where R(4.2) is the resistance of the sample at 4.2 K. The concentrations then were found from the measured values of ρ using $n\ (ppm) = (1.13) \times 10^4 \rho$. The constant 1.13×10^4 was obtained from the work of Hurd et al.[47] and Garbarino et al.[48] The Fe concentrations determined by residual resistance ratios are listed in the last column

of Table 1 and are the results of the average of two measurements of ρ for each sample. The determined values of n so found are much higher than the nominal concentrations for the low concentration samples. It is probable that the slice of master alloy used in preparing the low concentration samples was more Fe-enriched than the average concentration of the alloy.

The Mn concentrations were determined by using two methods 1). measurement of the residual resistance ratios ρ and 2). measurement of the magnetic properties of the samples.

By measuring the resistances R at 4.2 K and 273 K, the residual resistance ratios were calculated. Then using the results obtained by Loram, Whall and Ford, [14] i.e., $n_1(\text{ppm}) = 8.81 \times 10^3 \rho$, the concentrations of Mn were found. The concentrations of Mn in Au can also be found by using the relations $C = n_2 g^2 \mu_B{}^2 S\,(S+1)/3k_B$ and $M_{sat} = n_2 g \mu_B S$ where C is the measured Curie constant, μ_B is the Bohr magneton, S is the spin of the impurity, k_B is Boltzmann's constant, and M_{sat} is the measured saturation magnetization. From these two relations, n_2 can be obtained by eliminating the spin S, with the result that $n_2 = M^2_{sat}/(3k_B C - g\mu_B M_{sat})$. The value of g is assumed to be equal to 2. [49] The values of concentration n to be used in the analysis were chosen to be the average of n_1

Table 1

Fe Concentrations of AuFe Alloys Studied.

n_0 (ppm Fe-nominal)	n_1[a] (ppm Fe)	n_2[a] (ppm Fe)	n[b] (ppm Fe)
10	19	17.8	18 ± 1
20	44	41	42 ± 2
50	92	96	94 ± 2
100	167	171	169 ± 2
200	258	225	242 ± 16
500	580	565	572 ± 8
1000	1230	1070	1160 ± 70
2000	2350	2100	2225 ± 125
6000	6400	5700	6050 ± 350

a) Concentrations determined from residual resistance ratios ρ and n (ppm Fe) = $1.13 \times 10^4 \rho$ (see text).

b) Concentrations determined by averaging the values of n_1 and n_2 from this table, and used in the analysis of the data.

Table 2

Mn Concentrations of AuMn Alloys Studied.

n_0 (ppm Mn-nominal)	n_1[a] (ppm Mn)	n_2[b] (ppm Mn)	n[c] (ppm Mn)
50	50	58	54 ± 4
100	97	113	105 ± 8
200	225	207	216 ± 9
500	557	485	521 ± 36
1000	1030	980	1005 ± 25
2000	2060	2160	2110 ± 50

a) Concentrations determined from residual resistance ratios ρ and n_1 (ppm Mn) = $8.81 \times 10^3 \rho$ (see text).

b) Concentrations determined from measured values of the Curie constant C and saturation magnetization M_{sat}, listed in Table 3, using $n_2 = M_{sat}^2/(3k_BC - g\mu_BM_{sat})$.

c) Concentrations determined by averaging the values of n_1 and n_2 from this table, and used in the analysis of the data.

and n_2. These values of concentration for all the AuMn samples studied are listed in Table 2. The measured values of C and M_{sat} are listed in Table 3.

B. Experimental apparatus.

Magnetization and susceptibility were measured using Faraday's method, in a cryostat with a uniform magnetic field and gradient field provided by superconducting magnets. The measuring device used was a Cahn RH Electrobalance. A schematic of the experimental arrangement is shown in Figs. 1 and 2. A simple description of the apparatus is given in this section. A more detailed description is given in Jim Haddad's thesis.[50] (p.91-112)

1. Superconducting magnets.

a. Uniform field.

The uniform field was provided by a Westinghouse superconducting solenoid. The solenoid was powered by a Magnion CFC-100 power supply. The maximum field of the solenoid was 50 Kilogauss with a current constant of (52.7 $\pm$ 1 %) amperes per 50 kG as given by Westinghouse. The field of the solenoid is quoted to have a uniformity of better than 0.1 % over a 1 cm axial distance. A one milliohm standard resistor was put in series with the solenoid and the voltage across the resistor was used as a measure of the magnet current and hence the magnetic

FIG. 1

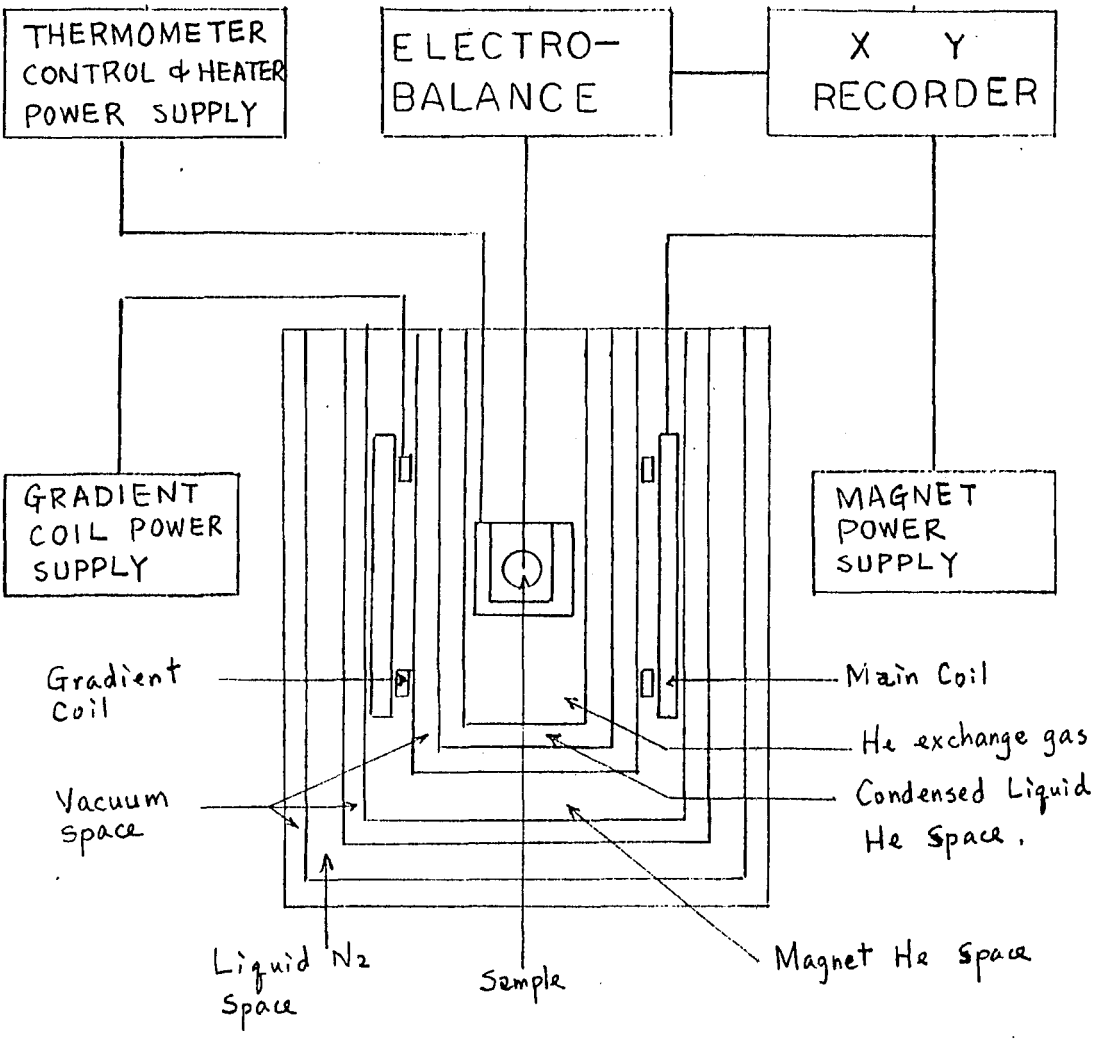

FIG. 1

Schematic diagram of the measuring apparatus and cryogenics.

field. The magnetic field can be increased or decreased automatically or manually. For the samples with high impurity concentrations ($n \geqslant 94$ ppm) data were taken with the field going up automatically from 0 to 50 kG in 10 min. For the low impurity samples, eddy currents contributed a large factor to the measurements when the field was increased at this rate. For these samples, the data were therefore taken point by point with the applied field increased manually.

b. Gradient field.

The gradient coils were mounted on a stainless steel tube insert. For dimensions and details refer to Fig. 3. An cylindrical epoxy coil form was mounted on the insert for proper coil positioning. Each coil was circular, with a square cross section of 10 layers of 11 turns each. The wire used was 7.5 mil NbTi with copper cladding and Formvar insulation. The gradient field was 53.8 I gauss/cm (from p.44 of Zijlstra),[51] where the gradient current I is in units of amperes. Typical currents of either 6 or 9 amperes were used in the coil. The brass spacer shown in Fig. 3 fit the inner diameter of the main solenoid to insure that the insert was properly centered.

The power supply used to energize the gradient coil was a Hewlett-Packard 6264 B. The circuit used is

FIG. 2

A schematic diagram of the magnet and the insert. To show all of the details, the diagram has been expanded to cover two pages.

Symbol identification:

A superconducting magnet (uniform field).
B superconducting magnet (gradient field).
C copper block with thermometers imbedded.
D sample.
E vacuum space.
F magnet helium space.
G condensed helium space.
H sample space.
J brass spacer.
K brass washer.
L connector for gradient coil lead.
M removable tube.
N demountable connector.
P connector for heater and thermometer lead.
R flange.
S teflon funnel.
Z teflon spacer.

Fig. 2 — 1

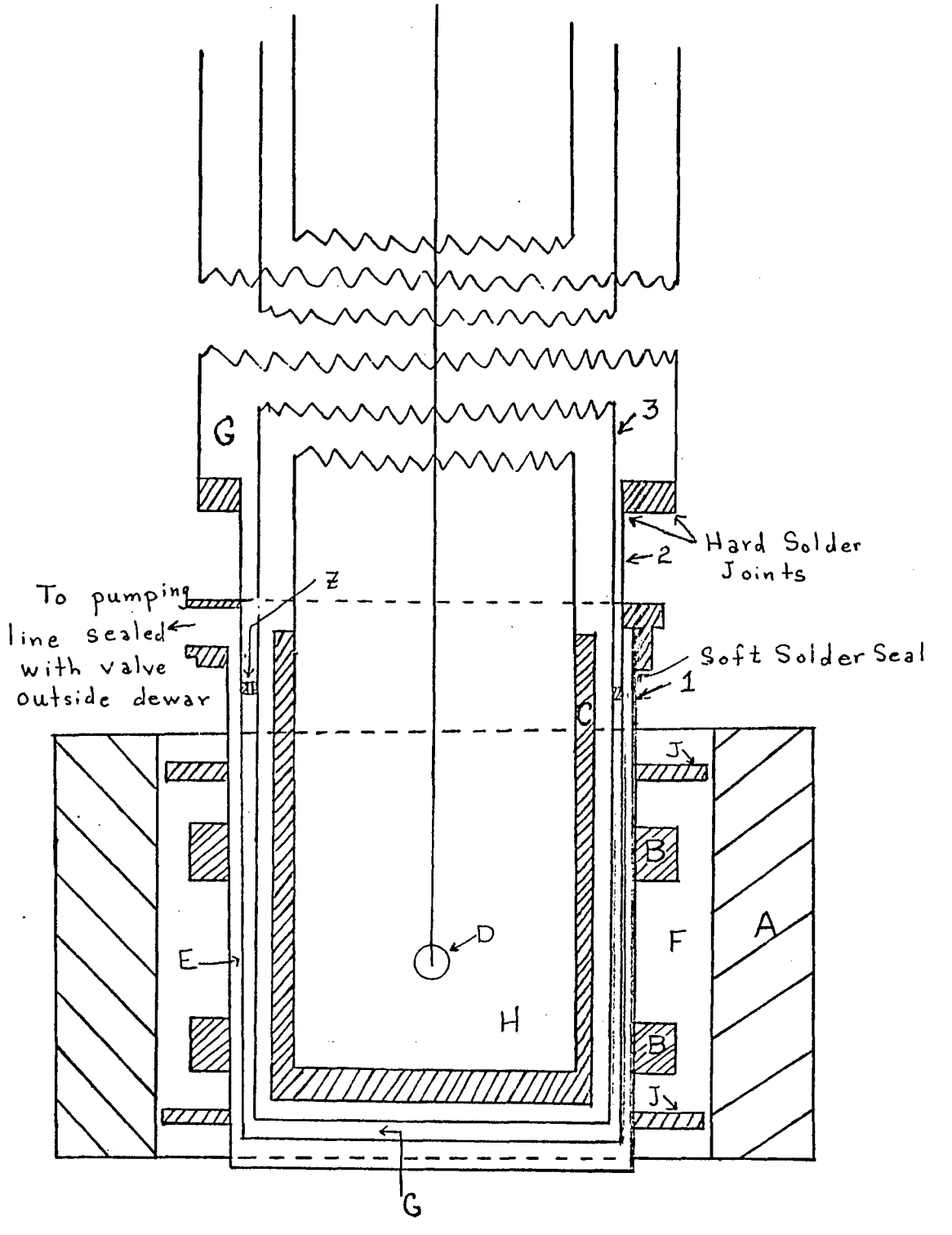
G
3
2
Hard Solder Joints
To pumping line sealed with valve outside dewar
Z
Soft Solder Seal
1
C
J
B
A
F
E
D
H
B
J
G

Fig. 2—2

Flange R includes provisions for He transfer, level detection, and leads for magnet current.

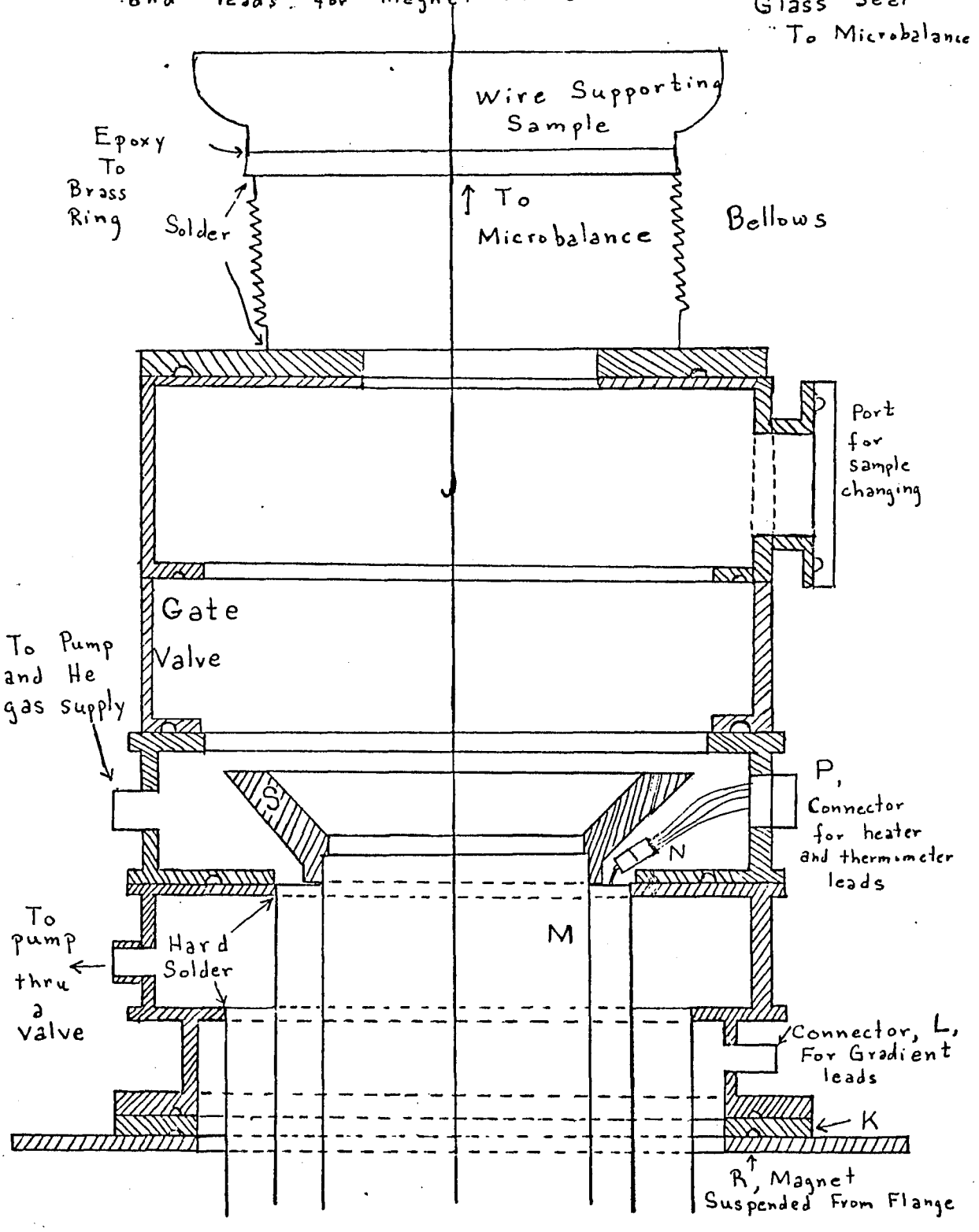

FIG. 3

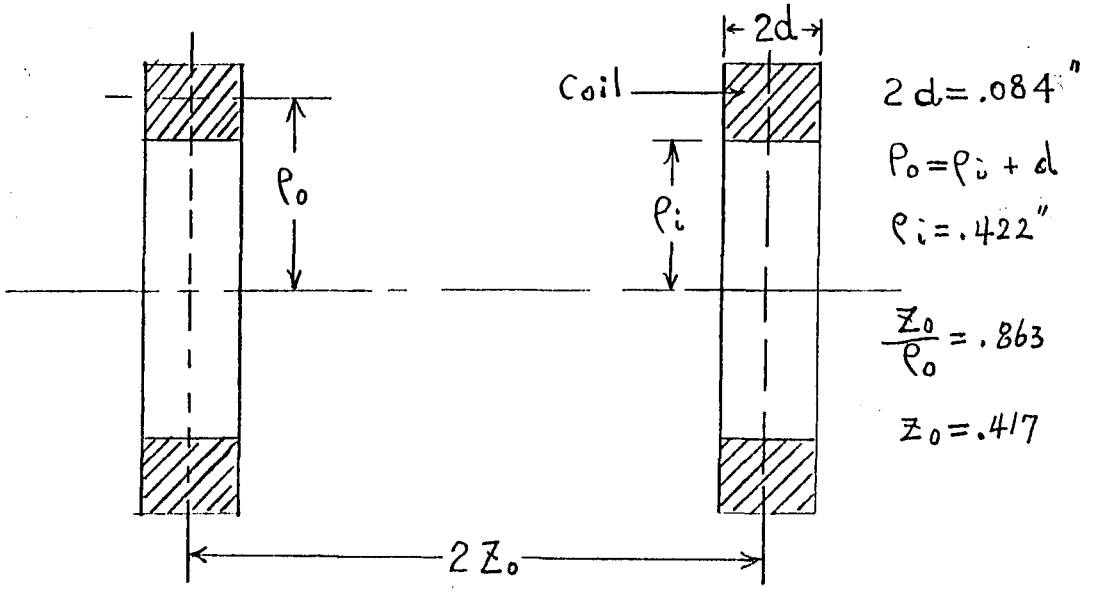

DIMENSION OF GRADIENT COIL

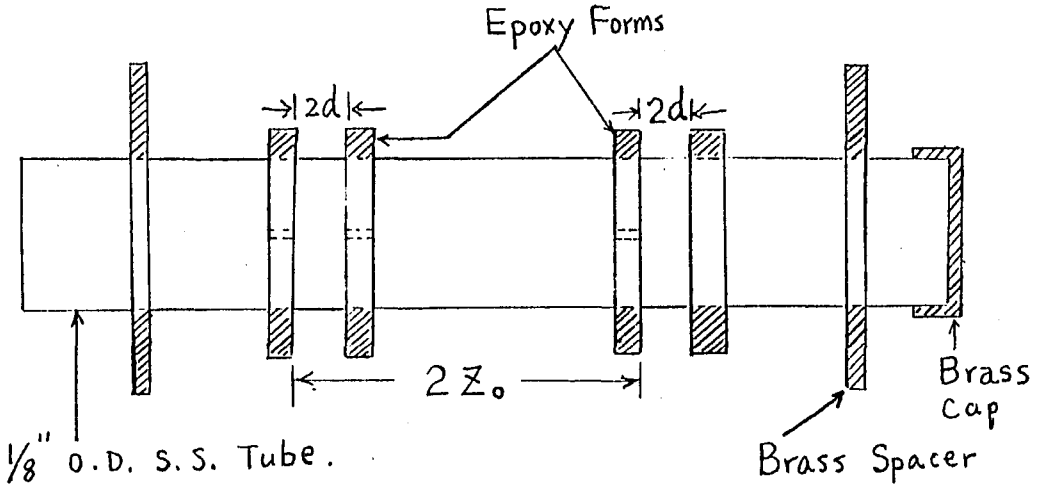

COIL FORM AND SPACER

FIG. 3

A schematic diagram of the gradient coils and the gradient coil form.

also contained in Haddad's thesis.[50]

2. Microbalance.

The force on the sample, $F = \chi mH\partial H/\partial Z$, was measured by a Cahn RH Electro-balance, and an effective change in mass of 2 micrograms could be detected. A Medistor microvoltmeter was used in balancing the sample initially, and was also used in measurements of some of the low impurity samples. For the high impurity samples, the output of the microbalance was connected to the Y input of a Hewlett-Packard 7001 XY recorder, while the voltage from the standard one milliohm resistor in series with the magnet was connected to the X input of the recorder. The microbalance was mounted on a lathe with 3-dimensional position control to allow positioning of the sample in the center of the magnetic field.

3. Thermometry and temperature control.

A stainless steel tube was inserted inside the sample space, see Fig. 2. The bottom part of the tube was OFHC copper capped with a half inch thick plug of OFHC copper. Inside the copper plug, a carbon resistor and a platinum resistor were mounted. The resistances of the thermometers were measured using a 4-terminal method. The thermometer current was provided by a 9.45 volt battery with 7 current-limiting resistors. A switch was provided for the purpose of selection of thermometers or

decade resistor. A Leeds and Northrup K-3 potentiometer and a Leeds and Northrup DC-null detector (Cat. No. 9834-1) were used for the measurement of voltage across the thermometer. Measurements were made by first adjusting the potentiometer for a null indication on the null detector. Then the decade resistor was substituted for the thermometer, and adjusted until the null detector read null again. The reading of the decade resistor was then the resistance value of the thermometer.

For temperatures below 4.2 K, the temperature was controlled by pumping on the condensed liquid helium. By fine adjustment of the pumping speed a steady vapor pressure can be achieved. For temperatures above 4.2 K, the desired temperature was obtained by using the off-balance output of the null-detector as an error signal to control the output of a Hewlett-Packard 6200B power supply, which provided current to a heater wound on the copper block inside the sample space.

The thermometers used were a calibrated 550 ohm platinum resistor supplied by Rosemont Engineering and an Allen-Bradley 80 ohm carbon resistor. The platinum resistor was used for temperatures above 40 K, while the carbon resistor was used for the temperature range 1.2 to 40 K. The temperature was calibrated against a calibrated germanium thermometer and also several

samples of chrome potassium alum. Since the susceptibility of the chrome potassium alum is known to follow a Curie law to very low temperatures, this also provided a check on the thermometer calibration. The uncertainty in temperature is $\pm$ 1 % for the whole range of temperatures between 1.2 to 100 K. The magneto-resistance of the carbon thermometer will cause the temperature to change 1 % when the magnetic field increases from 0 to 50 kG. In studies of the susceptibility, only low field data is used, and the magneto-resistance error will not be important; i.e., less than 0.1 %.

C. Experiment.

The step-by-step experimental procedure is as follows :

1. Positioning the sample.

The sample, with a small hole (Dia. 0.03 inch) drilled through it, was cleaned and dried before being tied to the end of a #40 copper wire. The sample suspended from the wire was then guided into the sample space through the sample port, and the top of the wire was then attached to a hook hanging down from the microbalance. The initial weight difference between the two sides of the microbalance was monitored by connecting the output of the microbalance to a Medistor (used as a null detector). Additional weight was then added until

a balance between the two sides was achieved.

2. Horizontal centering of the sample.

Since the inner tube was positioned in the center of the main field and gradient field initially, the centering of sample was made possible by using the tube as a guide. The output of the microbalance was connected to the X-Y recorder. Any irregular noise shown on the recorder indicated that the sample was touching the wall of the tube. By a lateral check of the clearance of the sample inside the tube, the center of the field could easily be found.

3. Pump out.

The whole system including the sample space, condensed helium space, and the pressure gauge, was pumped out by a central mechanical pump (Leybold-Heraeus Type DK - 200) for more than one hour.

4. Cooling down.

With the pump closed, 200 mm Hg of helium exchange gas was admitted into the sample space, and 1 atm. of He gas was introduced into the condensing space. Then liquid nitrogen was transferred to both the liquid nitrogen and magnet spaces. The temperature of the sample space was monitored using the platinum thermometer. Fifteen minutes after transfering of the liquid nitrogen, the temperature reached approximate 77 K. The liquid nitrogen

in the magnet space was then forced out by inserting a tube to the bottom of the magnet space and pressurizing the magnet space. After all the liquid nitrogen was forced out, the transfer of liquid helium was then started. It took approximately half an hour and 8 liters of liquid helium to fill the magnet space. With the magnet space filled with liquid helium, helium gas at a pressure of 3 psi over 1 atm. was connected to the condensing helium space for 7 minutes. The sample space exchange gas was then pumped down to 2mm Hg.

5. Sample weight monitoring and vertical positioning.

The weight of the sample was monitored on the X-Y recorder for 10 minutes. If the system was not leak-tight, air would condense onto the sample, and an increase of weight of the sample would be seen. The gradient field was then used to center the sample vertically. The sample was at the center of the gradient coil if there was no net change in force with the gradient current positive, negative and zero.

6. Experiment.

The power supply for the main field was turned on, and the field was run up and down automatically using 5 min./full scale to train the magnet. The voltage from the one milliohm standard shunt (i.e. the monitoring of the magnet current) was connected to the X input of the

recorder, the output of the microbalance was connected to the Y input of the recorder. The field was increased at a rate of 10 min./full scale. The magnetization curve at each temperature was recorded on the recorder. Data were first obtained at 4.2K. After the 4.2K run the temperature was lowered by pumping on the condensed liquid helium, controlled by adjusting the pumping speed, and monitored by both an oil manometer and a carbon resistance thermometer.

After the lowest temperature run, i.e., 1.25 K, had been completed and after all liquid helium had been pumped out of the condensed space, helium exchange gas at a pressure of 40 mm Hg was introduced into the condensed space. For the higher temperature runs, the decade resistor was set to a chosen value, the potentiometer was adjusted until the null detector read zero, and then the potentiometer was switched back to the thermometer. The output of the null-detector provided a signal to the heater power supply which supplied current to the heater inside the sample space to maintain a constant sample temperature.

IV. EXPERIMENTAL RESULTS AND ANALYSIS.

A. Calibration of Faraday method.

The experimental data were recorded directly on a Hewlett-Packard 7001 X-Y recorder. The Y -input to the recorder was the output of the microbalance, V_M, which is proportional to the force on the sample in the magnetic field; i.e., $F = mM(H)\,\partial H/\partial Z = mH\chi(H)\,\partial H/\partial Z = K_o V_m$ where m is the mass of the sample and M is the magnetization of the sample. Since the gradient field was constant, the above-mentioned relation could be simplified to $mM = K_I V_M$. The value of K_I could be obtained by measuring some known sample, such as pure Au, and is assumed to be independent of the temperature of the sample.

The susceptibility of pure Au was measured from 1.25K to 100K, and the value of V_M was plotted as a function of 1/T. The extrapolated value of V_M to $1/T = 0$ was taken to be equal the susceptibility of pure Au, which is $\chi_{Au} = -0.1435 \times 10^{-6}$ emu/g.[52] Then by using the relation that $K_I = m\chi H/V_M$, the value of K_I was determined to be $(1.98 \pm 0.02) \times 10^{-3}$ emu/mv. The values of M and χ were then obtained from V_M and V_H by using the relations:

$$M = K_I \frac{V_M}{m} = 1.98 \times 10^{-3} \frac{V_M}{m} \text{ emu/gram}$$

$$\chi = \frac{\Delta M}{\Delta H} = 1.88 \times 10^{-6} \frac{\Delta V_M}{m\,\Delta V_H} \text{ emu/gram},$$

where V_H is the voltage input to the X-axis of the recorder. Both V_m and V_H are in units of millivolt, and m is in units of gram.

B. AuMn

1. The susceptibility of AuMn.

The susceptibilities of the AuMn samples with concentrations of 54, 105, 216, 521, 1005, 2110 ppm Mn were determined graphically from the slope of M versus H as $H \rightarrow 0$, for temperatures from 1.25K to 100K. The impurity susceptibility data, obtained by subtracting χ of pure Au from the measured total susceptibility, are listed in Table 4. The diamagnetic susceptibility of pure Au was determined by plotting the measured total susceptibility as a function of 1/T and extrapolating to 1/T = 0, with the extrapolation point taken to be χ_{Au}. The values of χ_{Au} are also listed in Table 4. The results for each alloy have been least - square - fitted to a Curie - Weiss law, $\chi(T) = C/(T+\theta)$, with the resulting values of C and θ given in Table 3. The resulting values of χ^{-1} have been plotted vs. T in Fig. 4. The only significant deviations from Curie - Weiss behavior occurred below 2K for n = 1005 ppm Mn and below 4K for 2110 ppm Mn. From the measured Curie constant C and impurity concentration n, the value of S can be calculated. The values of S obtained, with

Table 3

Magnetic Properties of AuMn Alloys Studied.

n (ppm Mn)	C[a] (10^{-6} $\frac{emuK}{g}$)	θ[a] (K)	M_{sat}[b] (10^{-3} $\frac{emu\ G}{g}$)	S[c]	S[d]
54	0.985±0.02	0	7.0 ±0.2	2.23± 0.04	2.29± 0.06
105	1.92 ±0.04	0	13.7 ±0.2	2.23± 0.04	2.30± 0.04
216	3.81 ±0.08	0	26.3 ±0.2	2.18± 0.04	2.15± 0.03
521	9.80 ± 0.2	+0.2± 0.1	65 ± 1	2.27± 0.04	2.20± 0.04
1005	20.2 ± 0.4	+0.02± 0.1	133 ± 3	2.34± 0.04	2.33± 0.04
2110	38.0 ± 0.8	-0.5± 0.2	267 ± 5	2.21± 0.04	2.23± 0.04

a) Measured Curie constant C and Curie-Weiss temperature θ determined from initial susceptibility data and $\chi = C/(T+\theta)$.

b) Measured saturation magnetization M_{sat} determined from magnetization data in the limit $1/H \to 0$ (see Fig.9 and text).

c) Values of the spin S per Mn atom determined from the measured Curie constants $C = ng^2\mu_B{}^2 S(S+1)/3k_B$, g = 2, and the concentrations n listed in this table.

d) Values of the spin S per Mn atom determined from the measured saturation magnetization $M_{sat} = ng\mu_B S$, g = 2, and the concentrations n listed in this table.

Table 4

Magnetic Susceptibility of AuMn Alloys.

Au + n-ppm Mn	T[a] (K)	χ[b] (10^{-6} emu/g)	Au + n-ppm Mn	T[a] (K)	χ[b] (10^{-6} emu/g)
n = 54	1.24	0.780	n = 216	1.24	3.11
	1.73	0.586		1.70	2.19
	2.10	0.479		2.03	1.85
	2.57	0.390		2.32	1.60
	3.03	0.327		2.71	1.40
	3.41	0.291		3.06	1.24
	3.87	0.258		3.30	1.16
	4.25	0.232		3.77	1.03
	5.85	0.170		4.27	0.886
	7.90	0.160		5.85	0.647
	12.2	0.088		7.94	0.483
	22.7	0.048		12.20	0.314
	36.9	0.027		22.78	0.173
	52.0	0.020		36.95	0.107
	77.9	0.008		52.0	0.074
	89.0	0.011		77.5	0.050
n = 105	1.24	1.57	n = 105	7.90	0.237
	1.68	1.11		12.2	0.164
	1.96	0.96		22.7	0.100
	2.35	0.789		36.9	0.061
	2.64	0.719		52.0	0.046
	3.00	0.636		77.5	0.027
	3.40	0.559		89.0	0.021
	3.83	0.494		124.3	0.017
	4.23	0.446		150.5	0.018
	5.85	0.334			

Table 4 (continued)

Au + n-ppm Mn	T^a (K)	χ^b (10^{-6}emu/g)	Au + n-ppm Mn	T^a (K)	χ^b (10^{-6}emu/g)
n = 521	1.24	6.70	n = 1005	1.24	13.7
	1.67	5.34		1.62	11.3
	1.94	4.69		1.98	10.1
	2.28	4.13		2.33	8.14
	2.58	3.60		2.58	7.81
	2.97	3.18		2.96	6.74
	3.40	2.81		3.37	5.96
	3.85	2.51		3.75	5.29
	4.25	2.21		4.28	4.62
	5.47	1.77		5.47	3.72
	5.85	1.63		5.64	3.46
	6.34	1.50		6.34	3.19
	7.00	1.37		7.90	2.47
	7.90	1.22		9.45	2.14
	9.45	1.01		12.2	1.61
	12.2	0.771		17.8	1.11
	17.8	0.535		22.7	0.884
	22.7	0.425		30.1	0.668
	30.1	0.330		36.9	0.546
	36.9	0.270		45.5	0.445
	45.5	0.213		59.0	0.344
	59.0	0.164		77.5	0.270
	77.5	0.123		89.0	0.227
	89.0	0.108		103.5	0.193
	103.5	0.092		124.5	0.155
	124.5	0.076			

Table 4 (continued)

Au + n-ppm Mn	T[a] (K)	χ[b] (10^{-6}emu/g)	Au + n-ppm Mn	T[a] (K)	χ[b] (10^{-6}emu/g)
n = 2110	1.24	22.2	n = 2110	9.45	4.32
	1.75	19.6		12.2	3.26
	2.03	18.6		17.8	2.32
	2.37	17.1		22.7	1.85
	2.72	15.5		30.1	1.39
	3.08	13.6		36.9	1.17
	3.47	12.0		45.5	0.965
	3.84	11.0		52.0	0.843
	4.25	9.88		59.0	0.748
	5.47	7.77		66.3	0.673
	5.85	7.14		77.5	0.579
	6.34	6.61		89.0	0.413
	7.90	5.28		124.5	0.316

a) Temperatures are accurate to within $\pm$ 1 %.

b) Magnetic susceptibility results are estimated to be accurate to within $\pm$ 2 %. The values of χ listed in this table are the impurity contribution, corrected for the contribution of the pure Au host, which is obtained by extrapolating from the plot of total susceptibility vs. 1/T to 1/T = 0. The values obtained are as follows:

n ppm Mn	54	105	216	521	1005	2110
χ_{Au} ($10^{-6}\frac{emu}{g}$)	-0.1435	-0.130	-0.1435	-0.1435	-0.1435	0.1365

FIG. 4

Inverse impurity susceptibilities χ^{-1} for six AuMn alloys (54, 105, 216, 521, 1005 and 2110 ppm Mn) plotted as a function of temperature T. Error bars are estimated from the uncertainties of the magnetizations and the determinations of slope.

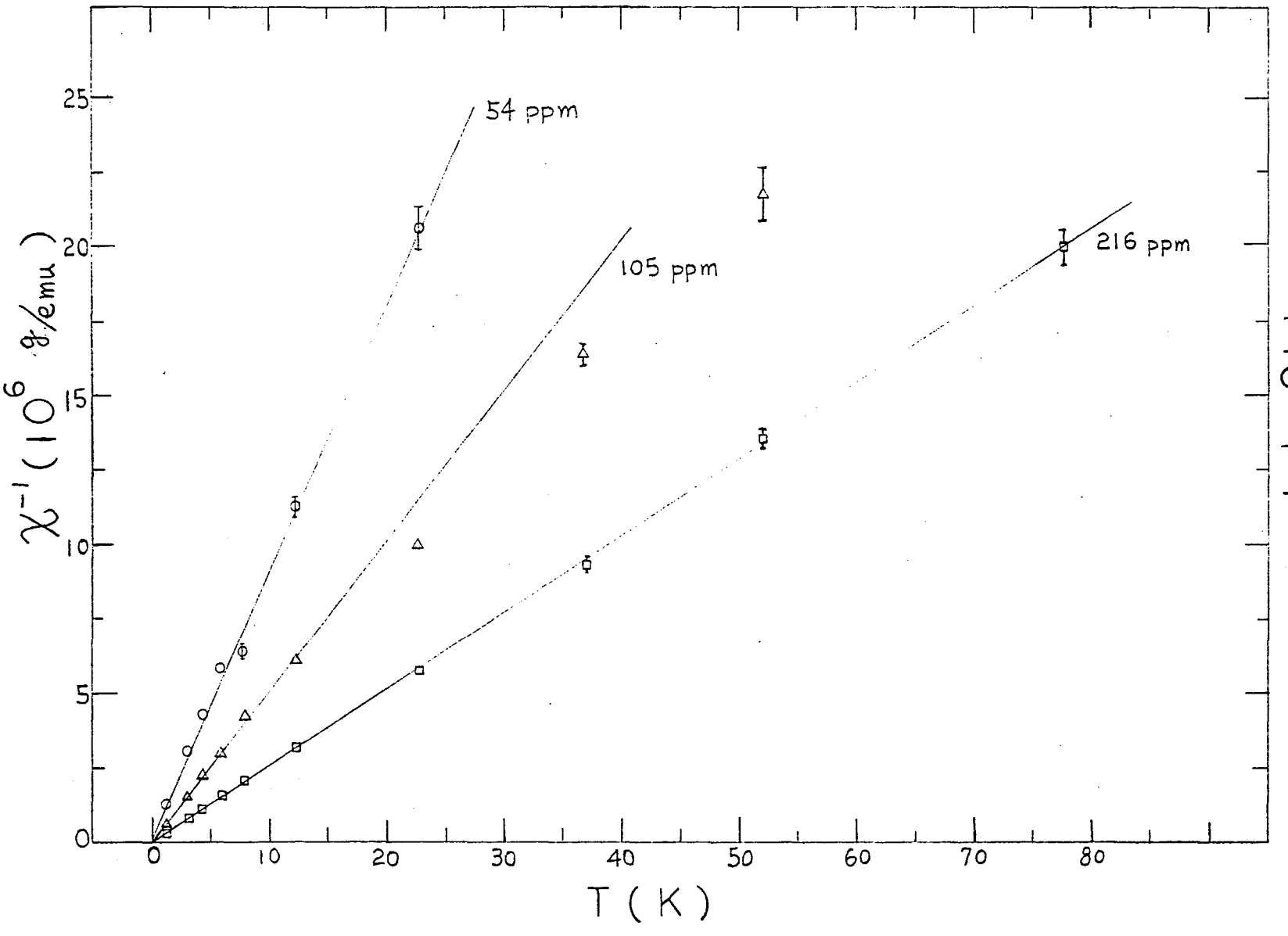
54 ppm
105 ppm
216 ppm
χ^{-1} (10^6 g/emu)
T (K)
0
5
10
15
20
25
0
10
20
30
40
50
60
70
80

FIG 4-1

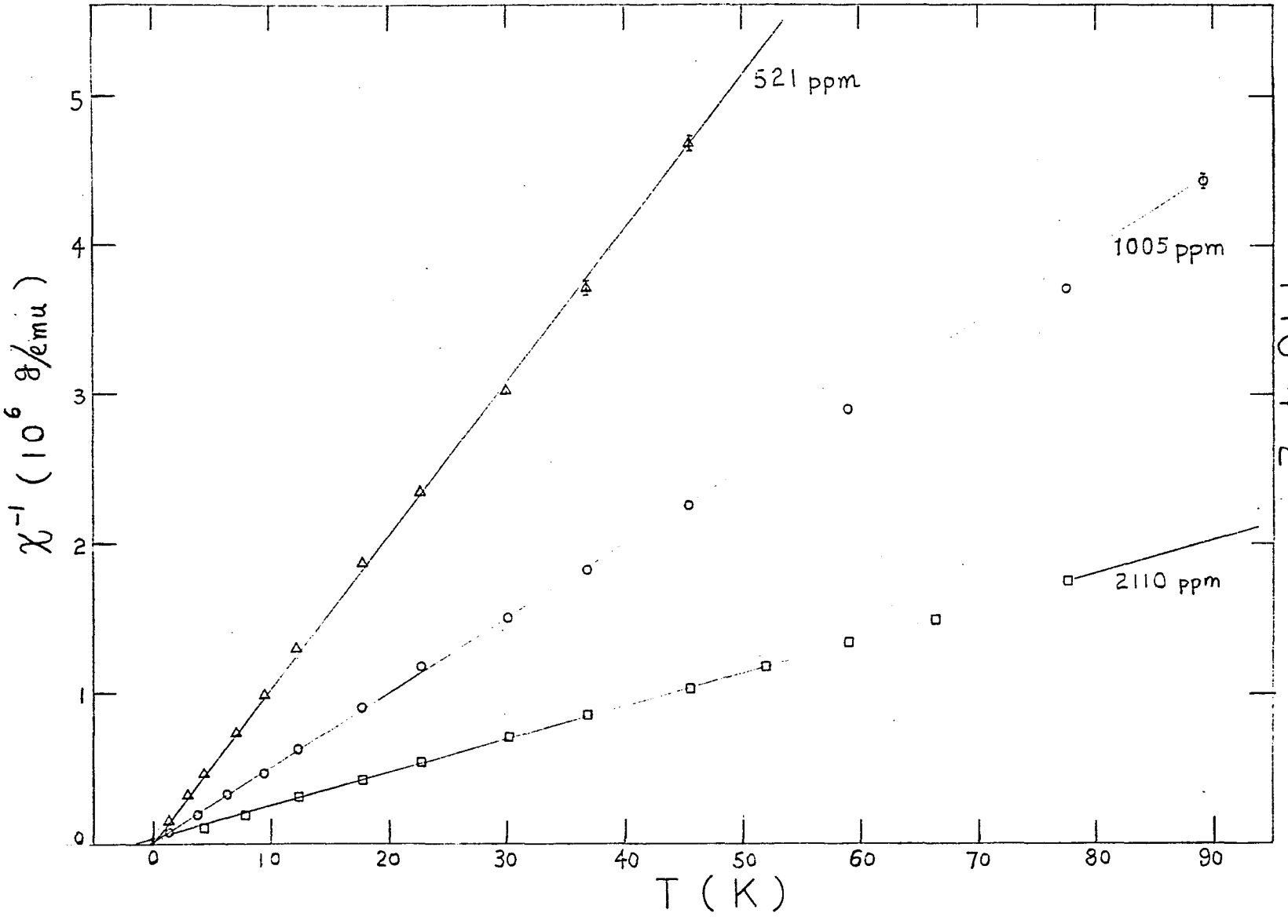
521 ppm
1005 ppm
2110 ppm
χ^{-1} (10^6 g/emu)
T (K)
0
1
2
3
4
5
0
10
20
30
40
50
60
70
80
90

FIG 4-2

g = 2 assumed, are also listed in Table 3. The values of S can also be calculated from $M_{sat} = ng\mu_B S$. The values obtained for S by using M_{sat} are also listed in Table 3.

2. The magnetization of AuMn.

The magnetization data for AuMn, corrected for the contribution due to the Au host, are listed in Table 5. The impurity magnetizations of AuMn of six different concentrations of Mn are plotted as a function of H/T for three different temperatures each in Fig. 5. Also shown in the Figure are Brillouin functions for the appropriate Mn spin S taken from Table 3. For the 54, 105 and 216 ppm Mn samples, within experimental error, the magnetization data are a function of H/T only, and the deviations from the Brillouin functions are small, but measurable. For higher concentration samples, the deviations from Brillouin functions are significant, and the deviations increase with Mn concentration. For all samples, the deviations increase with lower temperature.

3. Testing of scaling laws for AuMn.

In Fig. 6, the susceptibility $\chi(n, T)$ for all six samples is plotted as a function of T/n. The susceptibility data for these six alloys fall quite well on a universal curve, to within experimental error. In Fig. 7, the values of $M/M_{sat} = M/ng\mu_B S$ are plotted as a function of H/n for three alloys at fixed $T/n = (3.73 \pm 0.01) \times 10^{-3}$

Table 5

Impurity Magnetization Data of AuMn.

n = 54 ppm Mn

H^a(kG)	M^b (10^{-3} emu gauss/gram)			
T(K)	1.73	2.10	2.57	3.03
2.85	1.59	1.32	1.10	0.929
5.34	2.80	2.38	2.00	1.71
10.4	4.48	3.97	3.45	3.06
15.3	5.43	4.90	4.52	4.08
20.3	5.97	5.63	5.23	4.82
25.3	6.29	6.03	5.72	5.36
30.4	6.51	6.31	6.05	5.76
35.3	6.65	6.49	6.29	6.04
40.3	6.76	6.62	6.47	6.26
45.3	6.82	6.73	6.60	6.41
50.3	6.84	6.80	6.69	6.54

H^a(kG)			
T(K)	3.41	3.87	4.25
2.85	0.827	0.735	0.666
5.34	1.53	1.37	1.24
10.4	2.76	2.50	2.28
15.3	3.75	3.45	3.17
20.3	4.50	4.20	3.92
25.3	5.06	4.78	4.51
30.4	5.46	5.22	4.99
35.3	5.82	5.61	5.36
40.3	6.06	5.86	5.66
45.3	6.24	6.05	5.90
50.3	6.39	6.22	6.08

Table 5 (continued)

n = 105 ppm Mn

H^a(kG)	M^b (10^{-3} emu gauss/gram)				
T(K)	1.24	1.68	1.96	2.35	2.64
2.85	4.30	3.22	2.71	2.28	2.10
5.34	7.05	5.60	4.85	4.14	3.77
8.06	8.95	7.36	6.61	5.77	5.30
10.4	10.3	8.79	8.00	7.08	6.59
15.3	11.7	10.6	9.91	9.06	8.60
20.3	12.4	11.6	11.1	10.4	9.97
25.3	12.8	12.2	11.8	11.2	10.9
30.4	13.1	12.6	12.3	11.8	11.6
35.3	13.3	12.9	12.6	12.2	12.0
40.3	13.4	13.1	12.8	12.5	12.4
45.3	13.4	13.2	13.0	12.7	12.6
50.3	13.5	13.3	13.1	12.9	12.8

H^a(kG)				
T(K)	3.00	3.40	3.83	4.25
2.85	1.86	1.63	1.44	1.30
5.34	3.37	2.97	2.67	2.41
8.06	4.73	4.24	3.82	3.44
10.4	5.98	5.40	4.88	4.44
15.3	7.96	7.17	6.70	6.18
20.3	9.40	8.61	8.16	7.60
25.3	10.4	9.70	9.30	8.74
30.4	11.2	10.5	10.2	9.61
35.3	11.7	11.1	10.8	10.4
40.3	12.1	11.6	11.3	10.9
45.3	12.4	11.9	11.7	11.3
50.3	12.6	12.2	12.1	11.7

Table 5 (continued)

n = 216 ppm Mn

H^a(kG)	M^b (10^{-3} emu gauss/gram)				
T(K)	1.24	1.69	1.94	2.31	2.68
2.37	7.11	5.31	4.76	3.89	
4.74	12.5	9.85	8.93	7.56	6.69
7.12	15.6	13.4	12.2	10.7	9.65
9.49	18.8	16.2	15.0	13.3	12.1
14.2	21.8	19.9	18.7	17.2	15.9
19.0	23.5	22.1	21.0	19.8	18.7
23.7	24.4	23.3	22.5	21.5	20.6
28.5	24.9	24.1	23.4	22.7	21.9
33.2	25.3	24.7	24.1	23.5	22.8
38.0		25.1	24.6	24.6	23.5
42.7		25.4	24.9	24.4	24.1
47.4		25.5	25.1	24.8	24.5

H^a(kG)				
T(K)	3.06	3.42	3.85	4.25
2.37	3.02	2.74	2.36	2.09
4.74	5.87	5.32	4.75	4.18
7.12	8.50	7.74	6.95	6.21
9.49	10.8	9.88	9.01	8.08
14.2	14.4	13.5	12.5	11.4
19.0	17.2	16.2	15.3	14.1
23.7	19.2	18.3	17.5	16.4
28.5	20.6	19.8	19.2	18.2
33.2	21.7	21.0	20.5	19.6
38.0	22.5	21.9	21.6	20.7
42.7	23.1	22.6	22.4	21.6
47.4	23.6	23.1	23.0	22.3

Table 5 (continued)

n = 521 ppm Mn

H^a(kG)	M^b (10^{-3} emu gauss/gram)				
T(K)	1.24	1.67	1.94	2.28	2.58
2.37	15.4	12.5	11.2	9.73	8.61
4.74	27.1	23.4	21.1	18.7	16.8
7.12	35.3	31.3	28.8	26.1	23.7
9.49	41.6	37.5	35.0	32.0	29.7
14.2	49.6	46.0	43.7	40.9	38.7
19.0	54.2	51.4	49.4	47.0	45.1
23.7	57.0	54.9	53.2	51.2	49.5
28.5	58.7	57.1	55.8	54.1	52.7
33.2	59.7	58.6	57.5	56.3	55.1
38.0	60.4	59.7	58.7	57.8	56.8
42.7	61.0	60.3	59.4	58.9	58.1
47.4	61.4	61.0	60.1	59.8	59.1

H^a(kG)					
T(K)	2.97	3.40	3.85	4.25	5.47
2.37	7.62	6.64	6.08	5.24	4.19
4.74	14.8	13.2	11.9	10.5	8.46
7.12	21.2	19.1	17.4	15.6	12.6
9.49	26.9	24.3	22.4	20.3	16.5
14.2	35.7	33.0	30.6	28.3	23.5
19.0	42.2	39.6	37.2	34.7	29.6
23.7	47.0	44.7	42.3	40.0	34.6
28.5	50.5	48.4	46.3	44.2	38.9
33.2	53.3	51.4	49.6	47.5	42.3
38.0	55.2	53.6	52.0	50.1	45.2
42.7	56.8	55.4	53.8	52.1	47.2
47.4	58.0	56.8	55.3	53.7	49.0

Table 5 (continued)

n = 1005 ppm Mn

H^a(kG)	M^b (10^{-3} emu gauss/gram)			
T(K)	1.24	1.62	1.98	2.33
2.37	30.1	25.8	22.9	19.2
4.74	49.5	44.5	41.3	35.9
7.12	63.6	58.6	54.9	49.3
9.49	74.9	70.1	65.7	60.0
14.2	90.3	86.2	81.9	76.9
19.0	100	97.1	93.2	88.7
23.7	107	104	101	97.3
28.5	112	110	107	103
33.2	115	114	111	108
38.0	118	116	114	112
42.7	119	119	117	115
47.4	121	120	118	117

H^a(kG)				
T(K)	2.58	2.96	3.37	3.75
2.37	18.4	15.7	13.7	12.8
4.74	34.4	30.1	27.0	24.8
7.12	47.2	42.4	38.6	35.8
9.49	57.6	52.6	48.7	45.5
14.2	74.2	68.9	64.5	61.2
19.0	86.2	81.1	76.9	74.0
23.7	94.8	90.3	86.5	83.7
28.5	101	97.2	93.8	91.5
33.2	106	103	99.5	97.5
38.0	110	107	104	103
42.7	113	110	108	107
47.4	115	113	111	110

Table 5 (continued)

n = 1005 ppm Mn

H^a(kG)		M^b (10^{-3} emu gauss/gram)	
T(K)	4.28	5.47	7.90
2.37	11.2	8.83	5.78
4.74	21.9	17.5	11.6
7.12	31.8	25.8	17.5
9.49	40.9	33.5	23.0
14.2	55.6	47.4	33.5
19.0	68.1	58.8	42.9
23.7	78.1	68.7	51.6
28.5	85.8	76.9	59.0
33.2	92.3	83.6	65.9
38.0	97.4	89.4	72.0
42.7	101	94.2	77.5
47.4	104	98.5	82.3

n = 2110 ppm Mn

H^a(kG)		M^b (10^{-3} emu gauss/gram)		
T(K)	1.24	1.75	2.03	2.37
2.37	47.9	42.9	41.4	38.4
4.74	79.7	73.7	71.2	67.7
7.12	104	97.1	94.6	90.6
9.49	122	115	113	108
14.2	150	143	141	137
19.0	172	165	163	159
23.7	188	181	180	176
28.5	199	194	192	189
33.2	208	203	202	199
38.0	216	211	210	207
42.7	221	217	217	214
47.4	226	222	222	220

Table 5 (continued)

n = 2110 ppm Mn

H^a(kG)	M^b (10^{-3} emu gauss/gram)			
T(K)	2.72	3.08	3.47	3.84
2.37	35.4	31.4	28.4	26.4
4.74	63.7	58.2	53.7	50.2
7.12	86.6	80.1	75.1	70.6
9.49	104	97.9	92.9	87.9
14.2	132	126	121	
19.0	165	148	142	137
23.7	172	165	160	155
28.5	185	179	174	170
33.2	196	190	186	182
38.0	205	199	196	192
42.7	212	206	204	200
47.4	218	212	210	207

H^a(kG)			
T(K)	4.25	5.47	7.90
2.37	22.9	18.9	13.1
4.74	45.2	37.2	25.7
7.12	65.1	54.1	38.0
9.49	81.9	69.9	49.4
14.2	109		70.6
19.0	132	116	88.8
23.7	150	134	104
28.5	163	150	119
33.2	175	163	132
38.0	186	174	144
42.7	195	183	155
47.4	202	192	163

Table 5 (continued)

a) Magnetic fields are accurate to within 1%.

b) Magnetization results are accurate to within 2%. The values of M listed in this table are the impurity contribution , corrected for the contribution of the pure Au host (see Table 4, Note b).

FIG. 5

Impurity magnetization M as a function of H/T for six AuMn alloys (54, 105, 216, 521, 1005 and 2110 ppm Mn), for several temperatures T and for H up to 47.45 kG. Also shown as the solid curves are the free-spin Brillouin functions $B_S(H/T)$, calculated using the spins S listed in the last column of Table 3 for the appropriate alloy concentrations.

FIG 5-1

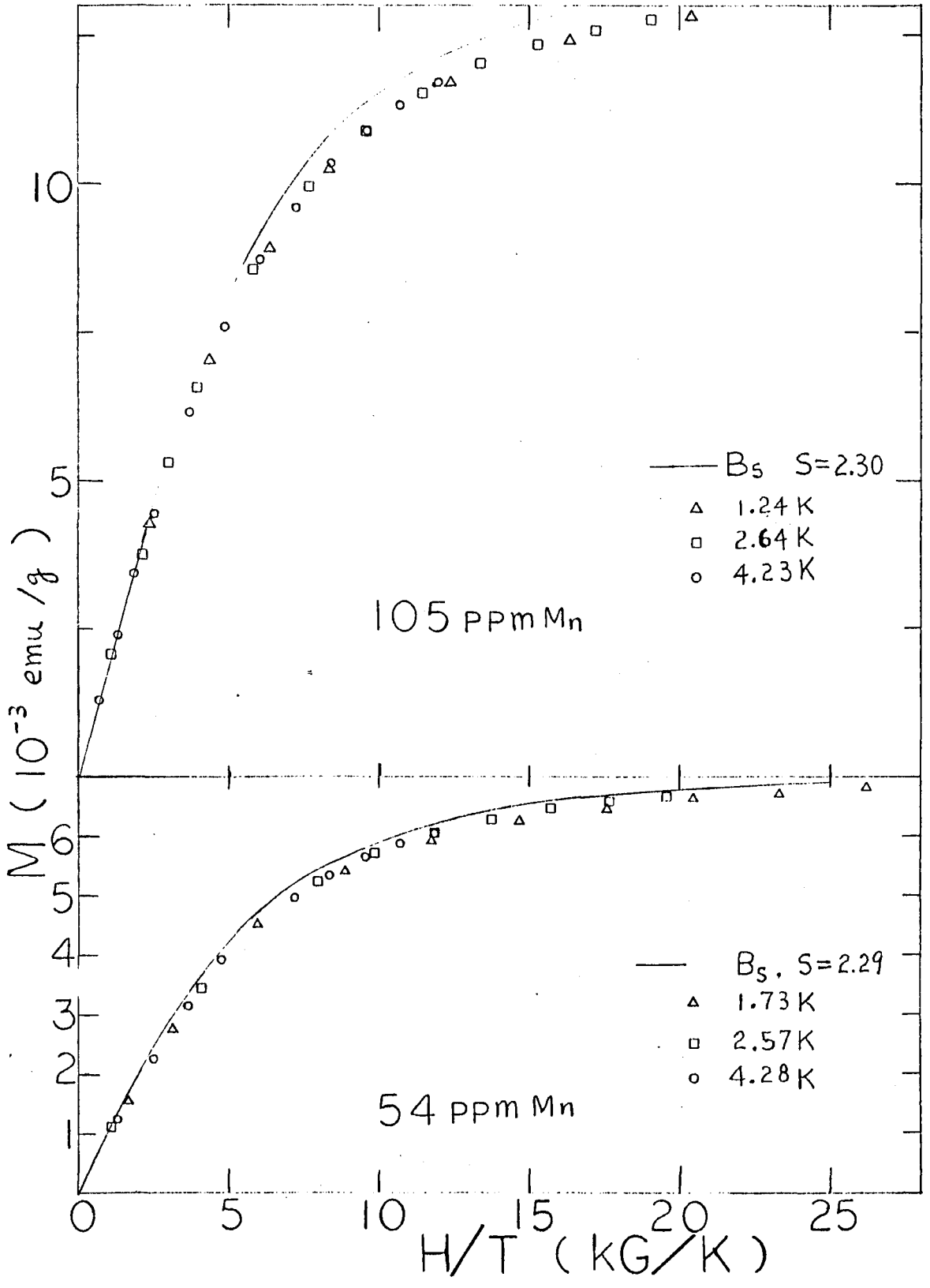
10
5
6
5
4
3
2
1
0
5
10
15
20
25
M (10^{-3} emu / g)
H/T (kG/K)
B_S S=2.30
1.24 K
2.64 K
4.23 K
105 ppm Mn
B_S, S=2.29
1.73 K
2.57 K
4.28 K
54 ppm Mn

FIG. 5-2

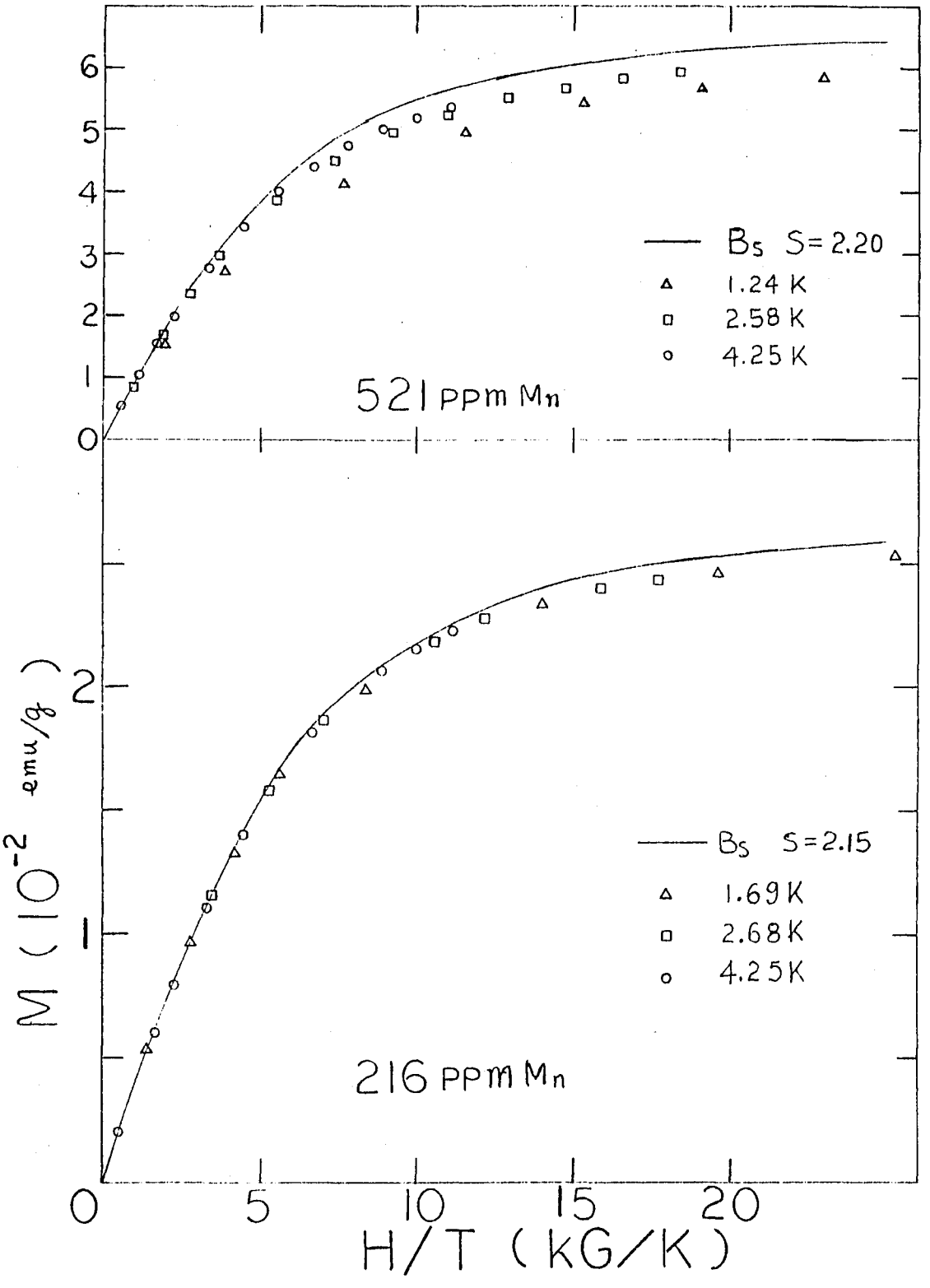
6
5
4
3
2
1
0
B_S S=2.20
1.24 K
2.58 K
4.25 K
521 ppm Mn
2
1
0
B_S S=2.15
1.69 K
2.68 K
4.25 K
216 ppm Mn
M (10^{-2} emu/g)
0
5
10
15
20
H/T (kG/K)

FIG. 5-3

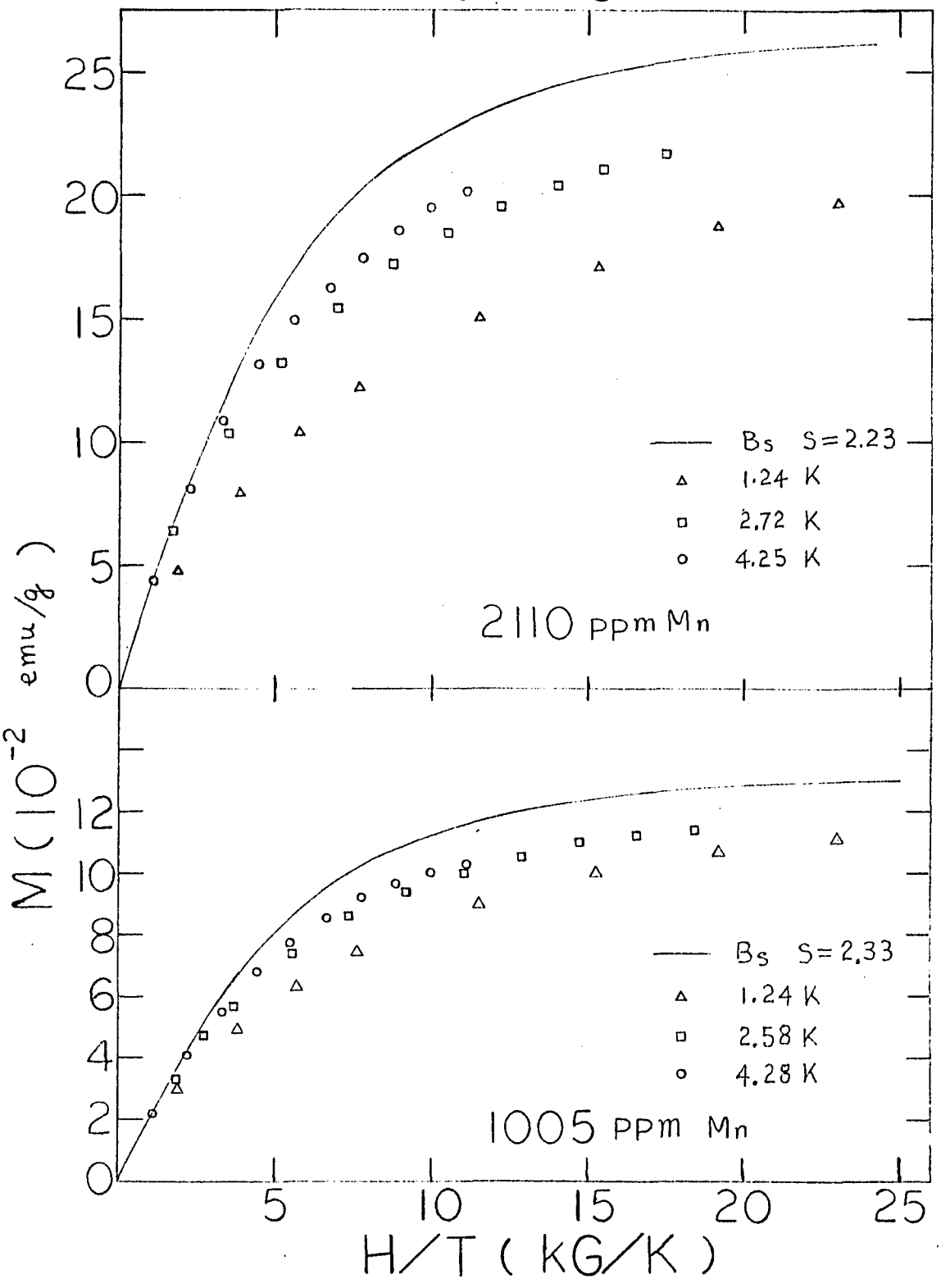
M (10^-2 emu/g)
H/T (kG/K)
Bs S=2.23
1.24 K
2.72 K
4.25 K
2110 ppm Mn
Bs S=2.33
1.24 K
2.58 K
4.28 K
1005 ppm Mn

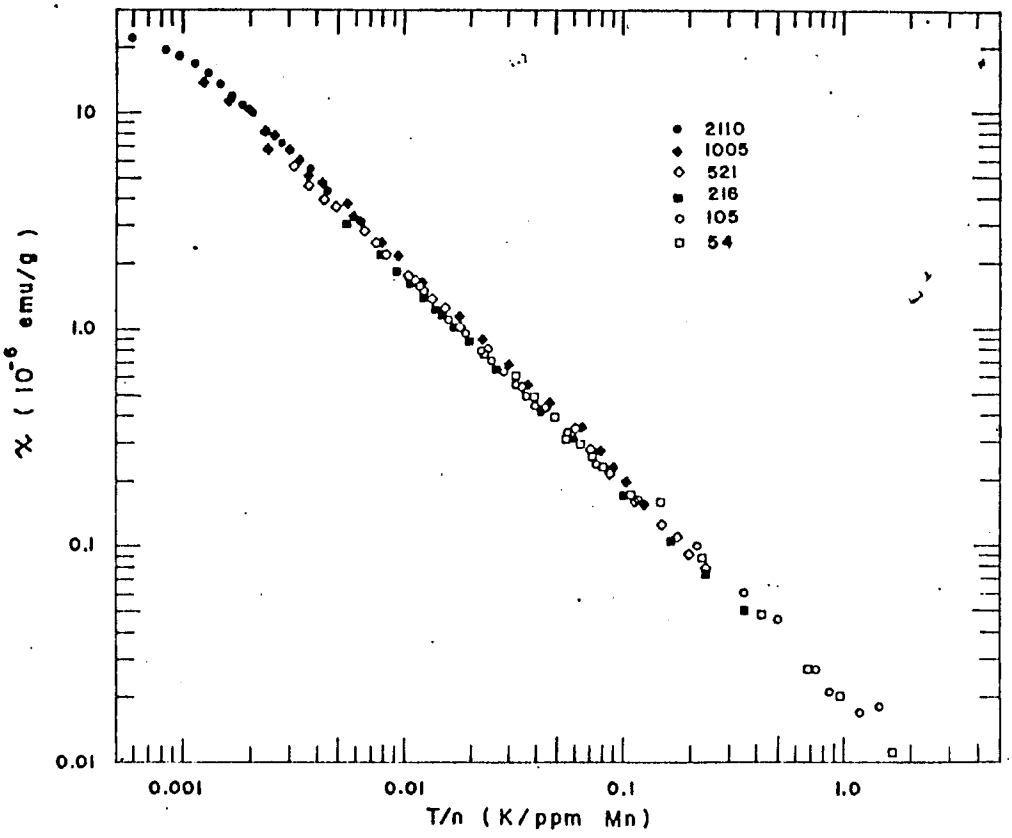

FIG. 6

Magnetic susceptibility $\chi(H \to 0)$ for six AuMn alloys (54, 105, 216, 521, 1005, 2110 ppm Mn) as a function of "reduced temperature" T/n. For clarity, overlapping data points have been omitted.

FIG. 7

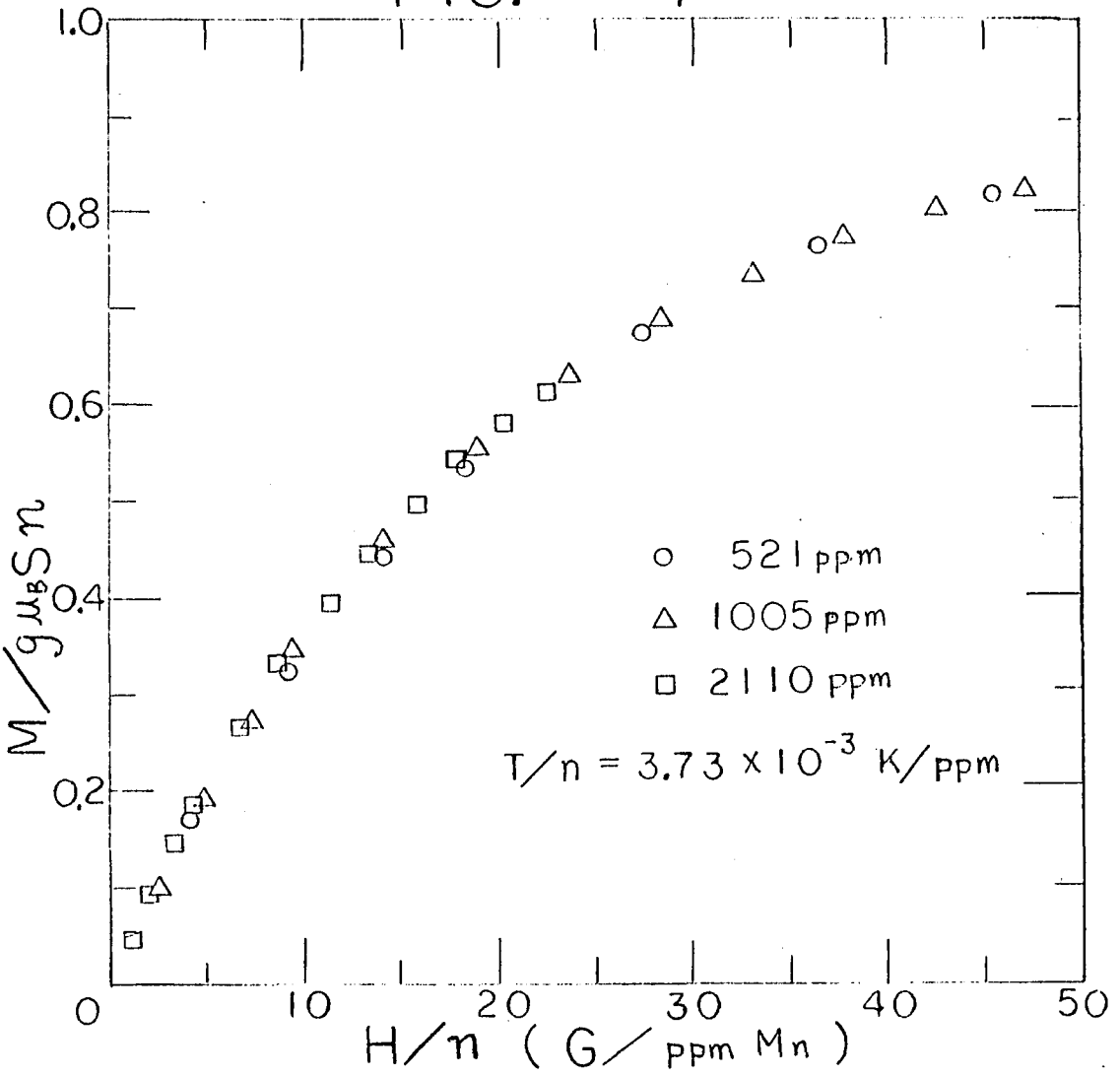

FIG. 7

Impurity magnetization M divided by M_{sat} = $g \mu_B Sn$ as a function of H/n at the "reduced temperature" $T/n = (3.73 \pm 0.01) \times 10^{-3}$ K/(ppm Mn). For n = 521, 1005, 2110 ppm Mn, the corresponding temperatures are T = 1.94, 3.75, 7.90 K, respectively.

K/ppm Mn. For a discussion of how M_{sat} was obtained, see below. The data superpose quite well on a single curve.

4. Strength of the RKKY interaction for AuMn.

To obtain the value of V_o, the values of M/M_{sat} were plotted as a function of n for T = (1.69 ± 0.06)K and (3.83 ± 0.04)K in a field of 47.45 kG in Fig. 8. According to Larkin et al.,[10]

$$m = \frac{M}{M_{sat}} = 1 - \frac{2\,(2S + 1)\,nV_o}{3g\mu_B H} \qquad (1)$$

Then $\Delta m/\Delta n = -BV_o/H$ where $B = 2\,(2S + 1)/3g\mu_B$. The initial linear decrease in M/M_{sat} as a function of n yields BV_o/H, and so V_o can be determined. From the slope at T = 3.83K, V_o is found to be $(2.1 \pm 0.3) \times 10^{-37}$ erg cm^3 while at T = 1.69K, V_o is found to be equal to $(2.7 \pm 0.3) \times 10^{-37}$ erg cm^3. In both cases g = 2 and S = 2.25 have been used in order to calculate B. The average value obtained is $V_o = (2.4 \pm 0.3) \times 10^{-37}$ erg cm^3. Also shown in Fig. 8 are the values of Brillouin functions for S = 2.25, g = 2, and the appropriate H and T. The linear extrapolations of M/M_{sat} to n = 0 fall about 1-2 % below these free spin predictions at both temperatures.

An alternative method of obtaining V_o from the magnetization data is to examine the approach to saturation of M. This is shown in Fig. 9, where M is plotted as a function of H^{-1} for the 521, 1005, 2110 ppm Mn samples. The

FIG. 8

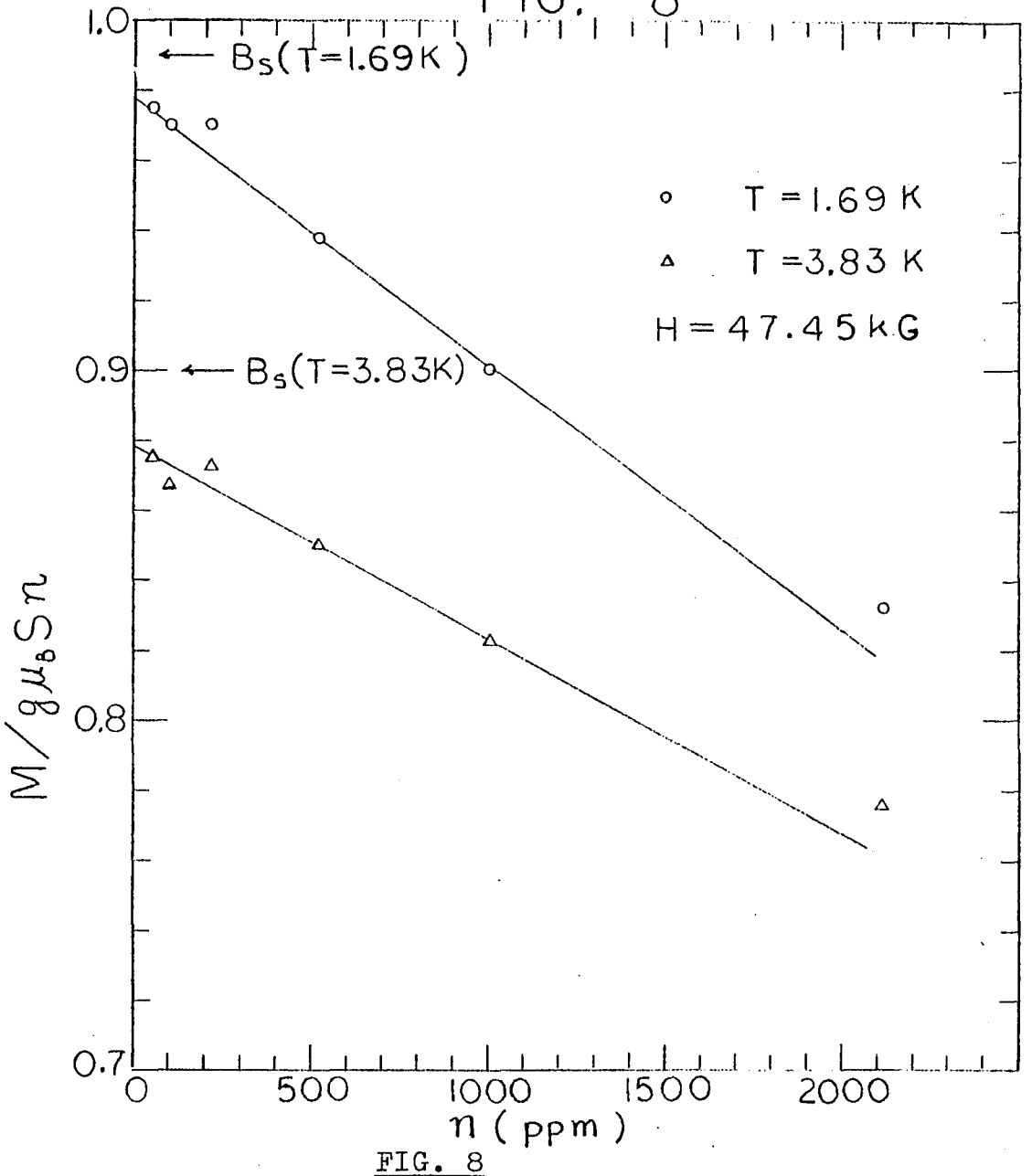

FIG. 8

Impurity magnetization M, normalized to $g\mu_B Sn = M_{sat}$, as a function Mn concentration n in a magnetic field H = 47.45 kG and at T = 1.69 and 3.83 K. Also indicated are the values of the free-spin Brillouin functions $B_S(H/T)$ for S = 2.25 at the appropriate H and T.

slope of M vs. H^{-1} is temperature-dependent and can be represented by the following expression:

$$M = g\mu_B Sn \left[1 - H_o(n,T)/H\right] \qquad (2)$$

where $H_o(n,T) = Ak_BT + BnV_o$. By comparison with Eq. (1), B can be identified with $2(2S + 1)/3g\mu_B$. By using the slope $\Delta M/\Delta(H)^{-1}$ from Fig. 9, H_o can be calculated from $H_o = \Delta M/\Delta(H)^{-1}/g\mu_B Sn$, where $M_{sat} = g\mu_B sn$ was obtained from the $(H)^{-1} \longrightarrow 0$ intercept of M. In Fig. 10, $H_o(n,T)/n$ is plotted as a function of T/n. Since $H_o(n,T)/n = Ak_BT/n + BV_o$, the straight line drawn through the data points has an intercept at T/n = 0 equal to BV_o and slope equal to Ak_B. The value of V_o thus obtained is $V_o = (2.4 \pm 0.2) \times 10^{-37}$ erg cm^3, using g = 2, S = 2.25 and $B = 2(2S+1)/3g\mu_B$. This value of V_o is identical with that found from the dependence of M/M_{sat} on n at fixed T and H. From the slope of the straight line, the value of Ak_B is found to be $(1.23 \pm 0.2) \times 10^3$ G/K. The data plotted in Fig. 9 for the 521 ppm Mn sample can not be represented by Eq. (2), due to a more rapid approach to saturation than H^{-1}. The same is also true for the three lower concentration samples.

C. AuFe.

1. The susceptibility of AuFe.

The susceptibility of the AuFe samples with concentra-

FIG. 9

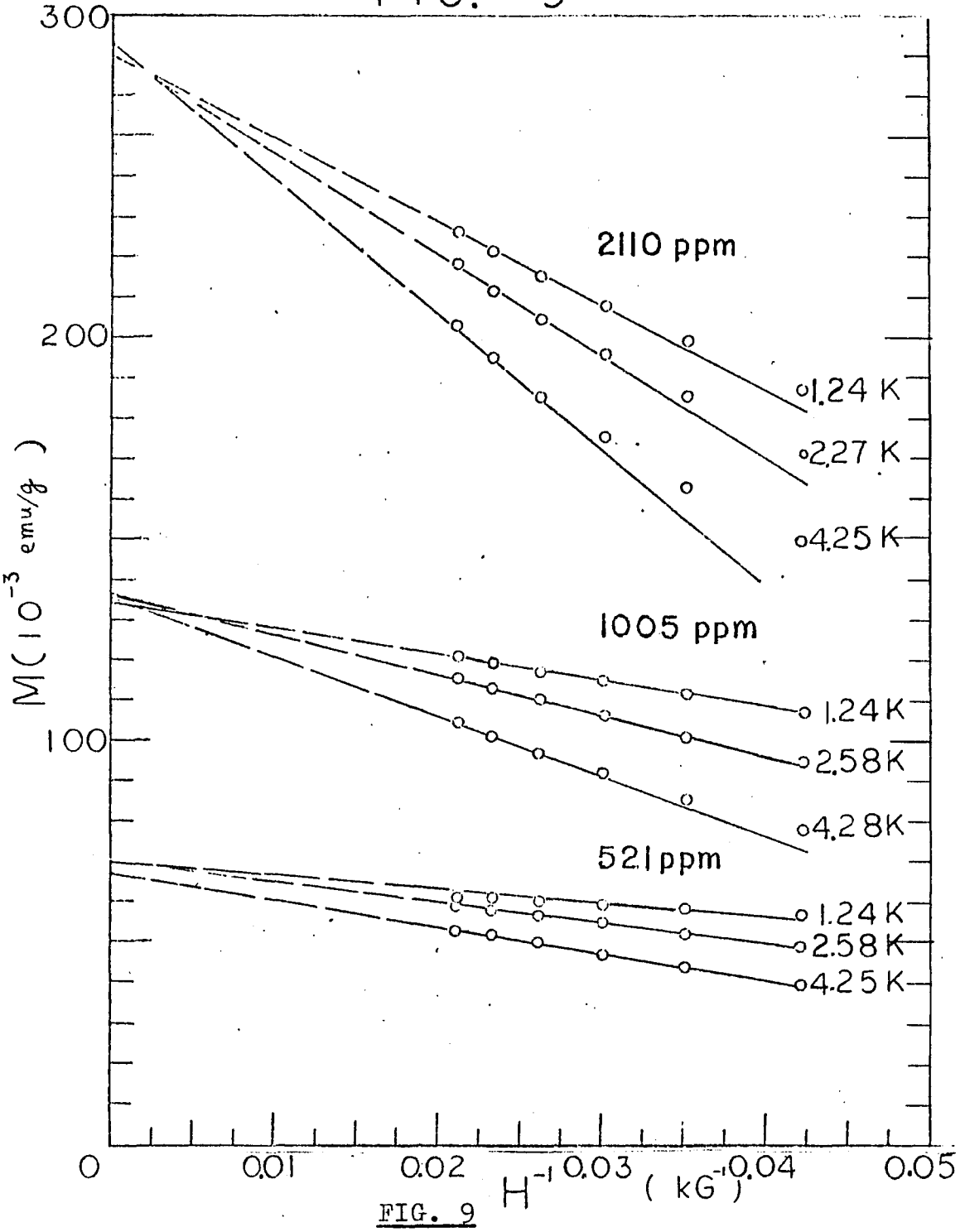

FIG. 9

Impurity magnetization M for the 521, 1005, and 2110 ppm Mn alloys as a function of the inverse of the magnetic field 1/H for several temperatures.

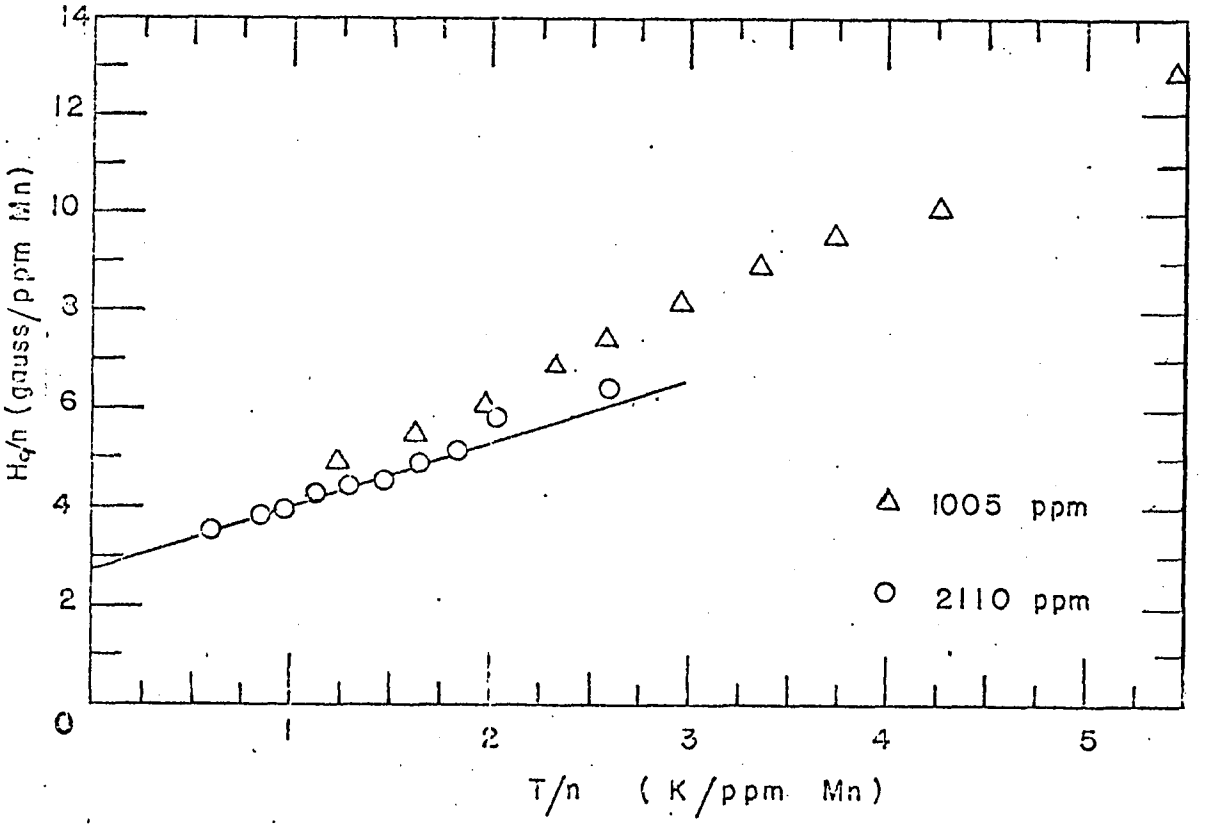

FIG. 10

$H_o(n,T)/n$ as a function of the "reduced temperature" T/n for the 1005 and 2110 ppm Mn alloys. The straight line indicates the fit to the equation $H_o/n=Ak_BT/n+BV_o$ for the 2110 ppm Mn data. See Eq. (2) for the definition of H_o.

tions 18, 42, 94, 169, 242, 572, 1160, 2225 and 6050 ppm Fe were determined graphically from the slope of M vs. H as $H \longrightarrow 0$, for temperatures from 1.25K to 100K. The impurity susceptibility data obtained by subtracting χ of pure Au from the measured total susceptibility are listed in Table 6. The χ_{Au} was determined by plotting the measured total susceptibility as a function of 1/T and extrapolating to 1/T = 0, with the extrapolation point taken to be χ_{Au}. The values of χ_{Au} are also listed in Table 6. The results for $\chi(T)$ for each alloy have been least-square-fitted to a Curie-Weiss law $\chi(T) = C/(T+\theta)$, with the resulting values of C and θ listed in Table 7. From the measured values of C and n, the spin S for each concentration can then be determined and these values are also listed in Table 7. The values of spin obtained from M_{sat} are also listed in Table 7. In Fig. 11, χ^{-1} is plotted as a function of T for all the alloys.

2. The magnetization of AuFe.

The impurity magnetization data for all nine AuFe samples are listed in Table 8, and are plotted as a function of H/T for three different temperatures each in Fig. 12. Also shown in the graphs are Brillouin functions for the appropriate Fe spin S taken from Table 7. For all the

Table 6

Magnetic Susceptibility of AuFe Alloys.

Au + n-ppm Fe	T[a] (K)	χ[b] (10^{-6} emu/g)	Au + n-ppm Fe	T[a] (K)	χ[b] (10^{-6} emu/g)
n = 18	1.25	0.0790	n = 18	4.28	0.0305
	1.75	0.0641		5.19	0.0247
	2.00	0.0561		5.64	0.0230
	2.28	0.0508		6.30	0.0212
	2.67	0.0437		6.99	0.0185
	3.02	0.0402		7.89	0.0167
	3.37	0.0380		9.46	0.0141
	3.67	0.0353		12.3	0.0110
n = 42	1.25	0.148	n = 42	6.30	0.0436
	1.70	0.113		6.99	0.0410
	2.00	0.102		7.89	0.0376
	2.28	0.0919		9.46	0.0324
	2.67	0.0815		12.3	0.0282
	3.02	0.0737		18.1	0.0238
	3.43	0.0660		22.7	0.0212
	3.87	0.0617		30.1	0.0186
	4.28	0.0574		39.6	0.0143
	5.19	0.0505		45.4	0.0134
	5.64	0.0488		56	0.0109
n = 94	1.25	0.272	n = 94	3.89	0.117
	1.64	0.221		4.27	0.108
	1.90	0.195		5.19	0.0897
	2.33	0.168		5.64	0.0844
	2.67	0.156		6.30	0.0769
	2.98	0.142		7.89	0.0629
	3.43	0.126		9.46	0.0548

Table 6 (continued)

Au + n-ppm Fe	T[a] (K)	χ[b] (10^{-6} emu/g)	Au + n-ppm Fe	T[a] (K)	χ[b] (10^{-6} emu/g)
n = 94	12.3	0.0414	n = 94	39.6	0.0156
	18.1	0.0285		45.4	0.0132
	22.7	0.0253		56	0.0119
	30.1	0.0199		75.2	0.0078
n = 167	1.25	0.531	n = 167	7.89	0.127
	1.67	0.430		12.3	0.0858
	1.99	0.377		18.1	0.0639
	2.37	0.325		22.7	0.0529
	2.73	0.294		30.1	0.0402
	3.12	0.268		39.6	0.0312
	3.50	0.242		45.4	0.0268
	3.90	0.225		50.8	0.0243
	4.28	0.206		56.0	0.0219
	5.19	0.179		67.5	0.0182
	5.64	0.166		75.2	0.0153
	6.30	0.153		103	0.0113
n = 242	1.25	0.700	n = 242	6.30	0.206
	1.74	0.537		7.89	0.173
	2.07	0.487		12.3	0.118
	2.33	0.448		18.1	0.0891
	2.62	0.408		22.7	0.0732
	2.99	0.377		30.1	0.0549
	3.36	0.341		39.6	0.0446
	3.81	0.312		56.0	0.0292
	4.26	0.279		75.2	0.0203
	5.19	0.242		103	0.0151
	5.64	0.226			

Table 6 (continued)

Au + n-ppm Fe	T[a] (K)	χ[b] (10^{-6} emu/g)	Au + n-ppm Fe	T[a] (K)	χ[b] (10^{-6} emu/g)
n = 572	1.25	1.72	n = 572	6.99	0.468
	1.65	1.40		7.89	0.420
	1.99	1.24		12.3	0.288
	2.37	1.09		18.1	0.210
	2.74	0.984		22.7	0.177
	3.11	0.884		30.1	0.136
	3.50	0.802		39.6	0.108
	3.95	0.738		44.4	0.0958
	4.28	0.699		56.0	0.0767
	5.19	0.592		75.2	0.0580
	5.64	0.553		104	0.0438
	6.30	0.507		151	0.0306
n = 1160	1.25	2.63	n = 1160	12.3	0.587
	1.62	2.51		18.1	0.428
	1.92	2.34		22.7	0.353
	2.37	2.09		30.1	0.278
	2.80	1.87		39.6	0.221
	3.20	1.71		45.4	0.196
	3.86	1.51		56.0	0.157
	4.28	1.38		75.2	0.116
	5.31	1.15		104	0.0890
	6.30	1.01		125	0.0755
	7.89	0.843		151	0.0628
	9.47	0.733		172	0.0543

Table 6 (continued)

Au + n-ppm Fe	T[a] (K)	χ[b] (10^{-6} emu/g)	n-ppm Fe	T[a] (K)	χ[b] (10^{-6} emu/g)
n = 2225	1.24	3.94	n = 2225	7.89	1.70
	1.78	3.77		12.3	1.17
	2.01	3.69		18.1	0.879
	2.28	3.63		22.7	0.722
	2.62	3.50		30.1	0.551
	3.04	3.34		39.6	0.453
	3.35	3.22		44.4	0.396
	3.80	2.99		56.0	0.320
	4.28	2.74		75.2	0.236
	6.30	2.07			
n = 6050	1.24	5.44	nn = 6050	9.46	4.95
	1.84	5.70		12.3	3.99
	2.13	5.82		18.1	2.92
	2.36	5.91		22.7	2.37
	2.70	6.04		30.1	1.85
	3.10	6.22		39.6	1.50
	3.42	6.30		44.4	1.35
	3.80	6.30		56.0	1.06
	4.25	6.33		75.2	0.802
	5.19	6.46		88.9	0.720
	5.64	6.58		112	0.586
	6.30	6.47		122	0.535
	6.99	6.22		151	0.457
	7.89	5.61			

Table 6 (continued)

a) Temperatures are accurate to within ± 1%.

b) Magnetic susceptibility results are estimated to be accurate to within ± 2%. The values of χ listed in this table are the impurity contribution, corrected for the contribution of the pure Au host, which is obtained by extrapolating from the plot of total susceptibility vs. 1/T to 1/T = 0. The values obtained are as follows:

n-ppm Fe	$-\chi_{Au}$ (10^{-6}emu/g)
18	0.1460
42	0.1475
94	0.1435
169	0.1435
242	0.1435
572	0.1435
1160	0.1410
2225	0.1435
6050	0.1435

FIG. 11

Inverse impurity susceptibilities χ^{-1} for nine AuFe alloys (18, 42, 94, 169, 242, 572, 1160, 2225 and 6050 ppm Fe) plotted as a function of temperature T. Error bars are estimated from the uncertainties of the magnetizations and the determinations of slope.

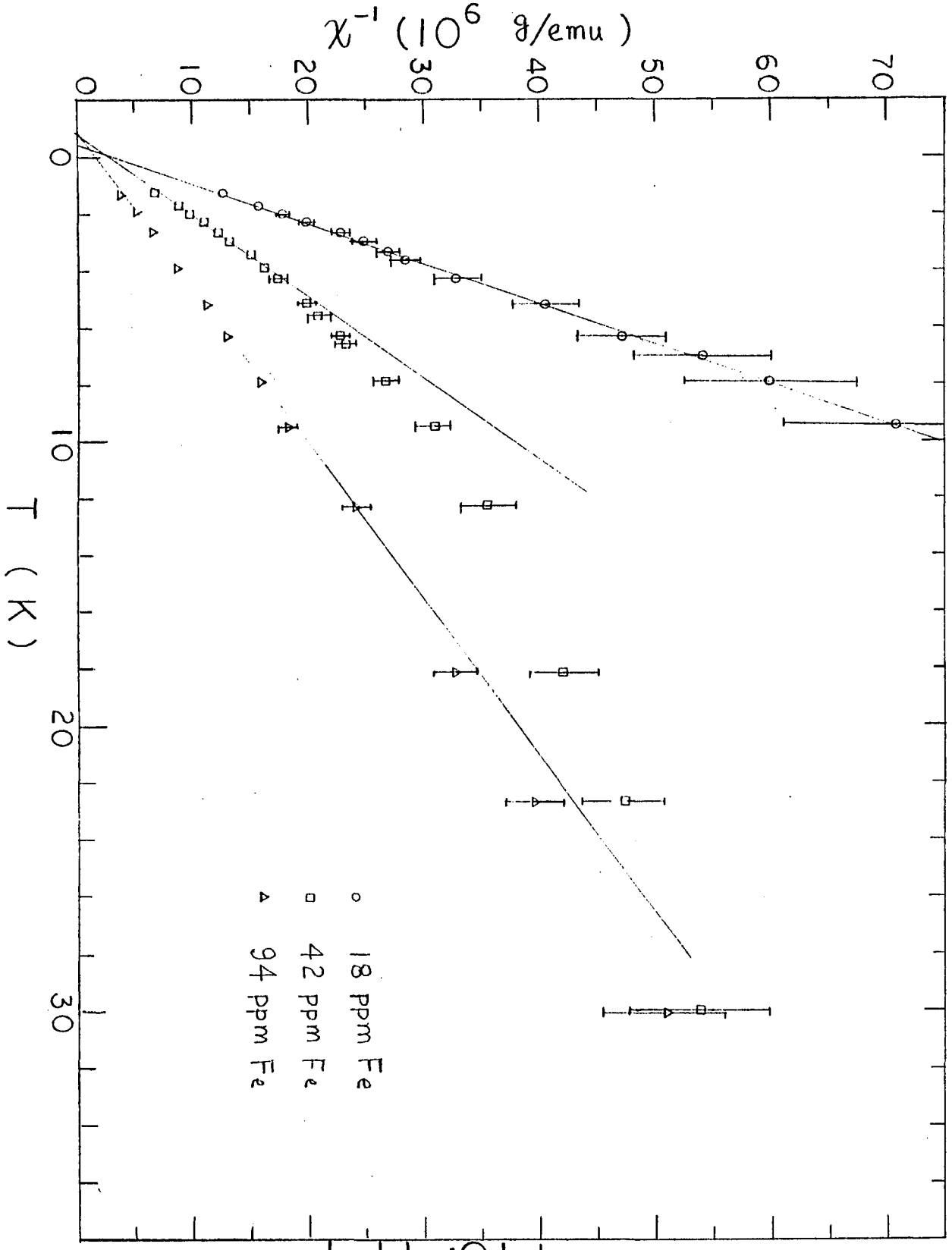
χ^{-1} (10^6 g/emu)
0
10
20
30
40
50
60
70
T (K)
0
10
20
30
18 Ppm Fe
42 Ppm Fe
94 Ppm Fe

FIG. II-1

T (K)
0
10
20
30
40
50
60
70
80
χ^{-1} (10^6 g/emu)
0
10
20
30
40
50
60
572ppm
242ppm
169ppm

FIG. II—2

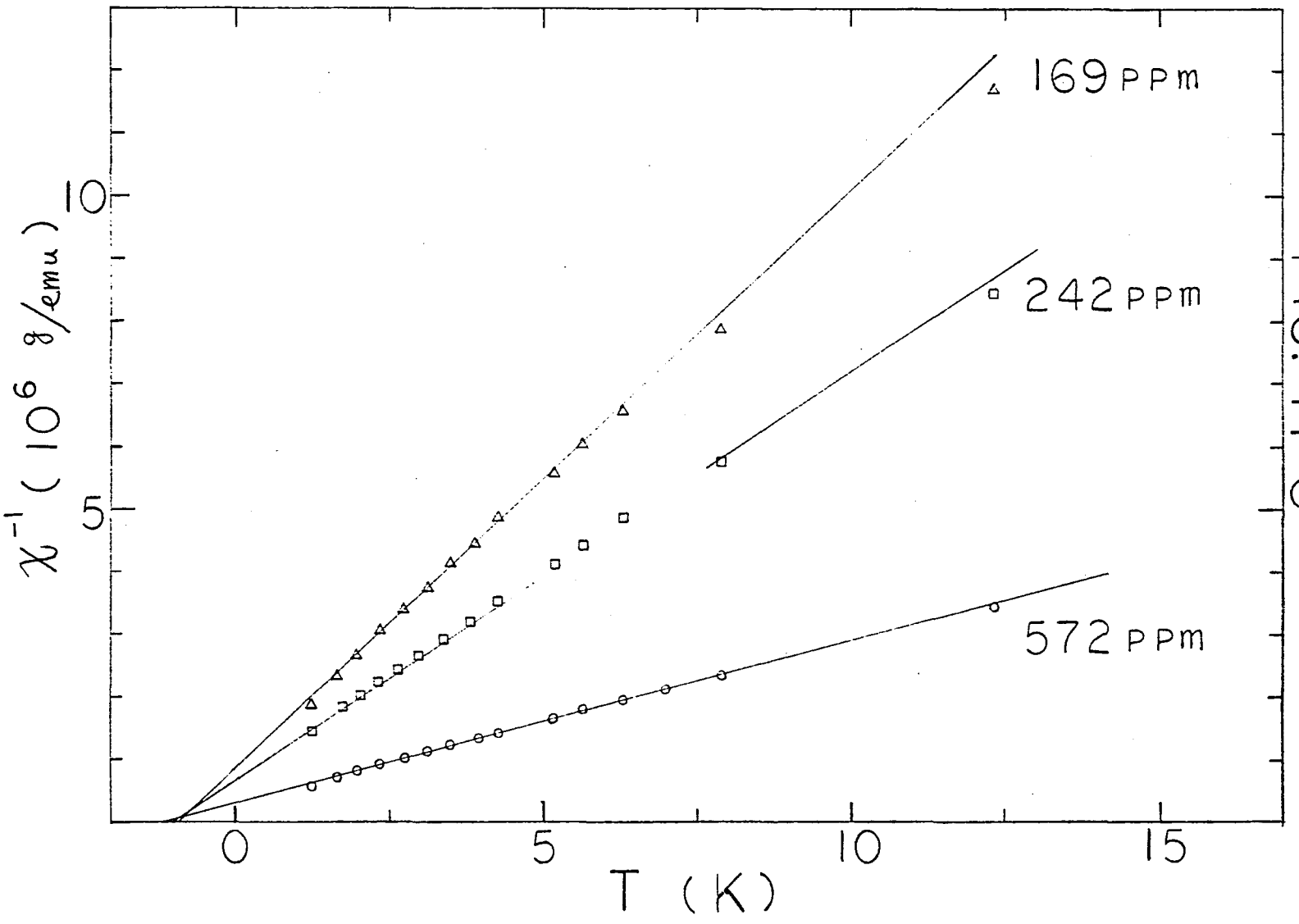

FIG. II-3

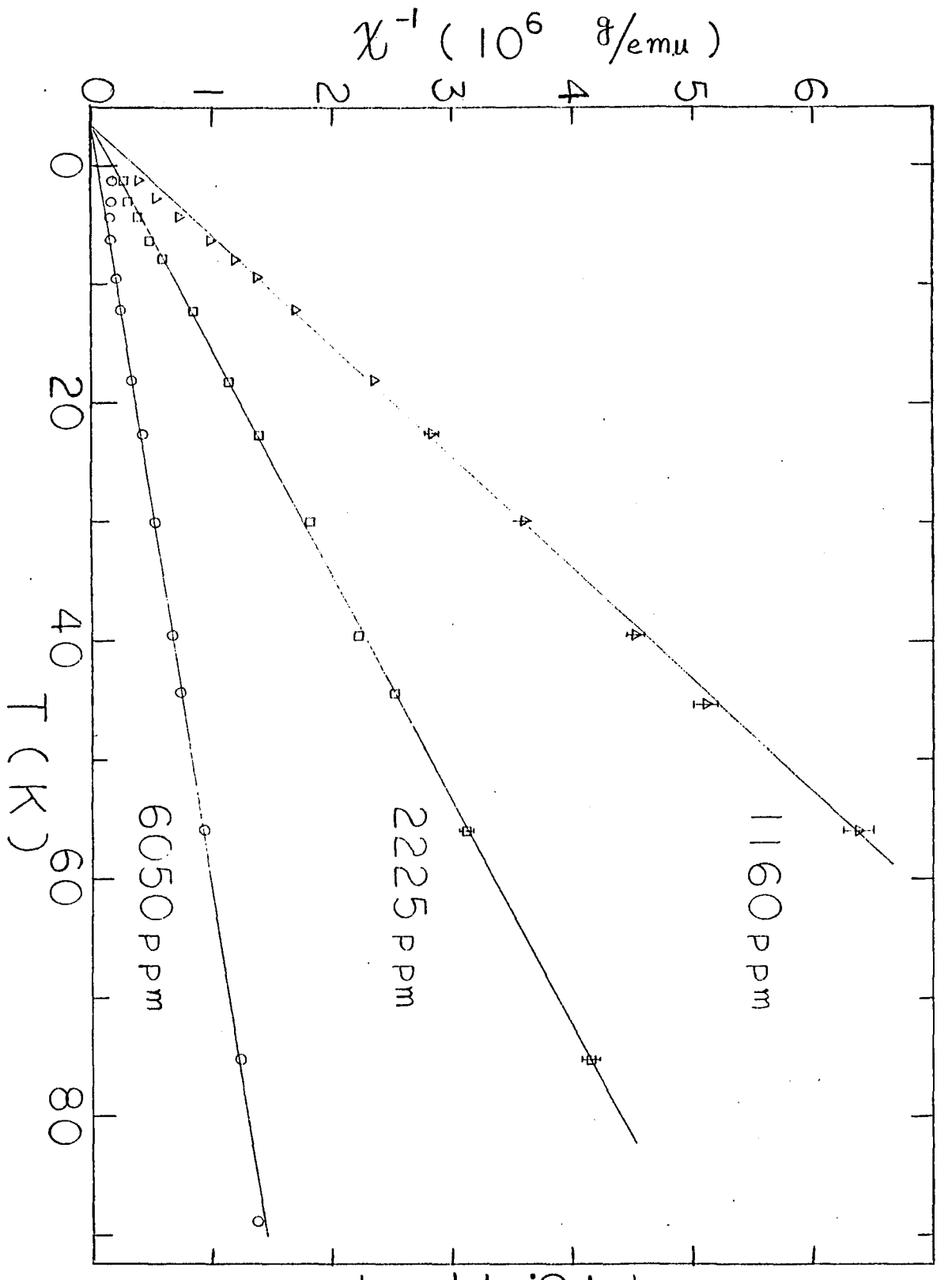
χ^{-1} (10^6 g/emu)
0
1
2
3
4
5
6
T (K)
0
20
40
60
80
1160 ppm
2225 ppm
6050 ppm

FIG. 11—4

FIG. II—5

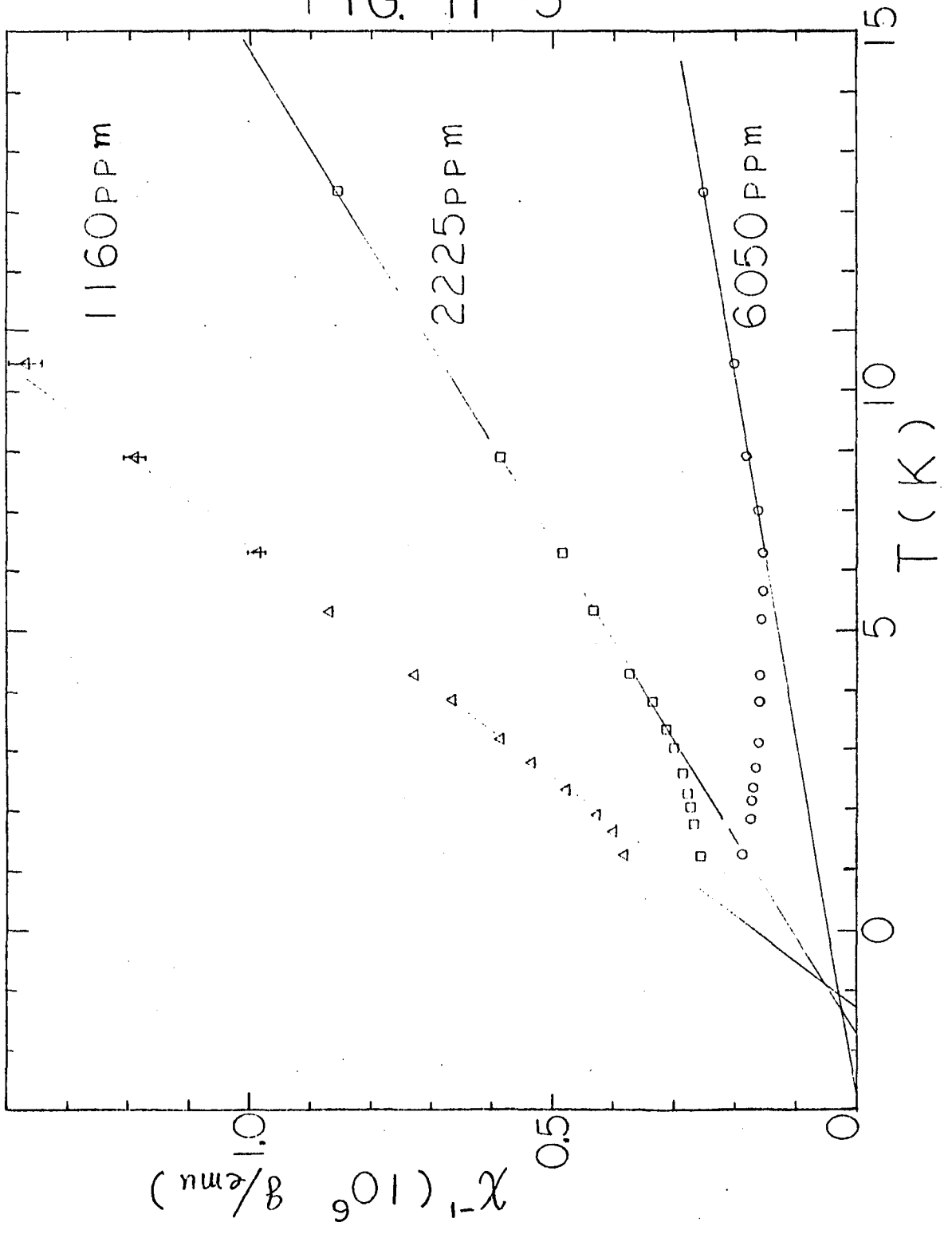

Table 7

Magnetic Properties of AuFe Alloys Studied

n (ppm Fe)	C^a ($10^{-6}\frac{emuK}{g}$)	θ^a (K)	$M_{sat}{}^b$ ($10^{-3}\frac{emuG}{g}$)	S^c	S^d	nV_o/k_B^e (K)
18 ± 1	0.140± 0.006	0.45± 0.05		1.32± 0.06		0.091± 0.012
42 ± 2	0.292± 0.020	0.8 ± 0.1	2.93± 0.05	1.23± 0.07	1.23± 0.08	0.214± 0.024
94 ± 2	0.549± 0.020	0.9 ± 0.1	5.82± 0.10	1.10± 0.03	1.09± 0.05	0.311± 0.024
169 ± 2	0.990± 0.020	0.9 ± 0.15	10.9± 0.2	1.10± 0.02	1.14± 0.04	0.324± 0.030
242 ± 16	1.51 ± 0.02	1.0 ± 0.15	15.5± 0.3	1.15± 0.05	1.13± 0.08	0.416± 0.038
572 ± 8	3.73 ± 0.04	1.1 ± 0.2	33.7± 0.7	1.18± 0.02	1.04± 0.04	0.661± 0.024
1160± 70	7.58 ± 0.10	1.25± 0.2	65.0± 2.0	1.18± 0.04	0.998± 0.061	1.05 ± 0.07
2225± 125	16.2 ± 0.5	1.7 ± 0.25		1.27± 0.05		1.17 ± 0.11
6050± 350	60.6 ± 1.2	2.7 ± 0.3		1.55± 0.06		2.66 ± 0.26

a) Measured Curie constant C and Curie-Weiss temperature θ determined from initial susceptibility data and $\chi = C/(T+\theta)$.

b) Measured saturation magnetization M_{sat} determined from magnetization data in the limit $1/H \rightarrow 0$ (see Fig. 15 and text).

Table 7 (continued)

c) Values of the spin S per Fe atom determined from the measured Curie constants $C = ng^2\mu_B{}^2S(S+1)/3k_B$, $g = 2$, and the concentrations n listed in this table.

d) Values of the spin S per Fe atom determined from the measured saturation magnetization $M_{sat} = ng\mu_B S$, $g = 2$, and the concentrations n listed in this table.

e) The strength $\frac{n V_0}{k_B}$ of the RKKY interaction determined from the limiting saturation magnetization (see Fig. 15, 16 and text).

Table 8

Impurity Magnetization Data of AuFe.

n = 18 ppm

H^a(kG)	M^b (10^{-3} emu gauss/gram)			
T(K)	2.00	2.67	3.37	4.28
2.73				0.085
5.17	0.285	0.228	0.188	0.149
7.64	0.406	0.329		0.223
10.1	0.514	0.421	0.352	0.287
15.1	0.721	0.613	0.511	0.431
20.0	0.873	0.754	0.650	0.548
24.9	0.997	0.882	0.763	0.663
29.9	1.09	0.983	0.872	0.770
34.6	1.16	1.05	0.939	0.854
39.8	1.22	1.15	1.06	0.951
44.8	1.26	1.19	1.12	1.03
49.6	1.27	1.21	1.14	1.06

n = 42 ppm

H^a(kG)				
T(K)	2.00	2.67	3.43	4.28
2.73	0.284	0.243	0.202	0.179
5.17	0.523	0.426	0.356	0.306
7.64				0.435
10.1	0.934	0.773	0.641	0.552
15.1	1.29	1.09	0.919	0.799
20.0	1.57	1.35	1.16	1.01
24.9	1.79	1.58	1.37	1.22
29.9	1.98	1.77	1.56	1.39
34.6	2.11	1.93	1.66	1.61
39.8	2.23	2.08	1.87	1.70
44.8	2.33	2.20	2.00	1.86
49.6	2.36	2.25	2.09	1.92

Table 8 (continued)

n = 94 ppm

H^a(kG)		M^b (10^{-3} emu gauss/gram)			
	T(K)	1.64	1.90	2.33	2.67
2.37		0.523	0.474	0.402	0.379
4.74		1.04	0.923	0.796	0.738
7.12		1.49	1.35	1.17	1.09
9.49		1.92	1.74	1.54	1.42
14.2		2.62	2.43	2.18	2.03
19.0		3.16	2.97	2.71	2.57
23.7		3.57	3.41	3.16	3.00
28.5		3.88	3.74	3.53	3.37
33.2		4.13	4.01	3.81	3.68
38.0		4.33	4.22	4.06	3.97
42.7		4.51	4.41	4.28	4.18
47.4		4.63	4.55	4.44	4.36

n = 94 ppm (continued)

	T(K)	2.98	3.43	3.89	4.27
2.37		0.338	0.302	0.277	0.258
4.74		0.670	0.598	0.554	0.510
7.12		0.990	0.881	0.821	0.760
9.49		1.30	1.16	1.08	1.01
14.2		1.87	1.70	1.59	1.48
19.0		2.38	2.19	2.06	1.91
23.7		2.82	2.62	2.48	2.32
28.5		3.19	3.00	2.85	2.70
33.2		3.52	3.33	3.18	3.01
38.0		3.80	3.61	3.50	3.33
42.7		4.04	3.89	3.76	3.59
47.4		4.22	4.09	3.98	3.83

Table 8 (continued)

n = 169 ppm

H^a(kG)	M[b] (10^{-3} emu gauss/gram)				
T(K)	1.25	1.67	1.99	2.37	2.73
2.37	1.25	1.02	0.900	0.782	0.694
4.74	2.42	2.01	1.79	1.54	1.40
7.12	3.44	2.89	2.60	2.28	2.07
9.49	4.28	3.68	3.35	2.97	2.71
14.2	5.59	4.99	4.63	4.17	3.85
19.0	6.57	6.02	5.66	5.18	4.84
23.7	7.29	6.81	6.48	6.03	5.67
28.5	7.83	7.43	7.13	6.71	6.37
33.2	8.24	7.90	7.66	7.26	6.96
38.0	8.57	8.28	8.08	7.73	7.45
42.7	8.82	8.59	8.43	8.10	7.85
47.4	9.03	8.84	8.70	8.40	8.20

n = 169 ppm (continued)

T(K)	3.12	3.50	3.90	4.28
2.37	0.635	0.571	0.532	0.503
4.74	1.27	1.15	1.06	0.998
7.12	1.89	1.73	1.60	1.48
9.49	2.47	2.26	2.10	1.97
14.2	3.56	3.28	3.06	2.85
19.0	4.51	4.20	3.93	3.68
23.7	5.33	5.00	4.72	4.45
28.5	6.04	5.71	5.41	5.13
33.2	6.63	6.31	6.02	5.74
38.0	7.15	6.83	6.55	6.27
42.7	7.58	7.28	7.01	6.75
47.4	7.94	7.68	7.42	7.15

Table 8 (continued)

n = 242 ppm

H^a(kG)		M^b (10^{-3} emu gauss /gram)			
	T(K)	1.24	1.78	2.12	2.34
2.37		1.55	1.20	1.11	1.03
4.74		2.97	2.39	2.20	2.03
7.12		4.22	3.50	3.20	2.98
9.49		5.30	4.48	4.15	3.84
14.2		7.00	6.18	5.76	5.41
19.0		8.29	7.52	7.11	6.75
23.7		9.29	8.59	8.23	7.87
28.5		10.1	9.48	9.13	8.83
33.2		10.7	10.2	9.92	9.62
38.0		11.3	10.8	10.6	10.3
42.7		11.7	11.4	11.1	10.9
47.4		12.2	11.8	11.6	11.4

n = 242 ppm (continued)

	T(K)	2.57	2.92	3.30	4.28
2.37		0.919	0.851	0.78	0.630
4.74		1.84	1.69	1.56	1.26
7.12		2.73	2.51	2.29	1.89
9.49		3.57	3.29	3.04	2.51
14.2		5.08	4.72	4.40	3.68
19.0		6.39	5.96	5.62	4.78
23.7		7.51	7.07	6.71	5.76
28.5		8.47	8.04	7.67	6.68
33.2		9.30	8.89	8.53	7.39
38.0		10.0	9.64	9.29	8.29
42.7		10.6	10.3	9.96	8.98
47.4		11.2	10.9	10.6	9.61

Table 8 (continued)

n = 572 ppm

H^a(kG)	M^b (10^{-3} emu gauss/gram)			
T(K)	1.25	1.65	1.99	2.37
2.37	3.79	3.28	2.88	2.54
4.74	6.93	6.19	5.55	4.97
7.12	9.44	8.63	7.91	7.17
9.49	11.7	10.7	9.95	9.10
14.2	15.2	10.8	13.4	12.5
19.0	17.9	17.0	16.2	15.3
23.7	20.1	19.2	18.5	17.6
28.5	21.9	21.1	20.4	19.5
33.2	23.6	22.6	22.0	21.2
38.0	24.6	23.9	23.4	22.6
42.7	25.6	25.0	24.5	23.8
47.4	26.5	25.9	25.5	24.9

n = 572 ppm (continued)

T(K)	2.74	3.11	3.50	3.95
2.37	2.33	2.10	1.83	1.73
4.74	4.53	4.13	3.72	3.49
7.12	5.92	6.02	5.52	4.81
9.49	8.43	7.82	7.21	6.30
14.2	11.7	10.9	10.2	9.04
19.0	14.5	13.6	12.8	11.5
23.7	16.8	16.0	15.2	13.7
28.5	18.8	17.9	17.2	15.7
33.2	20.5	19.7	18.9	17.5
38.0	22.0	21.2	20.4	19.1
42.7	23.2	22.5	21.8	20.5
47.4	24.3	23.6	22.9	21.7

Table 8 (continued)

n = 572 ppm

H^a(kG)	M^b (10^{-3} emu gauss/gram)				
T(K)	4.28	5.19	5.64	6.99	12.3
2.37	1.62	1.42	1.32	1.12	6.78
4.74	3.25	2.81	2.64	2.20	1.36
7.12	4.80	4.20	3.93	3.32	2.04
9.49	6.30	5.49	5.15	4.37	2.71
14.2	9.04	7.99	7.52	6.44	4.07
19.0	11.5	10.2	9.69	8.37	5.36
23.7	13.7	12.3	11.7	10.2	6.62
28.5	15.7	14.2	13.5	11.9	7.84
33.2	17.5	15.9	15.2	13.5	9.01
38.0	19.1	17.5	16.8	14.9	10.2
42.7	20.5	18.9	18.2	16.3	11.2
47.4	21.7	20.1	19.4	17.5	

n = 1160 ppm

T(K)	1.25	1.62	1.92	2.37	2.80
2.37	5.82	5.82	5.37	5.00	4.54
4.74	10.7	10.5	10.1	9.45	8.63
7.12	14.8	14.5	14.0	13.3	12.3
9.49	18.4	18.0	17.4	16.6	15.6
14.2	24.2	23.7	23.2	21.3	
19.0	29.2	28.6	28.0	27.0	25.9
23.7	33.4	32.7	32.2	31.1	30.1
28.5	37.0	36.3	35.8	34.7	33.7
33.2	40.0	39.5	38.9	37.9	36.9
38.0	42.8		41.7	40.7	39.8
42.7	45.2	44.7	44.1	43.2	42.4
47.4	47.5	46.8	46.5	45.6	44.5

Table 8 (continued)

n = 1160 ppm

H^a(kG)	M[b] (10^{-3} emu gauss/gram)				
T(K)	3.20	3.86	4.28	5.31	18.1
2.37	4.00	3.31	3.08	2.76	2.03
4.74	7.85	6.85	6.35	5.48	4.06
7.12	11.3	10.1	9.43	8.15	6.14
9.49	14.5	13.0	12.1	10.3	8.17
14.2	20.0	18.4	17.4	15.0	12.2
19.0	24.7	23.0	22.0	19.3	16.2
23.7	28.9	27.2	26.0	23.1	20.0
28.5	32.5	30.9	29.6	26.6	23.8
33.2	35.7	34.2	32.8	29.8	27.6
38.0	38.8	37.2	35.8	32.7	31.2
42.7	41.2	39.9	38.5	35.3	34.8
47.4	43.7	42.4	40.9	37.8	38.2

n = 2225 ppm

T(K)	1.24	1.78	2.06	2.28	2.62
2.37	8.96	8.54	8.33	8.33	8.12
4.74	16.2	15.8	15.4	15.2	14.8
7.12	22.5	21.6	21.2	21.0	20.4
9.49	27.6	26.8	26.2	26.0	25.3
14.2	36.5	35.5	34.9	34.6	34.0
19.0	43.9	42.9	42.5	41.8	41.4
23.7	50.0	48.9	48.6	48.1	47.6
28.5	55.8	55.0	54.5	53.9	53.5
33.2	60.9	60.3	59.7	59.0	58.8
38.0	65.8	65.2	64.5	64.0	63.5
42.7	72.4	69.3	69.2	68.5	67.8
47.4	74.4	73.5	73.0	72.4	71.9

Table 8 (continued)

n = 2225 ppm

H^a(kG)	M^b (10^{-3} emu gauss/gram)				
T(K)	3.04	3.35	4.28	5.31	5.83
2.37	7.70	7.69	6.44	5.81	5.60
4.74	14.2	14.1	12.2	11.2	11.0
7.12	19.9	19.7	17.6	16.4	15.7
9.49	24.8	24.7	22.4	20.9	20.3
14.2	33.4	33.4	30.6	29.2	28.1
19.0	40.7	40.6	37.8	36.5	35.3
23.7	46.6	47.1	44.6	42.9	41.7
28.5	52.4	52.7	49.7	48.2	47.2
33.2	57.7	57.7	54.8	53.6	52.3
38.0	62.4	62.4	59.7	58.5	57.0
42.7	66.8	66.9	63.9	62.8	61.6
47.4	70.8	70.9	68.0	67.1	65.9

n = 2225 ppm

T(K)	6.99	9.46	12.3	22.7
2.37	4.55	3.70	3.07	1.86
4.74	9.09	7.41	6.04	3.68
7.12	13.4	10.9	9.01	5.44
9.49	17.6	14.4	11.8	7.20
14.2	25.2	21.0	17.3	10.6
19.0	31.9	27.0	22.5	14.2
23.7	38.2	32.7	27.3	17.7
28.5	43.8	38.0	32.0	21.3
33.2	48.4	43.1	36.6	25.1
38.0	53.0	47.3	41.0	29.0
42.7	57.4	51.3	45.0	33.0
47.4	61.8	55.3	49.1	37.5

Table 8 (continued)

n = 6050 ppm

H^a(kG)	M^b (10^{-3} emu gauss/gram)				
T(K)	1.24	1.84	2.13	2.36	2.70
2.37	1.28	1.35	1.40	1.40	1.50
4.74	2.56	2.71	2.73	2.80	2.80
7.12	3.81	3.91	3.91	3.96	3.98
9.49	4.92	4.97	4.97	5.02	5.04
14.2	6.80	6.82	6.85	6.80	6.87
19.0	8.40	8.43	8.43	8.48	8.43
23.7	9.86	9.86	9.81	9.86	9.81
28.5	11.0	11.0	11.0	11.0	11.0
33.2	12.1	12.1	12.1	12.2	12.1
38.0	13.2	13.2	13.2	13.2	13.2
42.7	14.1	14.1	14.1	14.1	14.2
47.4	15.1	15.0	15.0	15.0	15.1

n = 6050 ppm

T(K)	3.10	3.42	3.80	4.25	7.89
2.37	1.48	1.50	1.52	1.50	1.35
4.74	2.85	2.85	2.85	2.80	2.51
7.12	4.06	4.03	4.01	3.96	3.57
9.49	5.09	5.07	5.04	4.97	4.53
14.2	6.92	6.87	6.85	6.77	6.21
19.0	8.48	8.43	8.38	8.33	7.64
23.7	9.86	9.77	9.72	9.67	8.98
28.5	11.1	11.0	10.9	10.9	10.1
33.2	12.2	12.1	12.1	12.0	11.2
38.0	13.3	13.2	13.1		12.3
42.7	14.3	14.2	14.1	14.0	13.2
47.4	15.1	15.1	15.0	15.0	14.1

Table 8 (continued)

a) Magnetic fields are accurate to within 1%.

b) Magnetization results are accurate to within 2%. The values of M listed in this table are the impurity concentration, corrected for the contribution of the pure Au host (see Table 6, Note b).

FIG. 12

Impurity magnetization M as a function of H/T for nine AuFe alloys (18, 42, 94, 169, 242, 572, 1160, 2225 and 6050 ppm Fe), for several temperatures T and for H up to 47.45 kG. Also shown as the solid curves are the free-spin Brillouin functions $B_S(H/T)$, calculated using the spins S listed in the fifth column of Table 7 for the appropriate alloy concentrations.

FIG. 12—1

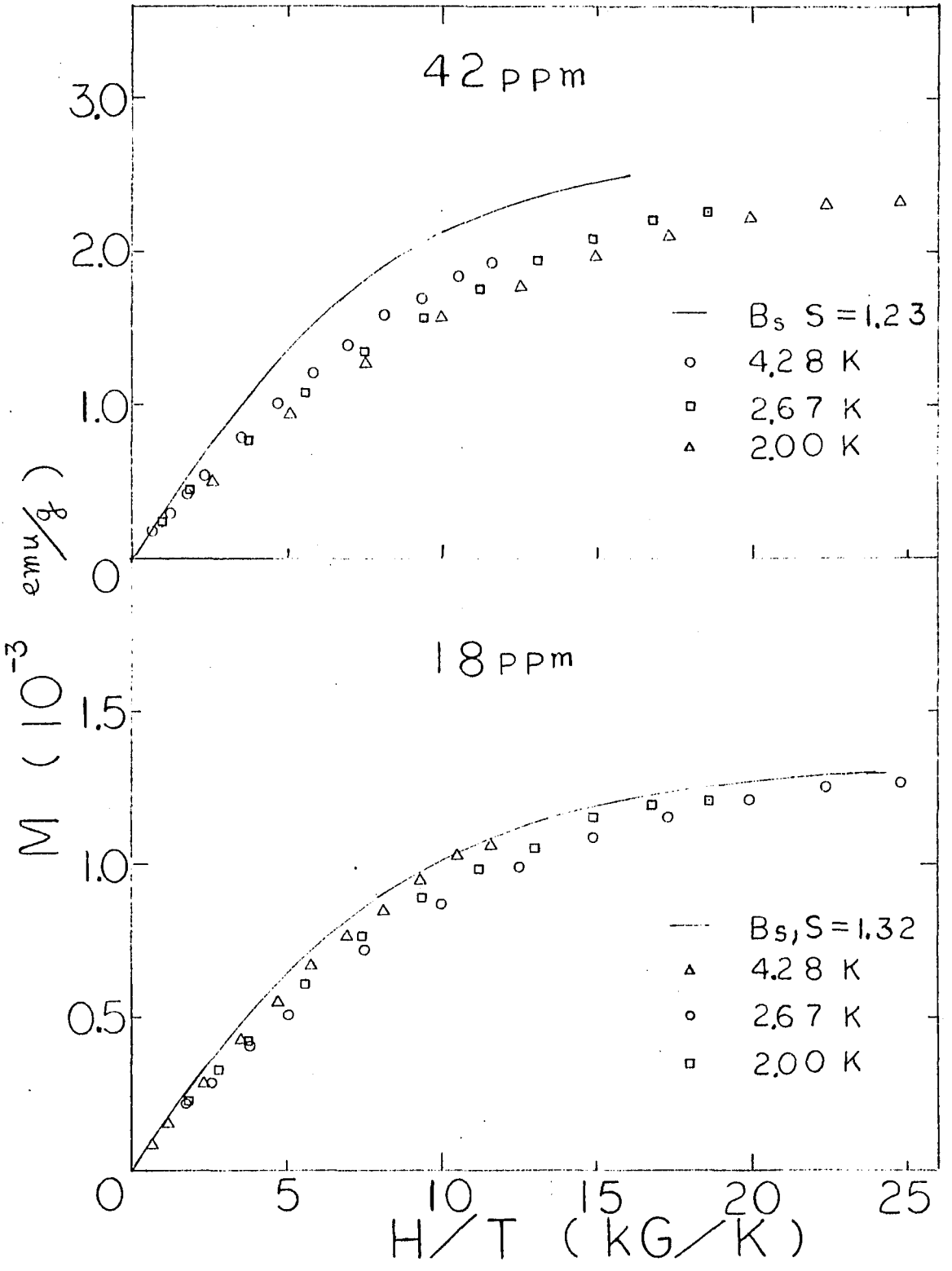
42 ppm
3.0
2.0
1.0
0
emu/g
B_S S = 1.23
4.28 K
2.67 K
2.00 K
18 ppm
M (10^{-3}
1.5
1.0
0.5
0
B_S, S = 1.32
4.28 K
2.67 K
2.00 K
5
10
15
20
25
H/T (kG/K)

FIG. 12-2

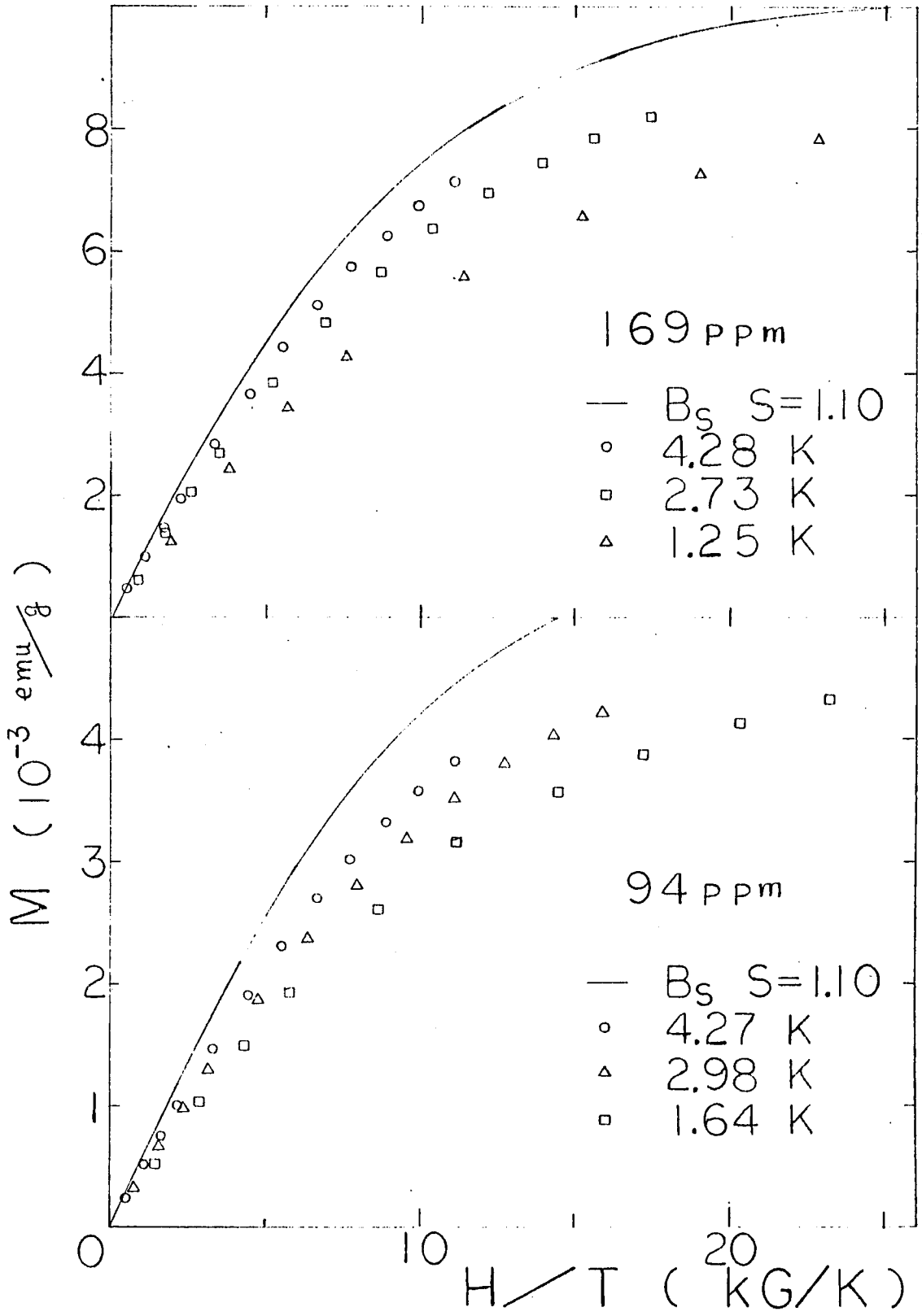
169 ppm
— B_S S=1.10
○ 4.28 K
□ 2.73 K
△ 1.25 K
94 ppm
— B_S S=1.10
○ 4.27 K
△ 2.98 K
□ 1.64 K
M (10^{-3} emu/g)
H/T (kG/K)
0
1
2
3
4
2
4
6
8
10
20

FIG. 12-3

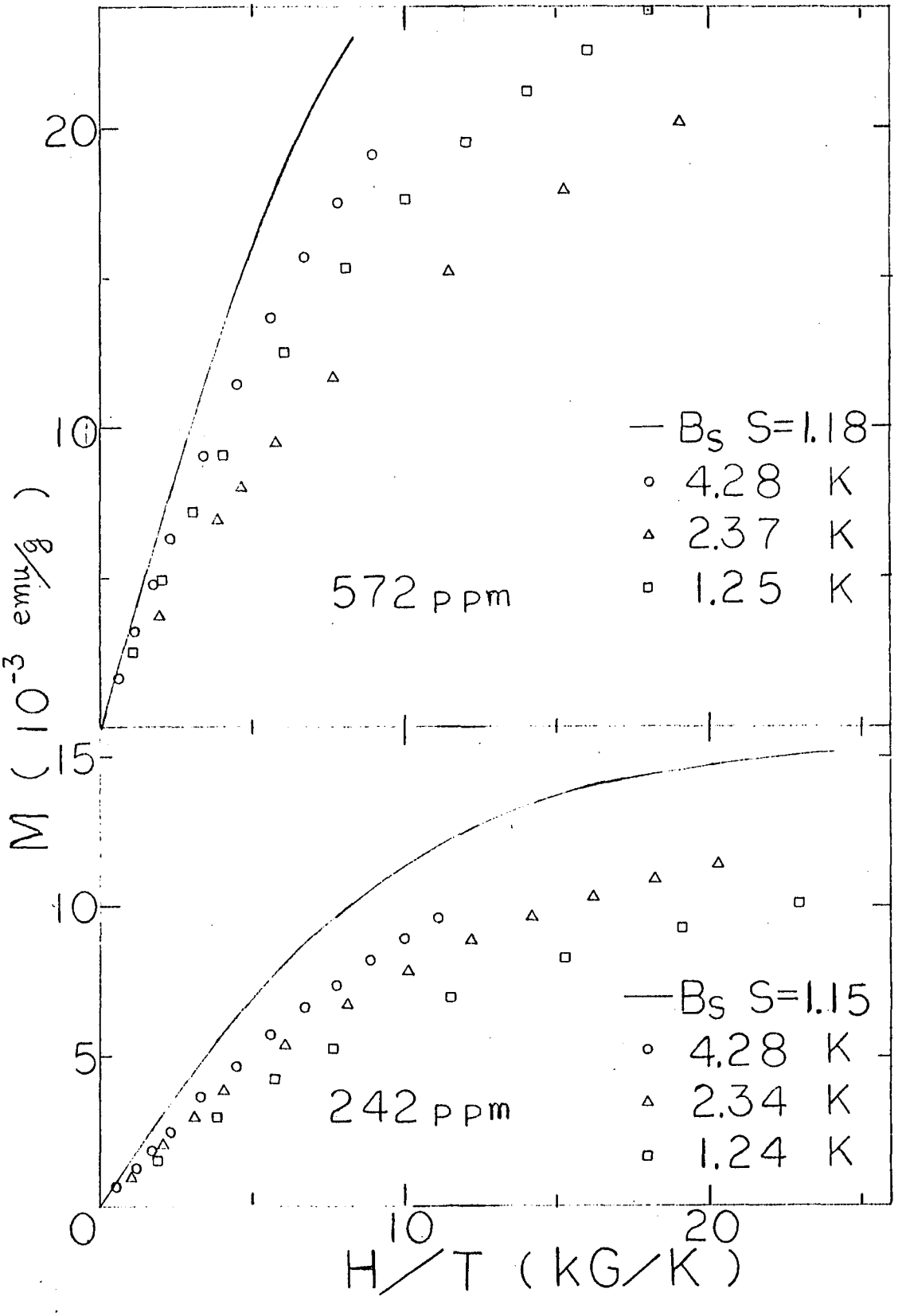
20
10
15
10
5
0
10
20
M (10^{-3} emu/g)
H / T (kG / K)
— B_S S=1.18
○ 4.28 K
△ 2.37 K
□ 1.25 K
572 ppm
— B_S S=1.15
○ 4.28 K
△ 2.34 K
□ 1.24 K
242 ppm

FIG. 12-4

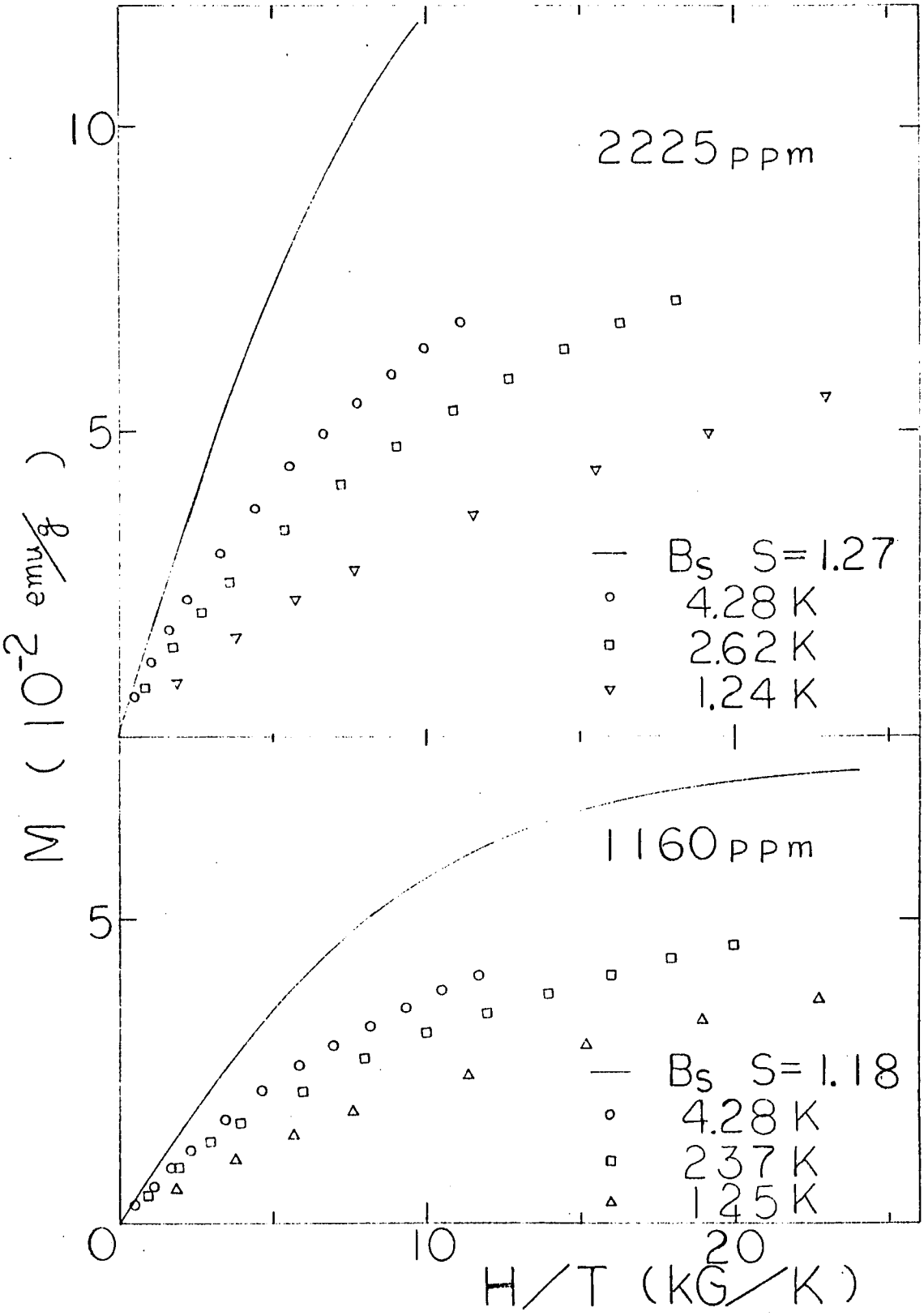
2225 ppm
— Bs S=1.27
4.28 K
2.62 K
1.24 K
1160 ppm
— Bs S=1.18
4.28 K
2.37 K
1.25 K
M (10⁻² emu/g)
H/T (kG/K)
0
5
10
20

FIG. 12-5

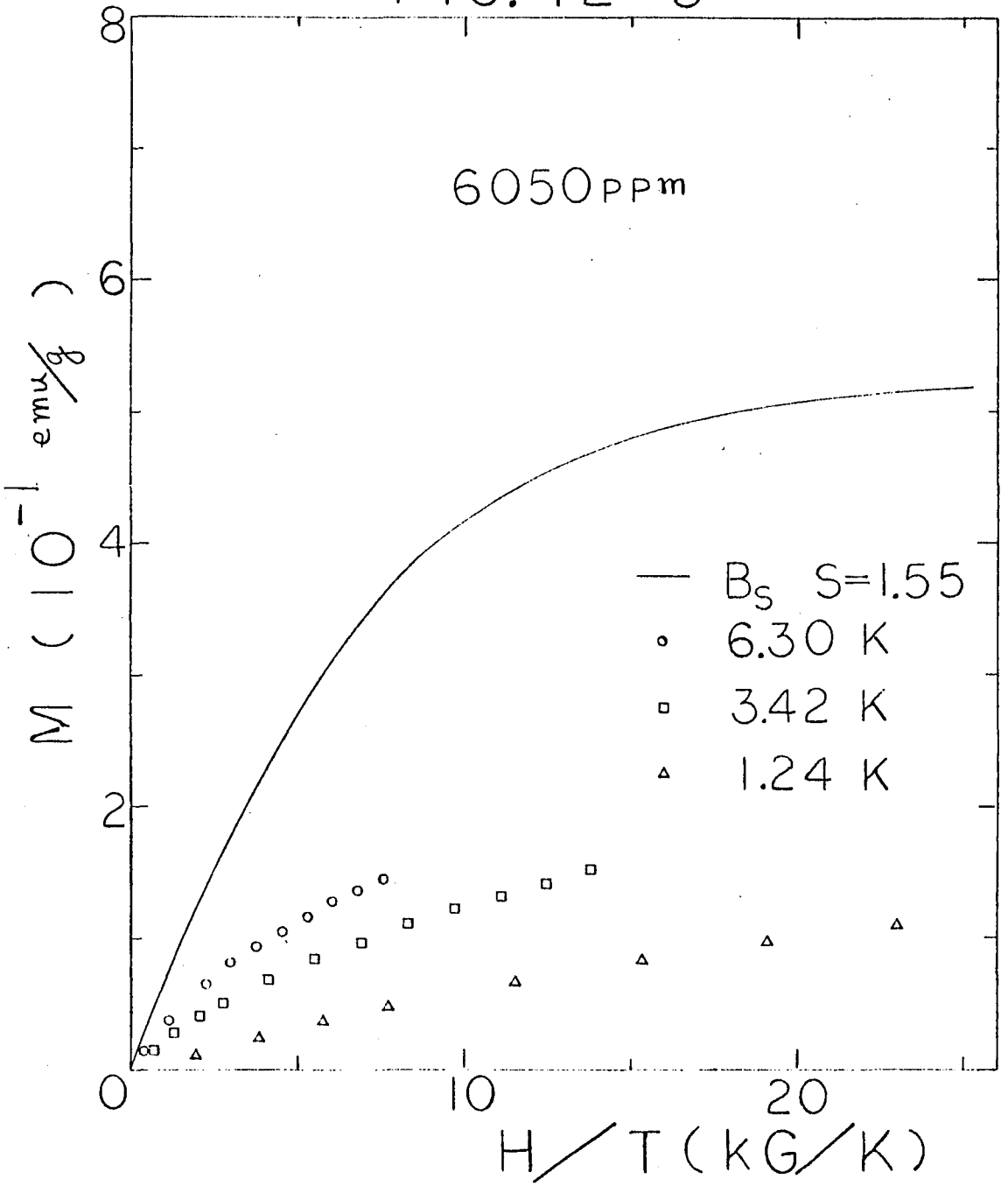

AuFe samples, the deviations from the Brillouin functions were large and the deviations increased with concentration of Fe impurity. The deviations from the Brillouin functions also increased with decreasing temperature.

3. Testing of scaling laws for AuFe.

In Fig. 13 the susceptibility χ (n,T) is plotted as a function of T/n for all the AuFe samples studied. The lack of scaling of χ with T/n is evident, in contrast to the alloy system AuMn (see Fig. 6). In Fig. 14 M/NS is plotted as a function of H/n for three alloys of concentration 572, 1060 and 2225 ppm at a fixed T/n = (2.8 $\pm$0.1) x 10^{-3} K/ppm. The lack of scaling is also quite obvious in contrast to AuMn (see Fig. 7).

4. Strength of the RKKY interaction for AuFe.

In Fig. 15, the magnetization M of six alloys is plotted vs. H^{-1}. The initial slope H_o (n,T) and limiting saturation magnetization M_{sat} can be found from the graph. As the magnetizations of the 6050 and 2225 ppm Fe samples have not approached saturation, this analysis was not possible in the available magnetic fields. This analysis was attempted for the 18 ppm sample, but was not conclusive, owing possibly to the uncertainty in pure Au magnetization, the smallness of the impurity magnetization, and the competition from single impurity effects. In Fig. 16, H_o(n,T)/n is plotted as a function of T/n for

FIG. 13

Magnetic susceptibility χ (H → 0) for nine AuFe alloys (18, 42, 94, 169, 242, 572, 1160, 2225 and 6050 ppm Fe) as a function of "reduced temperature" T/n. For clarity, overlapping data points have been omitted.

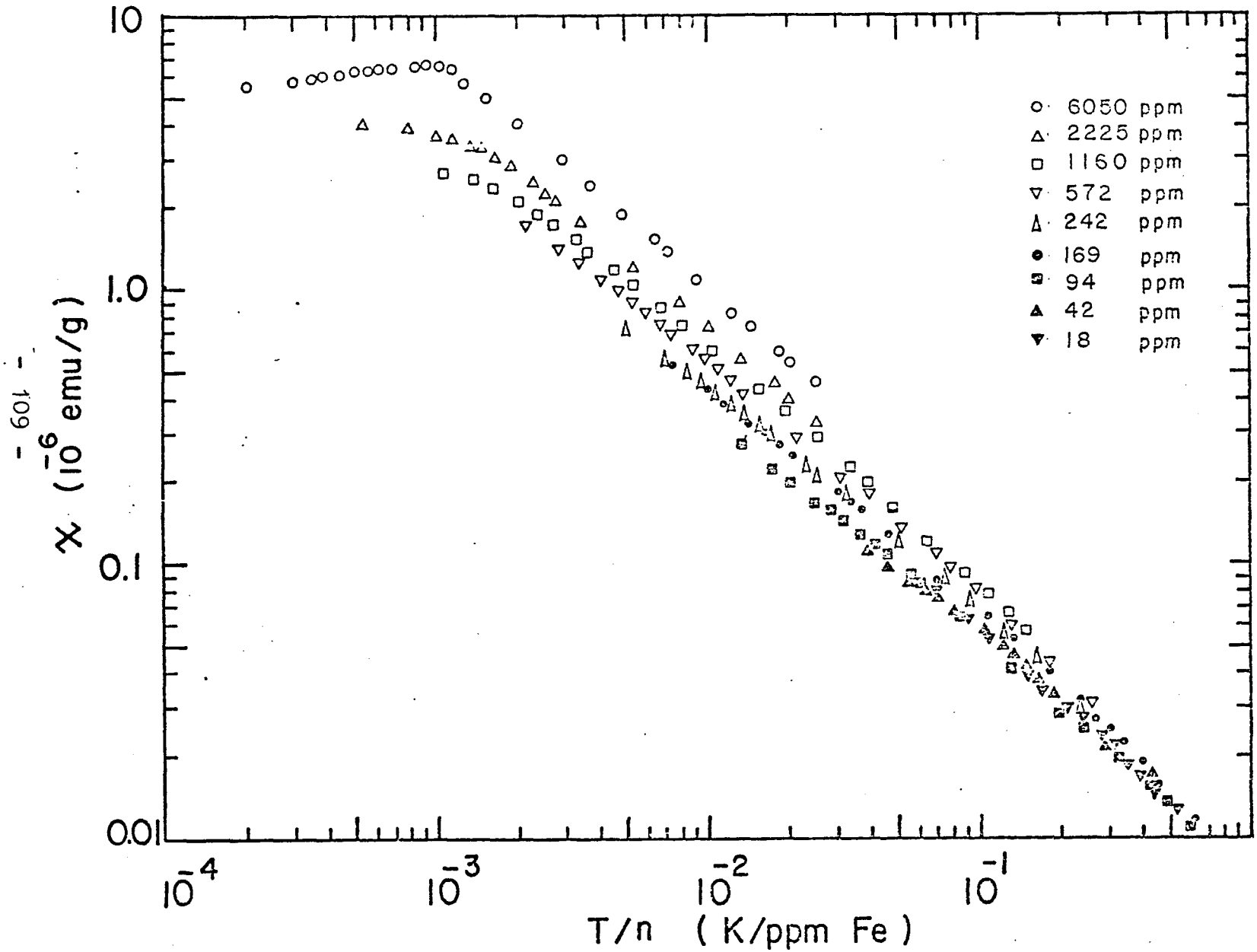
10
1.0
0.1
0.01
χ (10⁻⁶ emu/g)
10⁻⁴
10⁻³
10⁻²
10⁻¹
T/n (K/ppm Fe)
6050 ppm
2225 ppm
1160 ppm
572 ppm
242 ppm
169 ppm
94 ppm
42 ppm
18 ppm

FIG. 13

FIG. 14

Impurity magnetization M divided by concentration N and spin S as a function of H/n at the " reduced temperature" T/n = (2.81 $\pm$ 0.07)x10^{-3}K/(ppm Fe). For n = 572, 1160, 2225 ppm Fe, the corresponding temperatures are T = 1.65, 3.20, 6.30 K, respectively.

FIG. 14

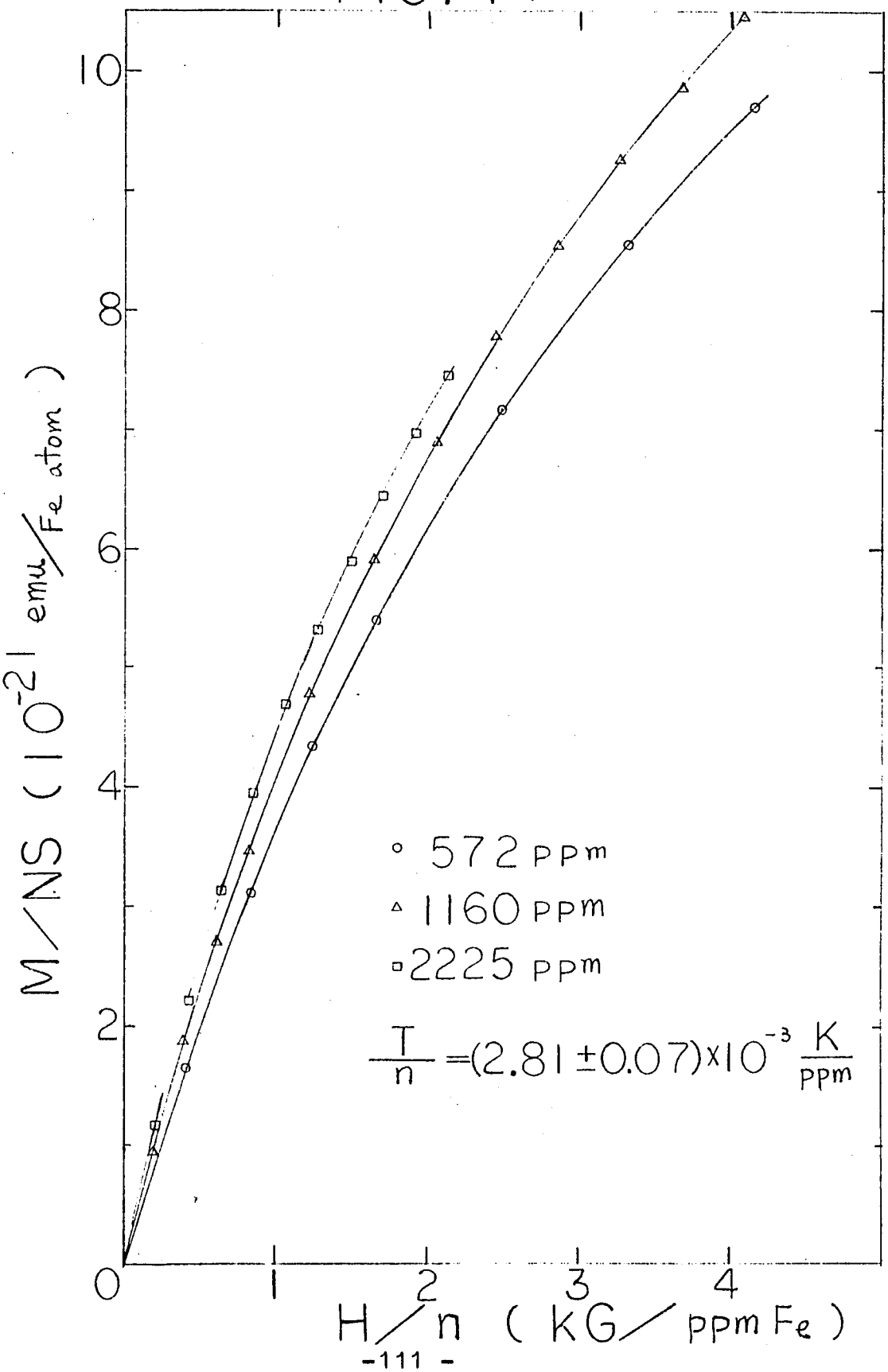
M/NS (10^{-21} emu/Fe atom)
H/n (KG/ppm Fe)
0
2
4
6
8
10
1
2
3
4
○ 572 ppm
△ 1160 ppm
□ 2225 ppm
$\frac{T}{n} = (2.81 \pm 0.07) \times 10^{-3} \frac{K}{ppm}$

FIG. 15

Impurity magnetization M for the 42, 94, 169, 242, 572 and 1160 ppm Fe alloys as a function of the inverse of the magnetic field 1/H for several temperatures.

FIG. 15-1

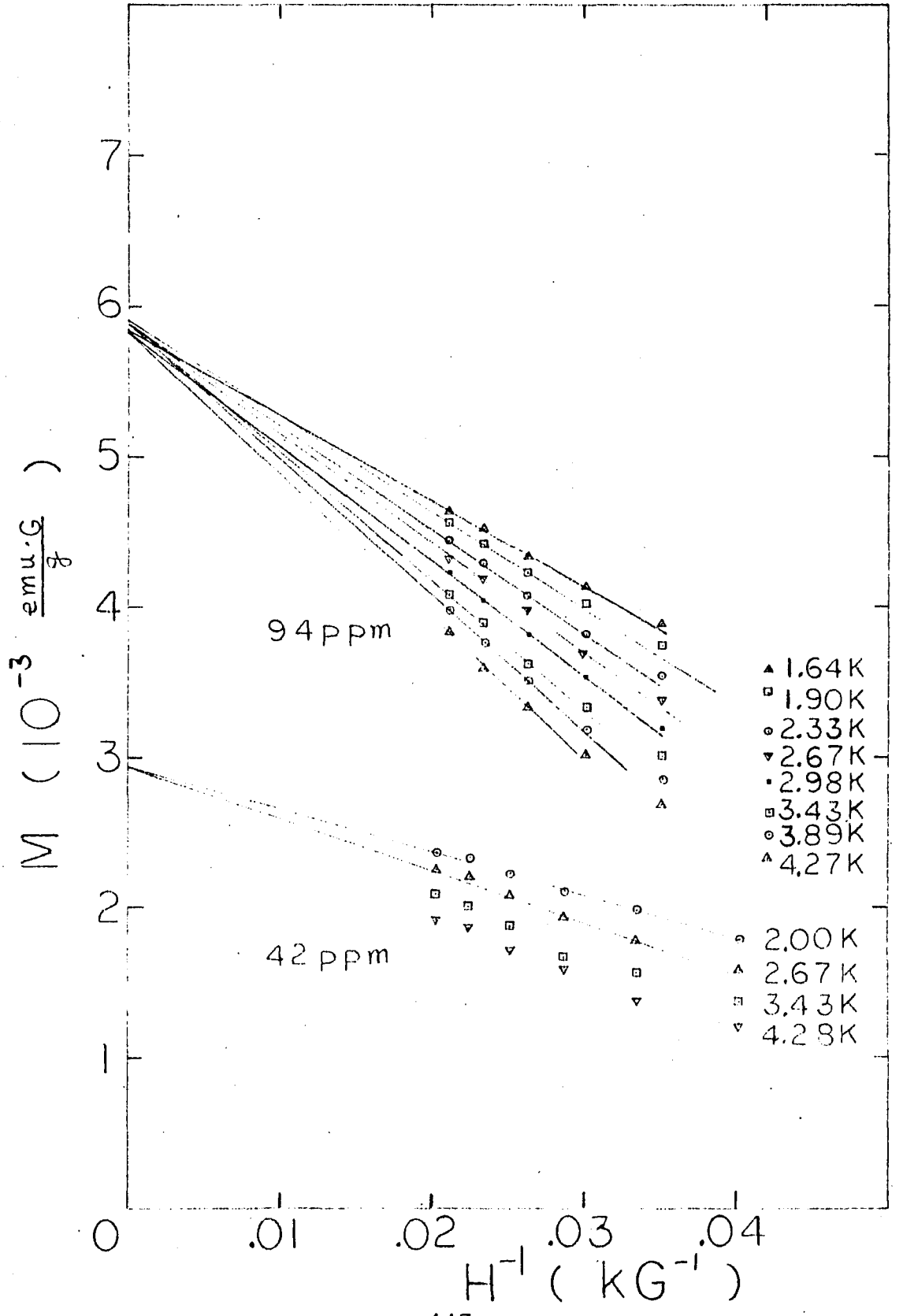
M (10^-3 emu·G / g)
7
6
5
4
3
2
1
0
.01
.02
.03
.04
H^-1 (kG^-1)
94ppm
42ppm
1.64K
1.90K
2.33K
2.67K
2.98K
3.43K
3.89K
4.27K
2.00K
2.67K
3.43K
4.28K

FIG. 15-2

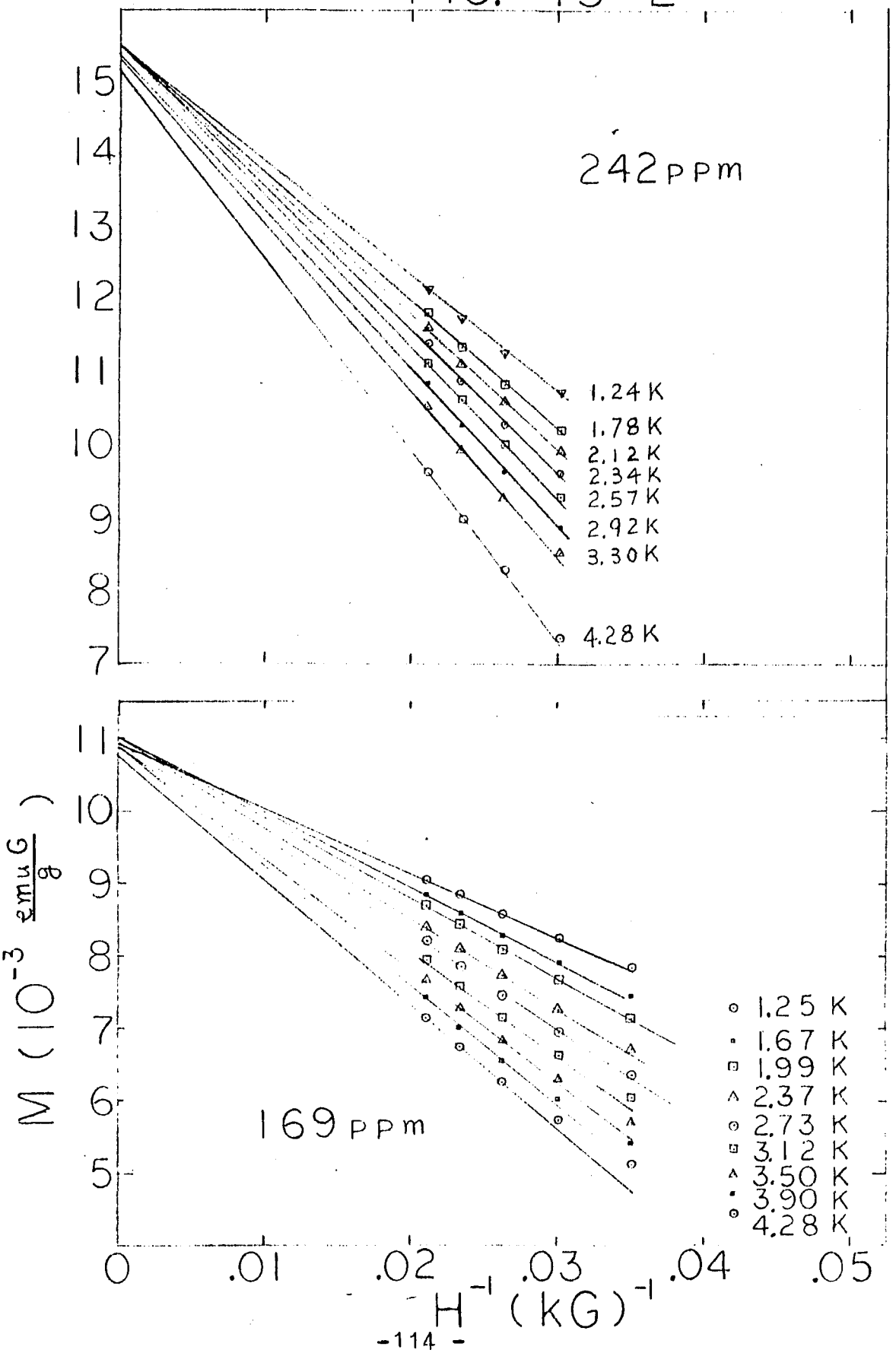
242 ppm
1.24 K
1.78 K
2.12 K
2.34 K
2.57 K
2.92 K
3.30 K
4.28 K
169 ppm
1.25 K
1.67 K
1.99 K
2.37 K
2.73 K
3.12 K
3.50 K
3.90 K
4.28 K
M (10^-3 emu/g)
H^-1 (kG)^-1
0
.01
.02
.03
.04
.05
15
14
13
12
11
10
9
8
7
11
10
9
8
7
6
5

FIG. 15-3

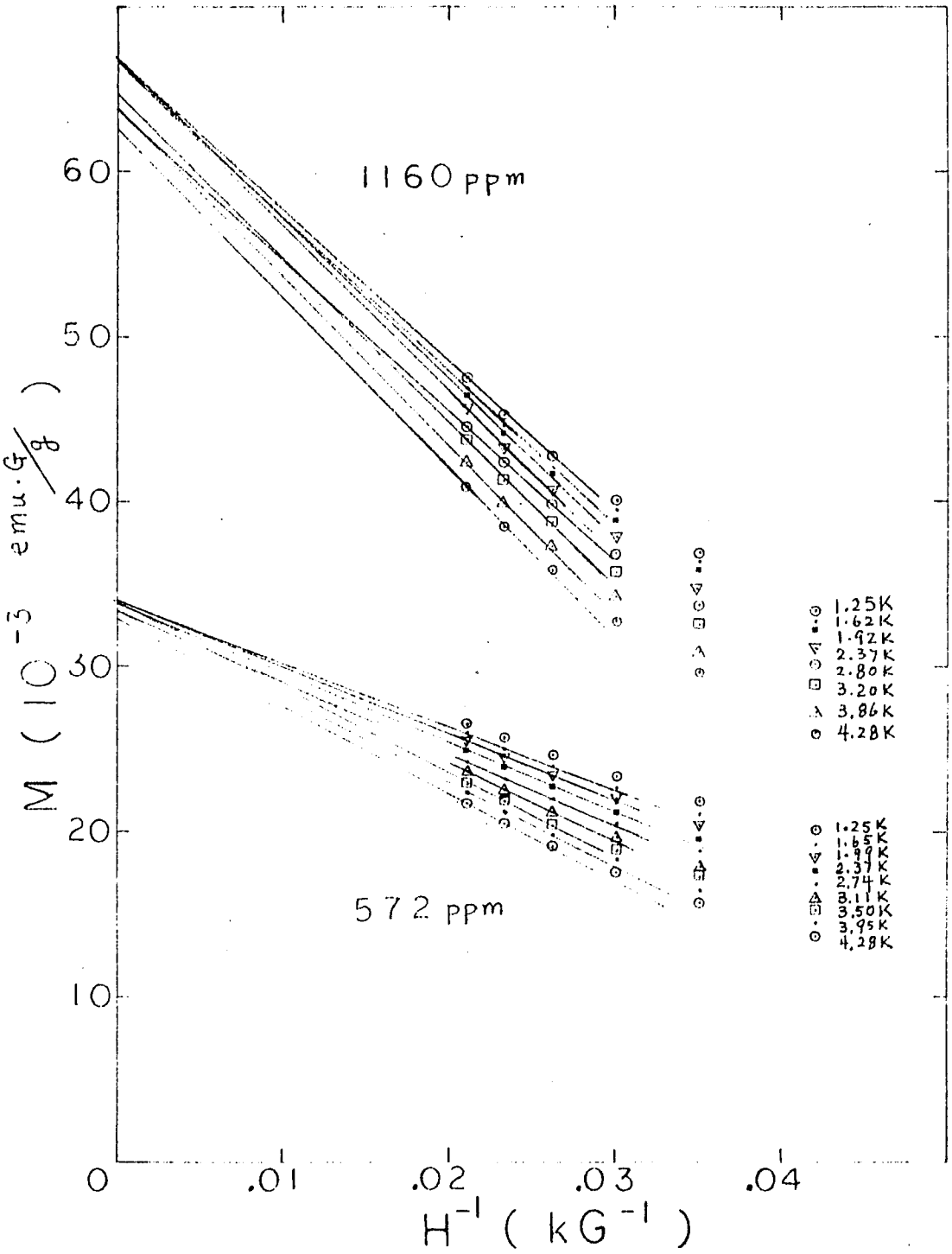
1160 ppm
572 ppm
M (10^-3 emu·G/g)
H^-1 (kG^-1)
0
10
20
30
40
50
60
.01
.02
.03
.04
1.25K
1.62K
1.92K
2.37K
2.80K
3.20K
3.86K
4.28K
1.25K
1.65K
1.99K
2.37K
2.74K
3.11K
3.50K
3.95K
4.28K

FIG. 16

$H_o(n,T)/n$ as a function of the reduced temperature T/n for the 42, 94, 169, 242, 572 and 1160 ppm Fe alloys. The straight lines indicate the fits to the equation $H_o/n = Ak_BT/n + BV_o$ for each sample. See Eq. (2) for the definition of H_o.

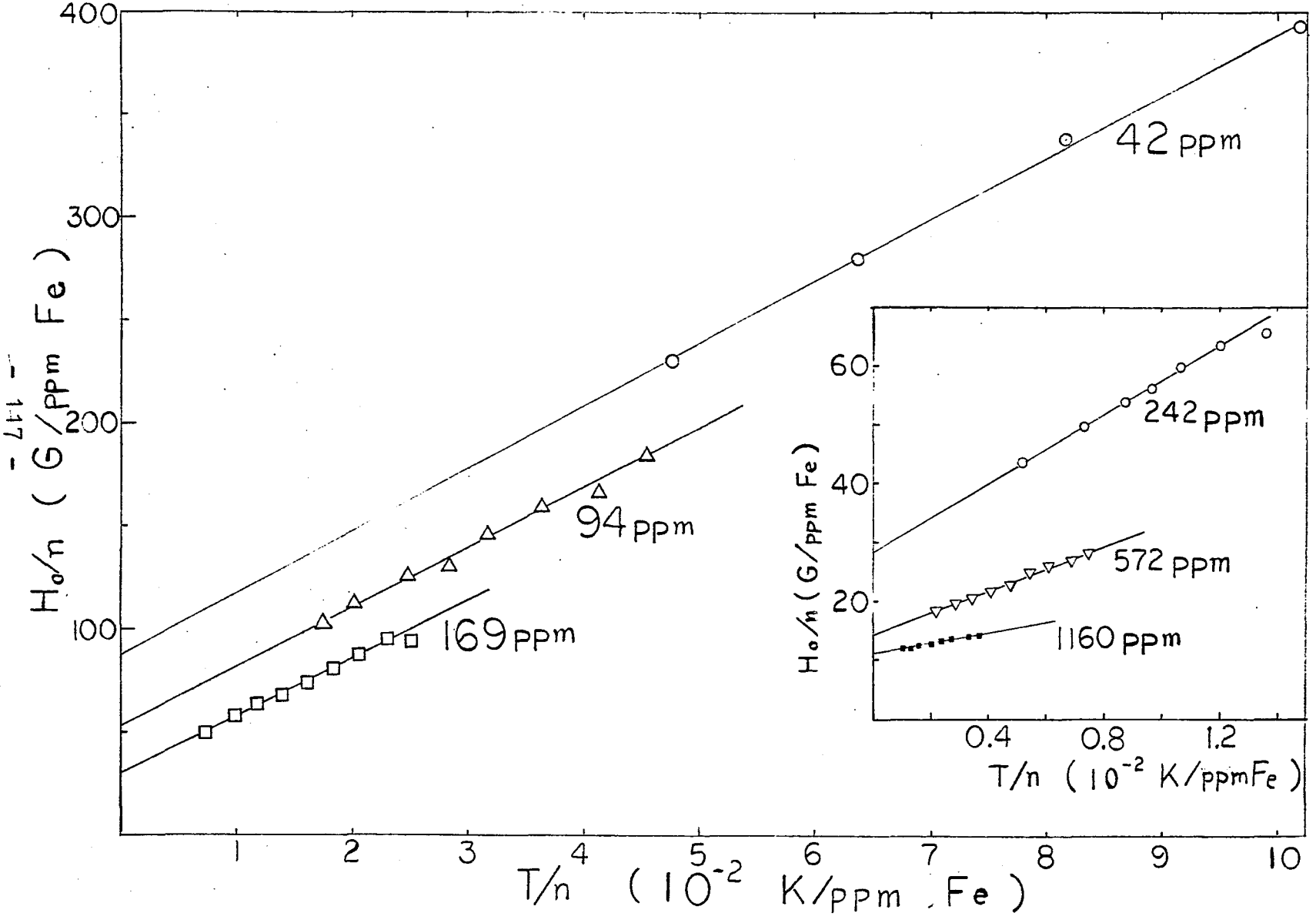
400
300
200
100
H_o/n (G/ppm Fe)
42 ppm
94 ppm
169 ppm
1 2 3 4 5 6 7 8 9 10
T/n (10^{-2} K/ppm Fe)
60
40
20
242 ppm
572 ppm
1160 ppm
0.4 0.8 1.2
T/n (10^{-2} K/ppmFe)

FIG. 16

these six alloys. From the graph, it is surprising to find that the values of BV_o, the straight line intercept on the T/n = 0 axis, are concentration-dependent. The resulting values of BV_o and V_o are listed in Table 9, using spin values S listed in Table 7, and g = 2.

5. New scaling laws for AuFe.

In Fig. 17, $\chi V_o/S(S+1)$ is plotted as a function of k_BT/nV_o for all nine samples, where V_o is obtained from Table 9. The data occupy 4x3 decades, and, when compared with Fig. 13, now appear to fall quite well on a single curve. In Fig. 18, M/NS is plotted as a function of H/NV_o for fixed T/nV_o, again using V_o from Table 9. The data for the three different concentrations fit reasonably well on a single curve.

6. Self-damping and $V_o(n)$.

According to Heeger et al.[45] and Walstedt and Walker,[25] self-damping of the RKKY interaction will contribute a factor of $e^{-r/\ell}$ to the RKKY interaction V(r), i.e., $V(r) = \left(V_o(\cos 2k_F r)/r^3 \right) e^{-r/\ell}$, where r is the distance between impurities, and ℓ is the electron mean free path. Thus one would expect that $V_o(n) \propto V_o(0)^{e^{-\langle r \rangle/\ell}}$, where $\langle r \rangle$ is the average distance between impurities, which can be determined from the impurity concentrations; i.e., $\langle r \rangle = n^{-1/3}$. The mean free path ℓ can be estimated by combining the measured residual resistivity ratios $\Delta\rho_r$ with the free electron model; i.e., $\rho\ell = 12\pi^3\hbar/e^2S_o$ and

Table 9

$V_o(n)$ of AuFe Alloy

n (ppm Fe)	$V_o(n)$[a] (10^{-36} erg cm^3)	$BV_o(n)$[b] (10^{-16} G cm^3)	$\ell^c_{4.2K}$ (10^2 A)	$\langle r \rangle$[d] (A)
18 ± 1			238	98.0
42 ± 2	11.9±1.35	14.8±0.9	133	73.9
94 ± 2	7.75±0.59	8.90±0.42	76.3	56.5
169 ± 2	4.49±0.37	5.16±0.34	45.4	46.5
242 ± 16	4.02±0.37	4.75±0.25	34.6	41.2
572 ± 8	1.96±0.07	2.37±0.09	15.5	31.0
1160± 70	1.54±0.10	1.87±0.12	8.25	24.5
2225±125	1.24±0.12		4.51	19.8
6050±350	1.03±0.10		1.78	14.1

a) The strength V_o of the RKKY interaction is determined from (b), using $B = 2(2S+1)/3g\mu_B$ and spin S from Table 7. The values of $V_o(n)$ for the 2225 and 6050 ppm Fe samples are obtained by fitting the susceptibility to the scaling law $\chi V_o/S(S+1) = f\,(T/nV_o)$.

b) The values of $BV_o(n)$ are obtained from Figs. 15 and 16 (see text).

c) The electron mean free path ℓ is obtained by using the free-electron model and measured residual resistivity ratio ρ_r (see text).

d) The average distance between impurities $\langle r \rangle = n^{-1/3}$ is determined by using impurity concentration n from Table 1 and 1ppm = 5.89 x 10^{16} atoms/cm^3 for Au.

FIG. 17

$\chi V_o/S(S+1)$ plotted as a function of k_BT/nV_o for nine AuFe alloys (18, 42, 94, 169, 242, 572, 1160, 2225 and 6050 ppm Fe). S is obtained from the measured Curie constants. V_o is obtained from Table 9.

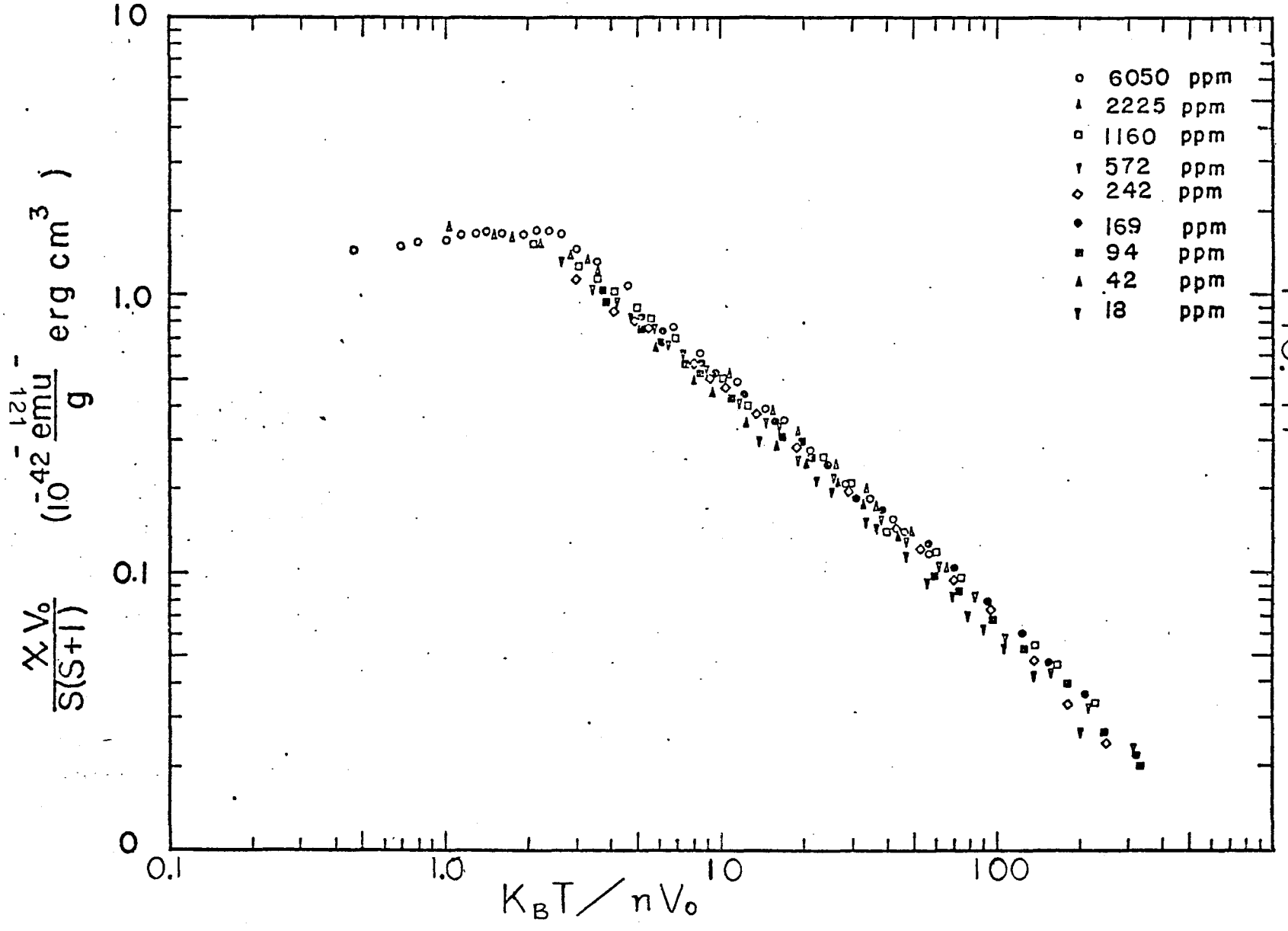
10
1.0
0.1
0
0.1
1.0
10
100
K_BT/nV_o
$\frac{\chi V_o}{S(S+1)}$ $(10^{-42}\frac{emu}{g}$ erg $cm^3)$
6050 ppm
2225 ppm
1160 ppm
572 ppm
242 ppm
169 ppm
94 ppm
42 ppm
18 ppm

FIG. 17

FIG. 18

Impurity magnetization M divided by concentration N and spin S as a function of H/NV_o at a fixed k_BT/nV_o. For n = 94, 169, 242 ppm Fe, the corresponding temperatures are 1.90, 1.99, 2.57 K, respectively, and $k_BT/nV_o = 6.15 \pm 0.06$. For n = 242, 572, 1160 ppm Fe, the corresponding temperatures are 1.78, 1.99, 3.20 K respectively, and $k_BT/nV_o = 4.21 \pm 0.07$.

FIG. 18-1

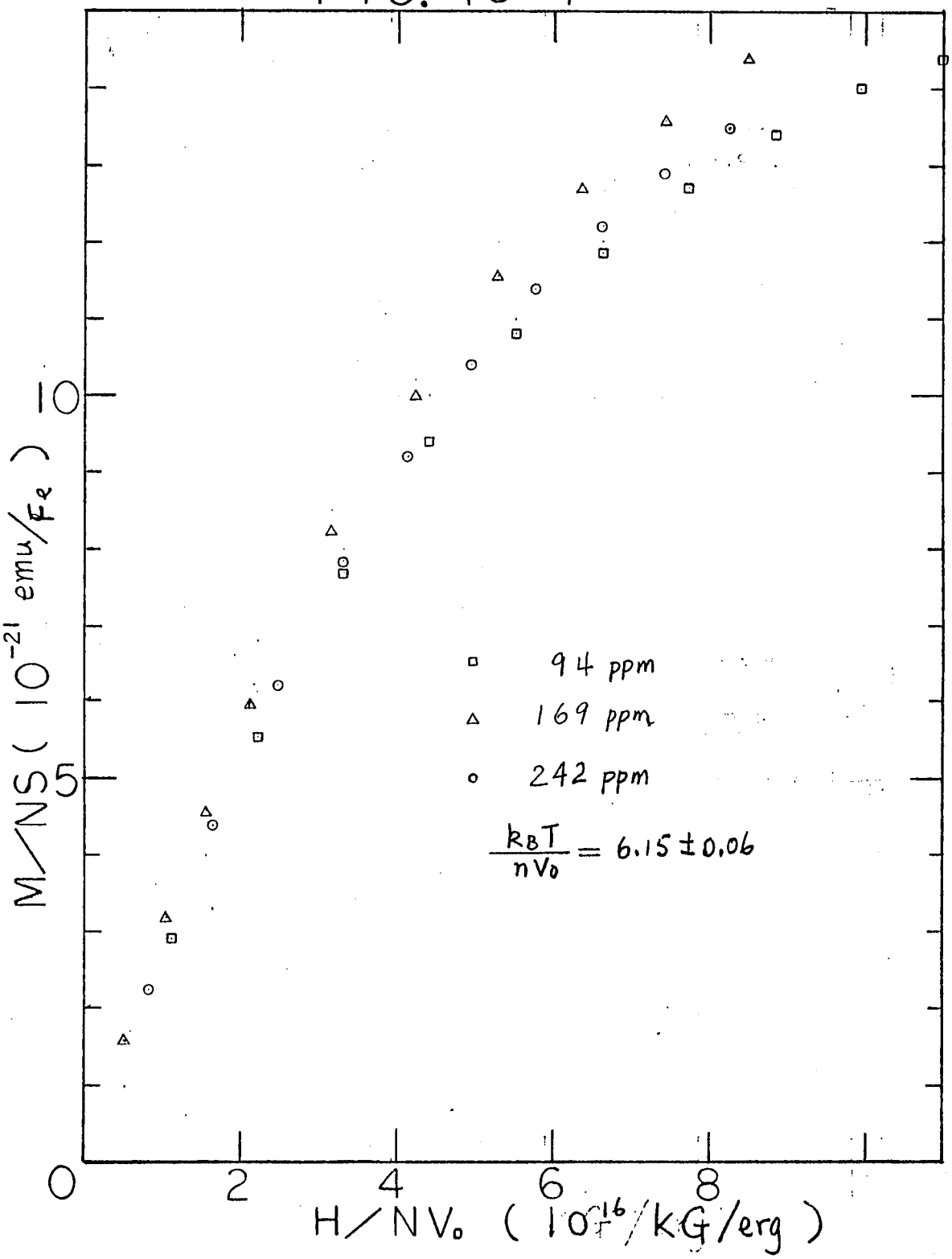
M/NS (10^{-21} emu/Fe)
H/NV$_0$ (10^{16}/kG/erg)
0
5
10
2
4
6
8
94 ppm
169 ppm
242 ppm
$\frac{k_B T}{n V_0} = 6.15 \pm 0.06$

FIG 18-2

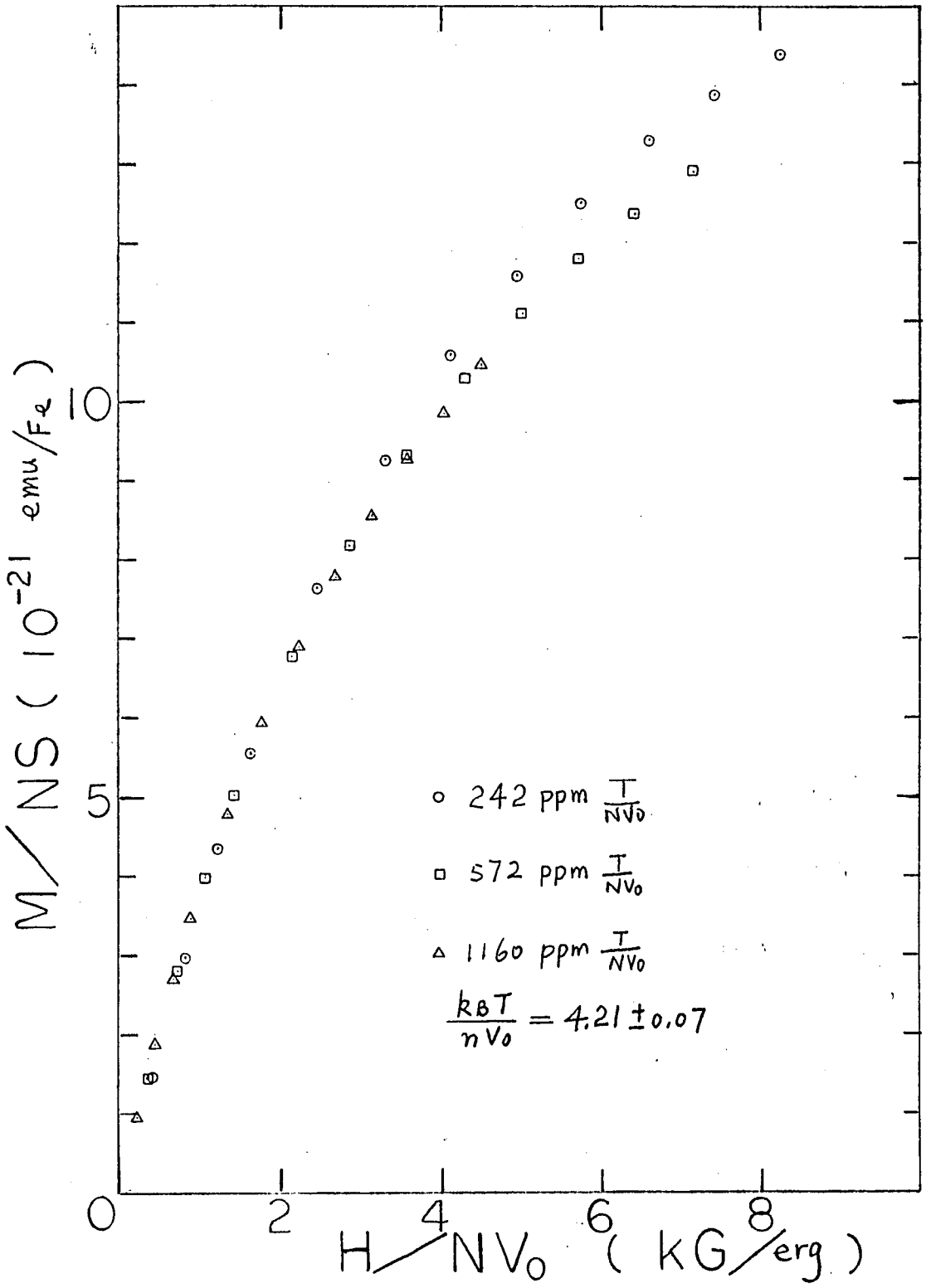
M/NS (10^{-21} emu/Fe)
0
5
10
2
4
6
8
H/NV$_0$ (kG/erg)
○ 242 ppm $\frac{T}{NV_0}$
□ 572 ppm $\frac{T}{NV_0}$
△ 1160 ppm $\frac{T}{NV_0}$
$\frac{k_B T}{nV_0} = 4.21 \pm 0.07$

$$\langle \ell \rangle_{4.2} = \frac{\langle \ell \rangle_{273}}{\Delta \rho_r} = \frac{\rho \ell}{\rho_{273} \Delta \rho_r} = \frac{367\ \text{Å}}{\Delta \rho_r}$$

where $S_o = 4\pi k_F^2$, $k_F = 1.208 \times 10^8\ cm^{-1}$ and $\rho_{273} = 2.35 \mu\Omega cm$. In Table 9, $\langle r \rangle$ and ℓ are listed for each n. In Fig. 19, $V_o(n)$ is plotted against $\langle r \rangle / \ell$.

7. The temperature of the susceptibility maximum for AuFe.

The broad susceptibility maximum at T = 5.5K of Au with 6050 ppm Fe is displayed in Fig. 11. The susceptibility of the 2225 ppm Fe sample was observed to approach a maximum around 1.5K. The approach of the susceptibility to a maximum of the 1160 ppm Fe sample at lower temperature is also indicated in Fig. 11.

8. Concentration-dependent spin and Curie-Weiss temperature Θ of AuFe.

The spin can be calculated either by using 1). the saturation magnetization $M_{sat} = ng\mu_B S$ or by 2). the Curie constant $C = nS(S+1)g^2\mu_B^2/3k_B$, with g = 2 assumed. In Table 7, the spin S for each concentration n is listed. An increase of S with concentration n is apparent. In Fig. 20, the spin S is plotted as a function of n. The spin may also have a minimum at the low concentrations, but the uncertainty in the data make it difficult to assert this with confidence. In Table 7, the values of Θ determined by least-mean-square fits are also listed, together

FIG. 19

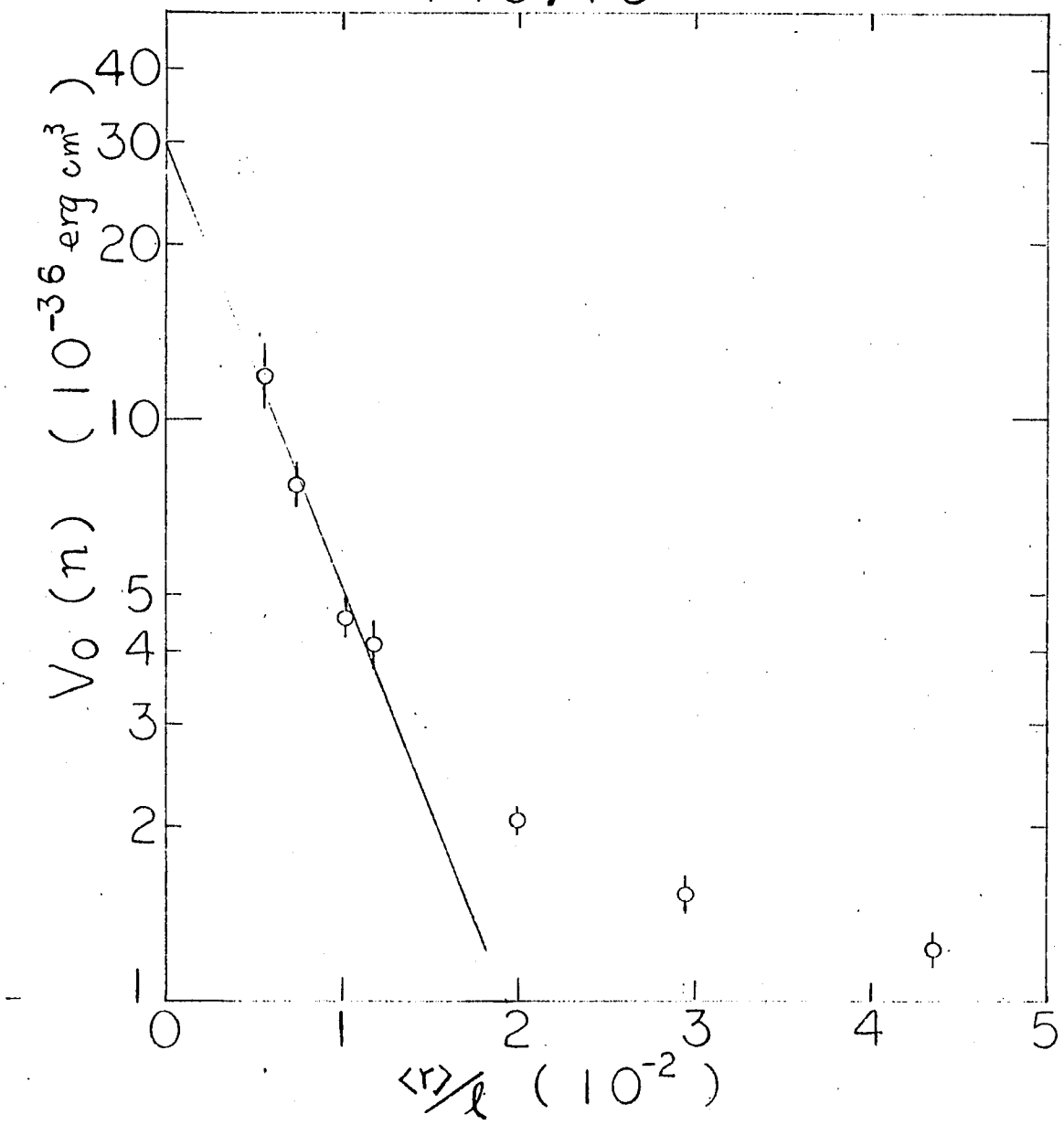

FIG. 19

The strength of the RKKY potential $V_o(n)$ plotted as a function of $\langle r \rangle / \ell$, where $\langle r \rangle$ is the average distance between impurities and ℓ is the electron mean free path.

FIG. 20

The spin S per Fe impurity plotted as a function of impurity concentration n. S is obtained from the measured Curie constants and Fe concentrations, assuming $\tilde{g} = 2$.

FIG. 20

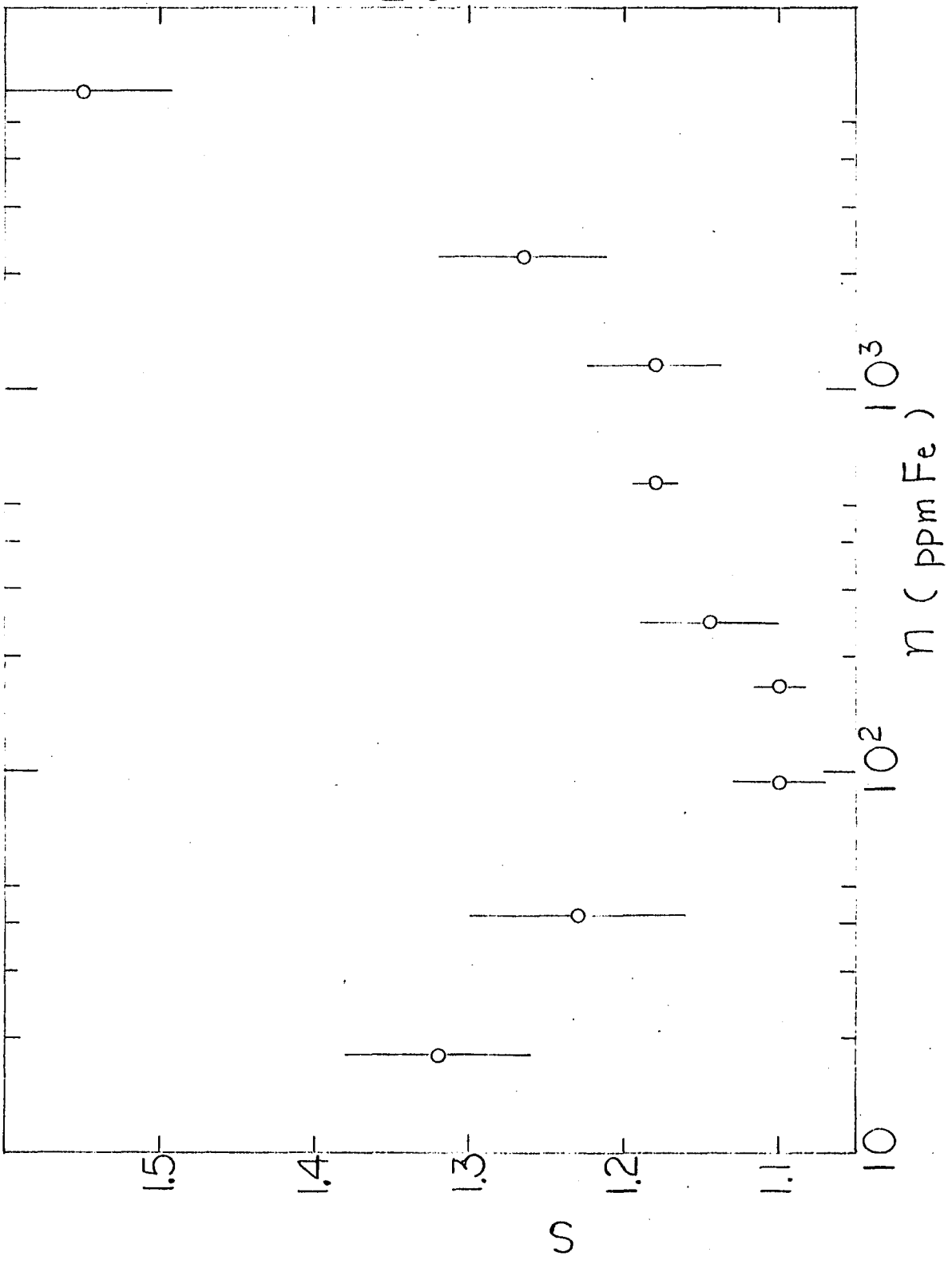

with nV_o for each concentration. The value of nV_o increases with concentration, but it does not relate to θ in a simple fashion.

V. DISCUSSION.

A. AuMn.

The initial susceptibility χ of our six AuMn alloys is plotted in Fig. 4. The susceptibility data of all six concentrations are observed to fit Curie-Weiss laws, except for the two higher concentration samples which approach susceptibility maxima at lower temperatures, i.e., for $T < 1K$. The values of $\frac{nV_0}{k_B}$ for the 1005 and 2110 ppm samples are 0.11K and 0.22K respectively. The deviations from Curie-Weiss behavior at low temperatures are characteristic of spin-glass behavior; they are due to the "freezing in" of the orientations of the Mn spins in the local molecular field. The impurity susceptibility $\chi(n,T)$ is also plotted as a function of T/n in Fig. 6. The susceptibility data for all six different concentration alloys fit very well on a single curve, with no noticeable deviations from scaling at either high or low concentrations such as have been observed previously in a similar plot for ZnMn.[53] The magnetization M at three different temperatures T is plotted as a function of H/T as shown in Fig. 5. Also shown on the graphs are Brillouin functions for the appropriate spin S, taken from Table 3. For the lowest concentration sample, 54 ppm Mn, the magnetization data are a function only of H/T for these three different temperatures. The magnetization data for this sample fall only slightly

(1–5 %) below the appropriate Brillouin function. The same behavior is found for the 105 and 216 ppm Mn samples. For the higher concentration Mn samples, the impurity magnetization is no longer a function only of H/T and deviations from the Brillouin function are significant. The deviations increase with increasing concentration and decreasing temperature. This behavior of the impurity magnetization has been observed previously for a series of ZnMn alloys where impurity-impurity interactions have been shown to be important.[53] The scaling behavior of the magnetization is tested in Fig. 7 by plotting $M/M_{sat} = M/ng\mu_B S$ as a function of H/n for three alloys at fixed $T/n = (3.73 \pm 0.01) \times 10^{-3}$ K/ppm Mn. The data superpose quite well on a single curve. There are almost no deviations from scaling observed for the 2110 ppm Mn sample such as that previously observed for a similar concentration ZnMn sample.[53] The three lower concentration AuMn samples also fit quite well on a single curve (not shown).

The strength of the RKKY interaction V_o is determined to be $(2.4 \pm 0.3) \times 10^{-37}$ erg $cm^3 = (1.04 \pm 0.13)$K/at. % (see details in Experimental Results and Analysis Section). As shown in Fig. 10, V_o is slightly concentration-dependent, but the difference is small between the 1005 ppm and 2110 ppm samples. The magnetization per impurity is plotted as a function of concentration n for a fixed tem-

perature and magnetic field in Fig. 8. The magnetization per impurity is observed to decrease with increasing n, which is an indication of interactions between the magnetic impurities. The same behavior is observed in the case of AuFe[21] for concentrations less than 1 % Fe. The linear extrapolation of M/M_{sat} to n = 0 falls about 1–2 % below the free spin prediction (the Brillouin function). For ZnMn a similar, but much greater, difference of about 10 % was observed as $n \longrightarrow 0$. This must be due to the weakness of the RKKY interaction strength V_o for AuMn compared with $V_o = 2 \times 10^{-36}$ erg cm^3 = 11.5 K/at. % for ZnMn.

The spin of the Mn impurity in Au is almost concentration-independent and equal to 2.25. Previous susceptibility measurements on AuMn have yielded S = 2.37,[54] while saturation magnetization results [55] yield S = 2.25, in excellent agreement with this work. The spin of Mn in Au is much larger than S = 1.25 obtained for Mn in Zn. The weaker coupling of the Mn impurity to the Au host electrons is reflected in the almost free-spin behavior of the Mn ion (S = 5/2 is the free spin value for Mn^{2+} with five 3d electrons, according to Hund's rule).

The magnetization is plotted as a function of H^{-1} in Fig. 9 to examine the approach to saturation of magnetization. The data for the 521 ppm Mn sample and the three lower concentrations can not be represented by

$M = g\mu_B Sn \left[1 - H_o (n,T)/H \right]$ due to a more rapid approach to saturation than H^{-1}. This is also characteristic of the Brillouin functions for free spins. Hence it appears that for the four lowest concentration Mn samples, the approach to saturation of the magnetization is not completely dominated by impurity-impurity interactions via the RKKY potential. It appears that single impurity effects are also important. If we assume that nV_o and $k_B T_K$ are comparable energies in this concentration region, then we obtain $T_K = (3 \pm 2) \times 10^{-2}$K by using $V_o = 2.4 \times 10^{-37}$ erg cm^3 and n = (300 $\pm$ 200) ppm Mn. This value of T_K is of the same order of magnitude as the result obtained from nuclear orientation measurements on AuMn,[56] and is many orders of magnitude larger than $T_K \sim 10^{-13}$ K obtained from the analysis of resistivity data for AuMn.[14]

B. AuFe.

The susceptibility of our nine AuFe samples is plotted in Fig. 11. The susceptibility data of all nine concentrations are observed to fit Curie-Weiss laws, except for some deviations at intermediate temperatures (10–70K). Previous studies of AuFe have found similar deviations.[16,52,57-59] The susceptibility for the three high concentration samples approaches maxima at T = 5.5K for the 6050 ppm sample, at T$\sim$1.5K for the 2225 ppm sample,

and at $T < 1K$ for 1160 ppm sample. The temperature T_o of the susceptibility maximum can be roughly fitted to the result of Lutes and Schmit,[15] i.e., $T = 8.00 \times n(at.\%)K$. The maximum of the susceptibility is observed to occur over a broad temperature range, in agreement with previous results,[15,17] but in contrast with the sharp peaks seen by Cannella and Mydosh,[20] observed in a small AC magnetic field ($\sim 5G$). Our results for χ are obtained with a superconducting magnet whose remanent field is of the order of 100 gauss. Tholence and Tournier [24] have attributed this sharp peak in the low field susceptibility to the presence of a remanent magnetization which appears for $T < T_o$ and $H < H_m$, where H_m is almost proportional to n and $H_m \sim 1000 \times n$ (at. %) gauss for AuFe.

The Curie-Weiss temperatures θ are listed in Table 7. Our results for θ are observed to increase with concentration, with θ increasing from 0.45 to 2.7K as the concentration increases from 18 ppm to 6050 ppm. These values of θ are much smaller than the high temperature susceptibility results of Hurd.[52] Our results for θ are obtained from Curie-Weiss fits to our low temperature data ($T < 50K$), where the data are most accurate. The θ of the 18 ppm Fe sample is $(0.45 \pm 0.05)K$, in good agreement with the result of Tholence and Tournier,[17] $\theta = 0.4K$, and that of Loram, Grassie and Swallow,[16] $\theta = 0.5K$. The θ of the highest

concentration sample (6050 ppm Fe) is (2.7 ± 0.3)K, in good agreement with the result for the 5000 ppm Fe sample of Lutes and Schmit,[15] i.e., θ = 3K. The effective spin S per impurity is also listed in Table 7. The spin is observed to decrease with concentration initially, go through a minimum at about 100 ppm, and then increase with concentration. Our values of S for the 18 ppm and 42 ppm Fe sample are 1.32 ± 0.06 and 1.23 ± 0.07, respectively, in reasonable agreement with Loram et al.,[16] i.e., S = 1.29 ± 0.03 for 20 - 100 ppm Fe. The uncertainties in concentration make it difficult to be sure of the decrease and minimum of the spin S at low concentrations. This decrease, however, was also observed by J. Haddad.[50] The increase in S with concentration for n > 100 ppm Fe is quite clear, however, as shown in Fig. 20.

The magnetization M at three temperatures for each of our samples is plotted as a function of H/T in Fig. 12. Also shown on the graphs are Brillouin functions for the appropriate spin S taken from Table 7. Unlike the AuMn alloys, the magnetizations fall significantly below the Brillouin functions, and are obviously not functions only of H/T. The deviations from the Brillouin functions increase with increasing concentration and decreasing temperature. This behavior of the impurity magnetization is qualitatively the same as observed for AuMn alloys with Mn

concentrations $n > 216$ ppm (see Fig. 5).

The impurity magnetization is plotted as a function of H in Fig. 21. The similarity between our results and those of Borg and Kitchens [21] is evident; i.e., the effects of temperature on the magnetization are greatest for the lowest concentration data and decrease with increasing concentration. The magnetization per impurity at fixed temperature and magnetic field is plotted as a function of n in Fig. 22. The values of magnetization per impurity decrease with concentration, as predicted by theories based on the RKKY interactions between magnetic impurities.

The scaling behavior of the AuFe samples is examined in Fig. 13 by plotting χ as a function of T/n. It is evident that the scaling behavior is not as good as that observed in a similar plot (Fig. 6) for our six AuMn samples. The scaling behavior of the magnetization is also tested by plotting M/M_{sat} as a function of H/n at fixed T/n for the 572, 1160 and 2225 ppm Fe samples in Fig. 14. The absence of scaling is again obvious.

The strength of the RKKY interaction V_o is determined as described in the "Experimental Results and Analysis Section". The values obtained for BV_o decrease with increasing concentration. The decreasing BV_o is determined to be the result of a decreasing V_o as the spin S actually

FIG. 21

The impurity magnetization plotted as a function of magnetic field H for three temperatures each for six AuFe alloys (42, 169, 572, 1160, 2225, and 6050 ppm Fe).

FIG. 21—1

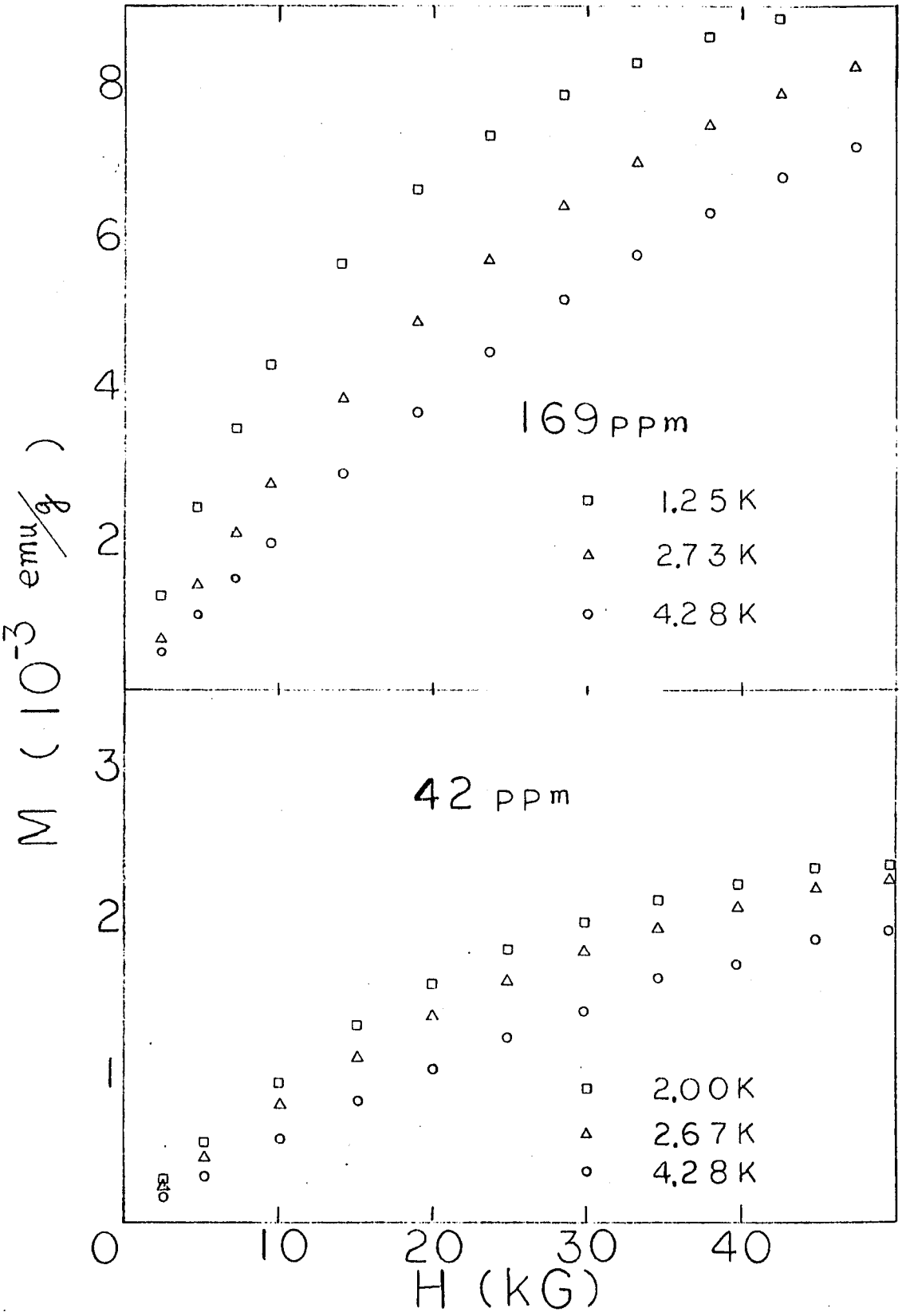
M (10^-3 emu/g)
8
6
4
2
169 ppm
1.25 K
2.73 K
4.28 K
3
2
1
42 ppm
2.00 K
2.67 K
4.28 K
0
10
20
30
40
H (kG)

FIG. 21-2

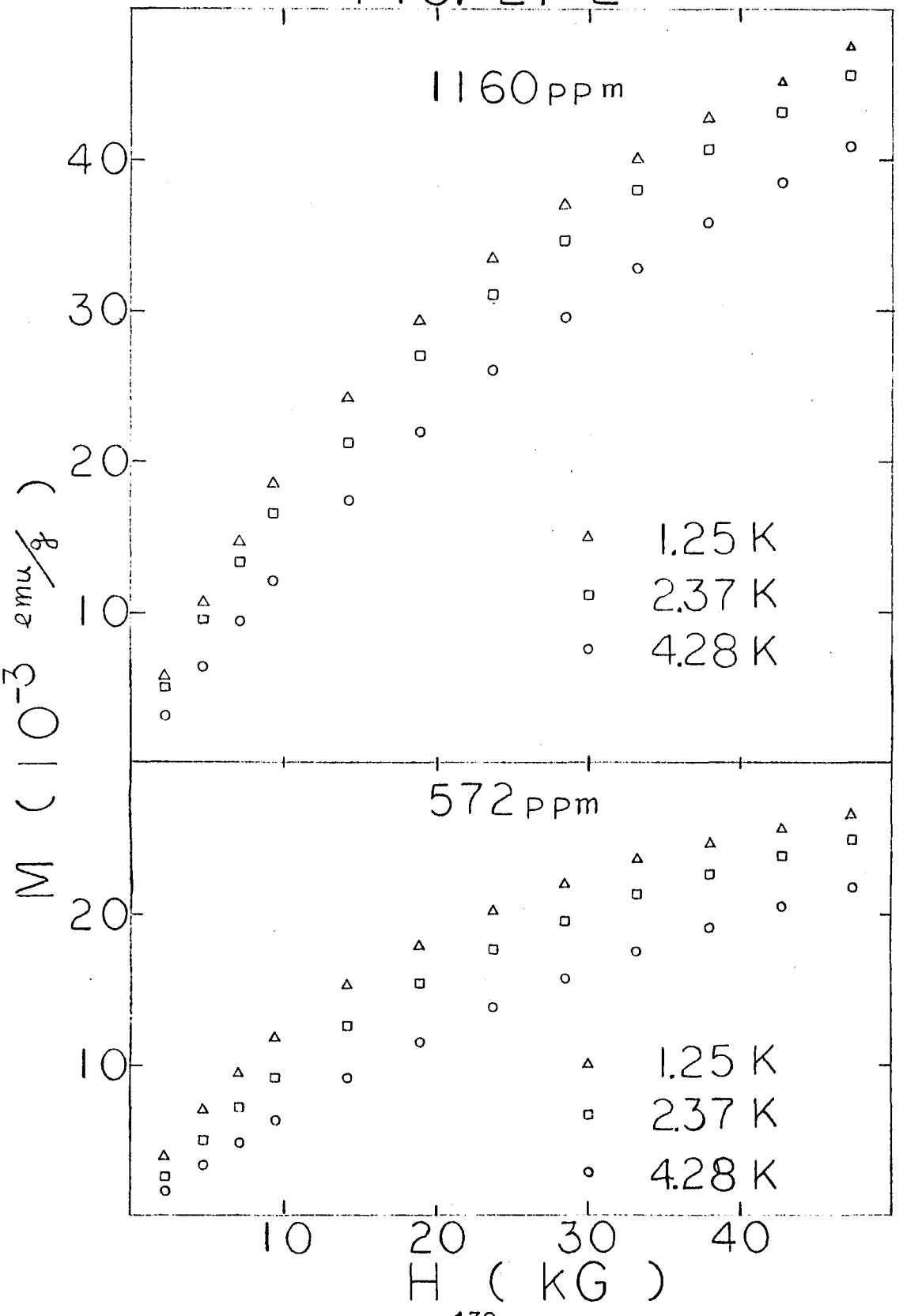
1160 ppm
572 ppm
1.25 K
2.37 K
4.28 K
1.25 K
2.37 K
4.28 K
40
30
20
10
20
10
10
20
30
40
M (10^{-3} emu/g)
H (kG)

FIG. 21-3

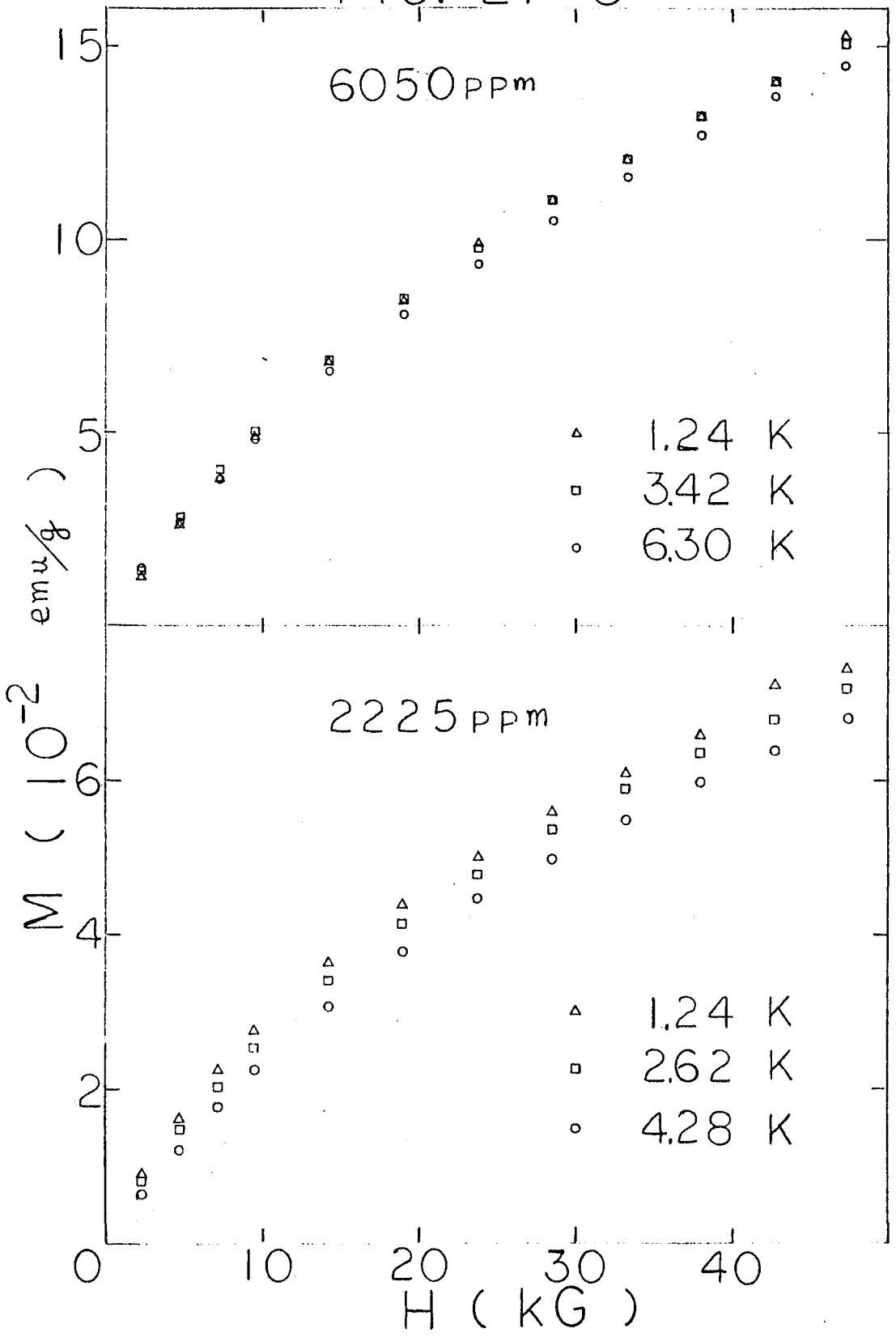
6050 ppm
1.24 K
3.42 K
6.30 K
2225 ppm
1.24 K
2.62 K
4.28 K
M (10^-2 emu/g)
H (kG)
0
2
4
6
5
10
15
10
20
30
40

FIG. 22

The impurity magnetization per Fe impurity M/n plotted as a function of impurity concentration n at fixed temperature T = 4.28K and fixed magnetic fields H = 47.45 kG and 23.73 kG.

FIG. 22

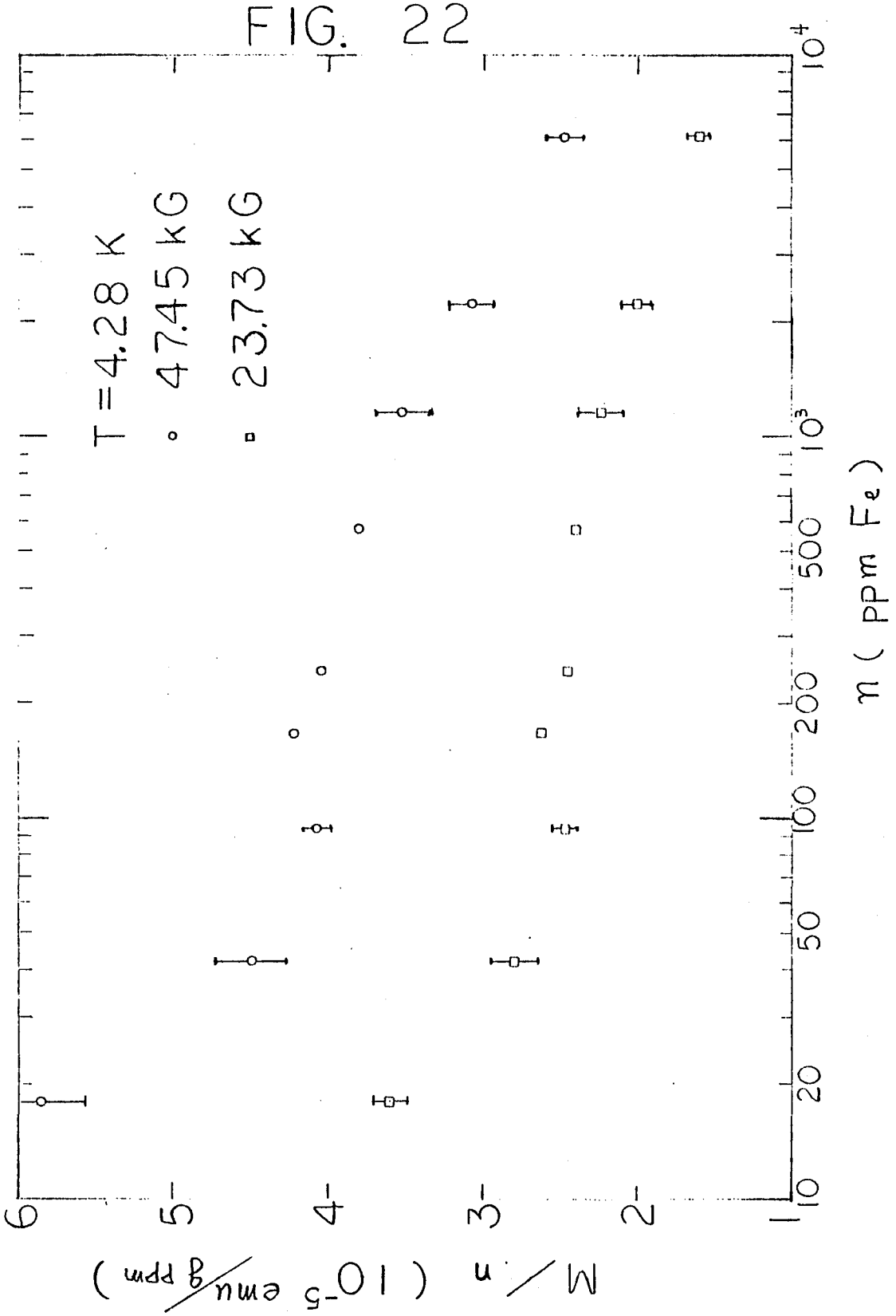
T = 4.28 K
47.45 kG
23.73 kG
M / n (10⁻⁵ emu/g ppm)
n (ppm Fe)
1
2
3
4
5
6
10
20
50
100
200
500
10³
10⁴

increases slightly as n increases. The values of V_o thus obtained are listed in Table 9. For the 42 ppm AuFe sample, $V_o = 11.9 \times 10^{-36}$ erg cm^3 (equivalent to 52K/at.% Fe), about fifty times greater than V_o obtained for a similar concentration AuMn sample. From the comparison of the alloy systems AuMn and AuFe, it can be concluded that the lack of dependence of V_o on n and the smallness of V_o for the AuMn alloys combine to make this alloy system an ideal "scaling law" spin glass.

Due to the rapid variation of V_o with n, the expression for the susceptibility due to Larkin et al,[10] $\chi = ng^2\mu_B^2 S(S+1)/3(k_BT+C_snV_o)$, should be reexamined. This formula can be written as

$$\chi V_o/S(S+1) = g^2\mu_B^2/3(k_BT/nV_o+C_s).$$

Thus $\chi V_o/S(S+1)$ should obey a scaling law when plotted as a function of k_BT/nV_o. This scaling law behavior is tested in Fig. 17. It is clear that the scaling of the susceptibility data is very much improved. By examining the formula

$$M = ng\mu_B S\left[1 - \frac{2(2S+1)nV_o}{3g\mu_B H}\right]$$

and the predicted scaling law $M/n = F(T/n, H/n)$, one is led to the modified scaling law $M/ng\mu_B S = F(T/nV_o, H/nV_o)$, where the variation of V_o with n is thus taken into consideration. In Fig. 18, M/nS is plotted as a function of H/nV_o for three different concentration alloys at the same

$k_B T/nV_o$. The improved fit to the modified scaling law is evident by comparison with Fig. 14. From the improved fits of the susceptibility and magnetization data to the above modified scaling laws, we feel that the magnetic properties of these AuFe alloys can be explained in terms of an RKKY interaction whose effective strength decreases rapidly with increasing Fe concentration n. The lack of scaling behavior observed in Fig. 17 for the 18 ppm Fe sample is probably due to some contribution from the single impurity Kondo effect. If $k_B T_K \approx nV_o$ is assumed to hold for this alloy, then using $V_o = 11.9 \times 10^{-36}$ erg cm^3, we find $T_K \sim 0.1$K, in good agreement with the result of Tholence and Tournier.[17]

We suggest that the rapid decrease of V_o with increasing concentration is due to self-damping of the RKKY oscillations; i.e., a damping of the RKKY interaction by the magnetic impurities which produce it. Walstedt and Walker [25] have concluded that the self-damping effect will contribute a factor $e^{-r/\ell}$ in the RKKY interaction potential, where ℓ is the electronic mean free path. If such an expression is correct, then V_o (n) should be proportional to $V_o(0)e^{-\langle r\rangle/\ell}$, where $\langle r\rangle$ is the average distance between magnetic impurities and $V_o(0)$ is the dilute-limit undamped RKKY interaction strength. In Table 9, the values of $\langle r\rangle$ and ℓ are listed for each n. In Fig. 19, $V_o(n)$ is plotted

against $\langle r \rangle / \ell$ on a semi-log graph. We find that $V_o(n)$ can be fitted to a straight line only for the 42,94,169 and 242 ppm samples; the slope of this line is -175, i.e., $V_o(n) = V_o(0) e^{-175 \langle r \rangle / \ell}$. Extrapolating to $\langle r \rangle / \ell = 0$ yields $V_o(0) \simeq (30 \pm 6) \times 10^{-36}$ erg cm^3. From our results for $V_o(n)$, $\langle r \rangle$, and ℓ, we conclude that the theoretical prediction has to be modified to account for both the magnitude of the coefficient in the exponent (i.e., 175 as compared to the predicted value of 1.61 and the deviations from the simple self-damping theory for $n > 242$ ppm Fe. It is probable that the mean free path obtained from the free electron model and residual resistivity ratios is very different from the mean free path of the electrons which participate in the RKKY interaction.

The observed decrease of V_o with n can help to clarify several anomalous experimental results previously observed for AuFe alloys. Souletie and Tournier [9] have shown that AuFe alloys with $n > 0.1$ at. % Fe are spin-glasses. They have examined the excess specific heat data of Dreyfus et al.[19] and claim to have shown that $\Delta C_p/n$ is a function of T/n only. The scaling behavior observed from their plot, however, is not very convincing. Dreyfus et al.[19] measured the excess specific heat ΔC_p due to the impurities in a series of AuFe alloys (0.2 to 8 at. % Fe). For the linear term, $\Delta C_p = AT$, observed for $k_B T \ll n V_o$, they found

that A increases with concentration n, in contrast to theoretical predictions [13] which specify that A is concentration-independent. However, since $A \propto V_o^{-1}$, a decrease in V_o as n increases will be reflected as an increase in A, as observed. Using the slope obtained from their ΔC_p vs. T plot and assuming that $\Delta C_p = A' V_o^{-1} T$, we use an interpolated value of $V_o = 1.06 \times 10^{-36}$ erg cm^3 for n = 0.5 at. % Fe from our results to determine a value of $A' = 3.5 \times 10^{-32}$ $erg^2/mole\ K^2$ for their 0.5 at. % Fe sample. Using their results for ΔC_p, values of V_o can be calculated for each of their concentrations. These results are listed in Table 10 and are plotted vs. n in Fig. 23. If this analysis is valid, then a continuing decrease of V_o above n = 1 at. % Fe is apparent.

Tholence and Tournier [24] have defined the range of concentrations in which AuFe behaves as a spin glass;i.e., from 400 ppm to 1 at. % Fe. This is the concentration range where T_o is approximately proportional to n. Our own results indicate that spin glass behavior exists for AuFe alloys down to 40 ppm Fe when we take into account the concentration-dependence of V_o.

Mydosh et al.[23] have measured the electrical resistivity of AuFe in the spin glass region (0.5 to 8 at. %Fe). The excess resistivity is found to be $\Delta \rho(T) = \Delta \rho_o + AT^{3/2}$ as $T \longrightarrow 0$, where A decreases very slowly with increasing

concentration in this concentration region. If $\Delta\rho(T)$ follows a scaling law, as it should, it should have a form $\Delta\rho/nV_o = f(T/nV_o)$. Thus in the above expression for $\Delta\rho$ A should be proportional to $(nV_o)^{-\frac{1}{2}}$. Letting $A = A_o/(nV_o)^{\frac{1}{2}} = 9.6\ n\Omega cm/K^{3/2}$ for their n = 0.5 at. % Fe result, and interpolating a value of $V_o = 1.06 \times 10^{-36}$ erg cm^3 for this concentration from our results for $V_o(n)$, we can calculate $A_o = 6.99 \times 10^{-18}(n\Omega cm/K^{\frac{3}{2}})(at.\%erg\ cm^3)^{\frac{1}{2}}$. Using this result for A_o and their results for A, we can calculate values of V_o for their alloys. These results are listed in Table 10 and are plotted in Fig. 23. If this analysis is valid, then a continuing decrease of V_o for n > 1 at. % Fe is again indicated.

Cannella et al.[20] have observed sharp peaks in $\chi(T)$ for n > 1 at. % Fe in Au and have found that $T_o \propto n^{2/3}$. Scaling theory predicts that $k_B T_o \propto nV_o$, so that $T_o \propto n$ if V_o is independent of concentration. It has been conjectured [60] that if at short distances the RKKY interaction varies as r^{-2} instead of r^{-3}, T_o should be proportional to $n^{2/3}$ instead of n. On the other hand, if V_o decreases with n roughly as $n^{-1/3}$, then the $n^{2/3}$ dependence of T_o would be explained. We feel that this latter explanation is correct. The $T_o \propto n^{2/3}$ behavior has been observed for a variety of dilute magnetic alloy systems for n > 0.1 at.% of impurity (e.g. AuCr,[61] AuCo,[61] AgMn,[61] CuFe,[61] AuMn,[62]

CuMn[62]). It may be that a decrease of V_o with increasing n is a general phenomenon in such systems. If we assume that $k_B T_o = nV_o(n)$, then we can calculate values of $V_o(n)$ from the results of Cannella et al.[20] for T_o as a function of n. These values of V_o (n) are listed in Table 10 and plotted vs. n in Fig. 23.

Table 10

The RKKY Interaction Strength $V_o(n)$ vs. n.

n (at. % Fe)	$V_o(n)^a$	$V_o(n)^b$ (10^{-36} erg cm^3)	$V_o(n)^c$ (10^{-36} erg cm^3)	$V_o(n)^d$ (10^{-36} erg cm^3)
0.0042	11.9			
0.0094	7.75			
0.0169	4.49			
0.0242	4.02			
0.0572	1.96			
0.116	1.54			
0.2		1.23		
0.2225	1.24			
0.5		1.06	1.06	
0.605	1.03			
0.8		0.97	1.00	
1		0.97	0.82	1.99
1.5			0.66	
2		0.83	0.53	1.63
3		0.75	0.39	
4			0.40	
5			0.32	1.04
6.5			0.26	
8		0.51	0.24	0.82
12				0.70
13				0.68

a) The values of $V_o(n)$ are obtained from Table 9, this work.

b) The values of $V_o(n)$ are obtained from the measured excess specific heat results of Dreyfus et al.[19] and assuming $\Delta C_p = A' V_o^{-1} T$ (see text).

Table 10 (continued)

c) The values of $V_o(n)$ are obtained from the electrical resistivity results of Mydosh et al. [23] and assuming $\Delta\rho/nV_o = f(T/nV_o)$ (see text).

d) The values of $V_o(n)$ are obtained from the magnetic susceptibility results of Cannella et al.[20] and assuming $k_B T_o = nV_{o(n)}$.

FIG. 23

The strength of the RKKY potential $V_o(n)$ plotted as a function of impurity concentration n from our results and the calculated results from Dreyfus et al,[19] Mydosh et al[23] and Cannella et al,[20] (see text).

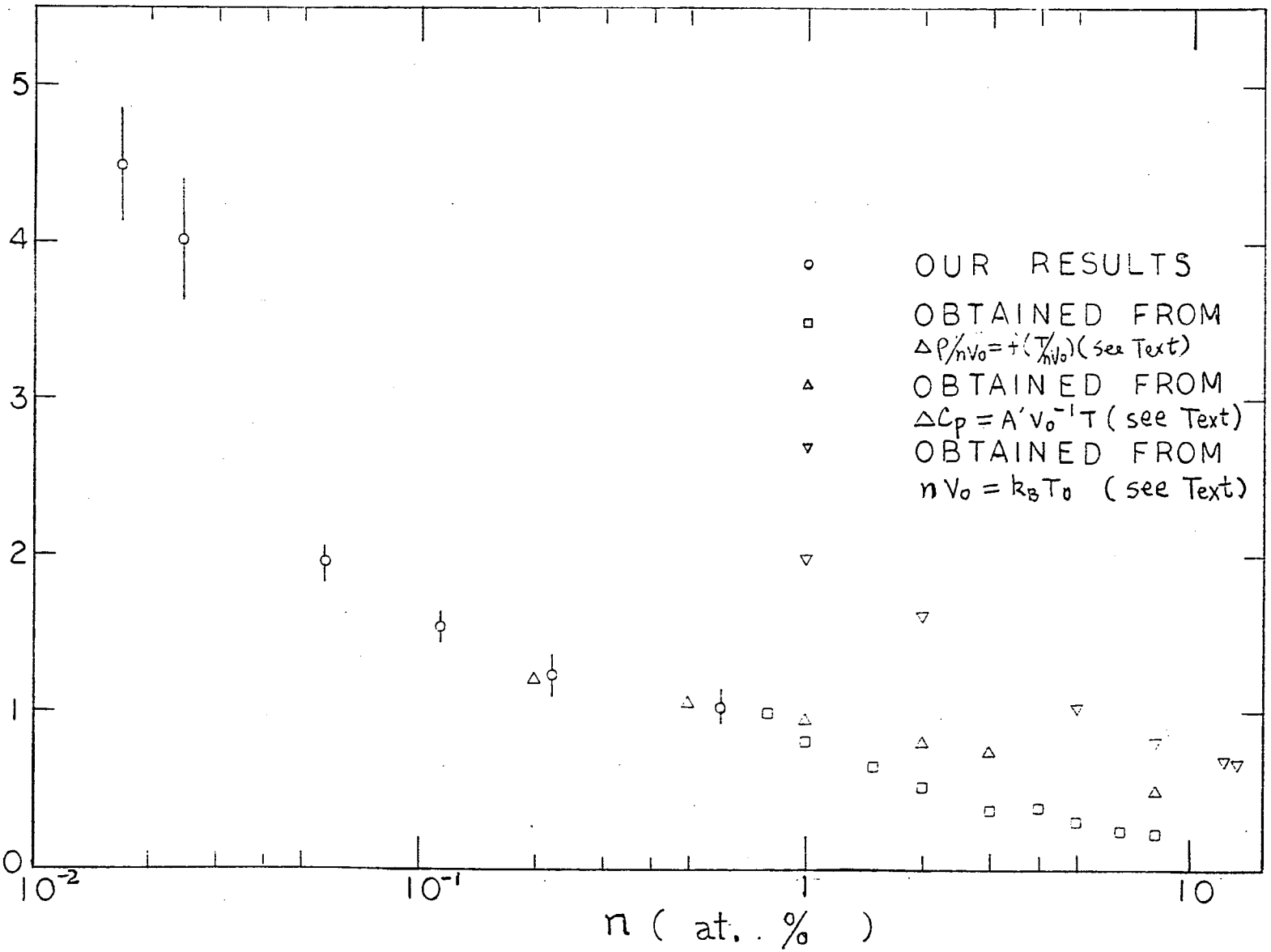
V_0 (n) (10^{-36} erg cm^3)
5
4
3
2
1
0
10^{-2}
10^{-1}
1
10
n (at. %)
OUR RESULTS
OBTAINED FROM
$\Delta\rho/nV_0 = +(T/nV_0)$ (see Text)
OBTAINED FROM
$\Delta C_p = A' V_0^{-1} T$ (see Text)
OBTAINED FROM
$n V_0 = k_B T_0$ (see Text)

FIG 23

VI. CONCLUSIONS

A. AuMn.

The susceptibility and magnetization of a series of AuMn alloys with concentrations n from 54 to 2110 ppm Mn have been measured. The susceptibility data can be fitted to Curie-Weiss laws except for the two higher concentration Mn samples for which the susceptibility approaches maxima at low temperatures. The spin S determined is essentially concentration-independent and equal to 2.25. The magnetizations M of the AuMn samples are very close to Brillouin functions for spin S = 2.25. The deviations from the Brillouin functions increase with increasing concentration and decreasing temperature. The strength of the RKKY interaction V_o is determined to be equal to 2.4×10^{-37} erg cm^3 (equivalent to 1.04 K/at. % Mn), almost independent of concentration. The strength of the s-d interaction J is determined to be 0.1 ev. The Kondo temperature is estimated to be equal to 10^{-2} K. The susceptibility and magnetization data fit very well to scaling laws predicted for spin glass alloys. The ideal spin glass behavior extends over a wider concentration range in AuMn than in either ZnMn or AuFe, both of which have higher Kondo temperatures and larger and concentration-dependent V_o's. The experimental results clearly indicate that the magnetic properties of AuMn alloys within the studied concentration range are

dominated by the RKKY interaction and correspond to ideal spin glass behavior.

For further investigation, we would suggest 1) measurement of susceptibility and magnetization of AuMn alloys with higher and lower Mn concentrations (n = 0.001 to 0.005 and n = 0.2 to 1 at. %) in order to study the scaling behavior and possible deviations in these limits. 2) measurement of susceptibility at lower temperatures (0.04K to 1K) and at low frequencies and low magnetic fields in order to study the possible sharp peak behavior of the susceptibility maximum.

B. AuFe.

The susceptibility and magnetization of a series of AuFe samples with Fe concentrations from 18 to 6050 ppm have been measured. The measured susceptibility data can be fitted to Curie-Weiss laws over a limited range of temperature, with concentration dependent Curie-Weiss temperatures Θ and spins S. For the higher concentration samples, the susceptibility approaches maxima at temperatures approximately proportional to n. The magnetization data deviate from Brillouin functions, with the deviations increasing with increasing concentration and decreasing temperature. The strength V_o of the RKKY interaction is found to decrease with increasing Fe concentration, and has a value of $V_o = (11.9 \pm 1.35) \times 10^{-36}$ erg cm^3 (equi-

valent to 54 K/at. % Fe) at n = 42 ppm Fe. The strength of the s-d interaction J is determined to be 1.2 ev. The decrease of V_o with increasing Fe concentration is attributed to the self-damping of the RKKY interaction. The measured V_o (n) does not satisfy the simple relation $V_o(n) = V_o(0)\, e^{-\langle r\rangle/\ell}$ derived by Walstedt and Walker,[25] where $V_o(0)$ is the dilute-limit strength of V_o. If one takes into account the variation of V_o with n, several previous anomalous experimental results on AuFe alloys can be explained. The variation of V_o with Fe concentration prevents the susceptibility and magnetization data from following the scaling laws predicted for spin glasses with concentration-independent V_o. We propose modified scaling laws of the form $\chi V_o/S(S+1) = F_1(T/nV_o)$, $M/nS = F_2(H/nV_o, T/nV_o)$. Our data for the susceptibility and magnetization of AuFe fit these scaling laws very well. We also feel that the variation of V_o with concentration is a common phenomenon existing in a variety of alloy systems.

For further investigation, we propose : 1) measurement of magnetic susceptibility and magnetization on AuFe alloys with Fe concentrations between 0.1 and 10 at. %, in magnetic fields up to 130 kG. By using higher magnetic fields, it will be possible to approach saturation in higher Fe concentration samples, thus allowing the deter-

mination of the strength of the RKKY interaction to higher concentrations of Fe. 2) measurements of χ (at low frequencies and low magnetic fields) from 0.04K to 1K on AuFe alloys with Fe concentrations between 0.001 and 0.1 at. %. By using low fields and lower temperature, it will be possible to study the sharp peak behavior at the susceptibility maximum for low Fe concentration AuFe samples, It will also be possible to measure the width Δ of the probability distribution function $P(H)$ for the random molecular field H by using the relation $\chi\ (T \longrightarrow 0) = 2ng^2S(S+1)\mu_B/3\pi\Delta$.

REFERENCES

For an experimental review of the dilute magnetic alloy problem see (1-4).

1. A. J. Heeger, Solid State Physics, edited by F. Seitz, D. Turnbull, and H. Ehrenreich, Vol. 23, p. 283 (Academic Press, New York, 1969).

2. G. J. Van den Berg, Progress in Low Temperature Physics, edited by G. J. Gorter, Vol. 4, Chapter 4 (North-Holland Publ. Amsterdam, 1964).

3. M. D. Daybell and W. A. Steyert, Rev. Mod. Phys. 40, 380 (1968).

4. Magnetism, Vol. 5, edited by H. Suhl (Academic Press, New York, 1973).

5. M. A. Ruderman and C. Kittel, Phys. Rev. 96, 99 (1954).

6. T. Kasuya, Progr. Theor. Phys. (Kyoto) 16, 45 (1956).

7. K. Yosida, Phys. Rev. 106, 893 (1957).

8. A. Blandin, Thesis, Paris University (1961); A. Blandin and J. Friedel, J. Phys. Radium 20, 160 (1959).

9. J. Souletie and R. Tournier, J. Low Temp. Phys. 1, 95 (1969).

10. A. I. Larkin and D. E. Khmel'nitskii, Zh. Eksp. i Theor. Fiz. 58, 1789 (1970) [Sov. Phys. JETP. 31, 958 (1970)]; A. I. Larkin, V. I. Mel'nikov, and D. E. Khmel'nitskii, Zh. Eksp. i Theor. Fiz. 60, 846 (1971) [Sov. Phys. JETP 33, 458 (1971)].

11. P. W. Anderson, Proceedings of the International Symposium on Amorphous Magnetism, edited by H. O. Hooper and A. M. deGraff, p. 1 (Plenum Press, New York, 1973).

12. M. W. Klein and L. Shen, Phys. Rev. B5, 1174 (1972).

13. M. W. Klein and R. Brout, Phys. Rev. 132, 2412 (1963); M. W. Klein, Phys. Rev. 136, A1156 (1964); 173, 552 (1968).

14. J. W. Loram, T. E. Whall, and P. J. Ford, Phys. Rev. B3, 953 (1971).

15. O. S. Lutes and J. L. Schmit, Phys. Rev. 134, A676 (1964).

16. J. W. Loram, A. D. C. Grassie, and G. A. Swallow, Phys. Rev. B2, 2760 (1970).

17. J. L. Tholence and R. Tournier, J. Physique. 32, C1-211 (1971).

18. B. Dreyfus, J. Souletie, J. L. Tholence, and R. Tournier, J. Appl. Phys. 39, 846 (1968).

19. B. Dreyfus, J. Souletie, R. Tournier, and L. Weil, Compt. Rend. 259, 4266 (1964).

20. V. Cannella and J. A. Mydosh, Phys. Rev. B6, 4220 (1972).

21. R. J. Borg and T. A. Kitchens, J. Phys. Chem. Solids, 34, 1323 (1973).

22. P. A. Beck, Metallurgical Transactions. 2, 2015 (1971).

23. J. A. Mydosh, P. J. Ford, M. P. Kawatra, and T. E. Whall, Phys. Rev. B10, 2845 (1974).

24. J. L. Tholence and R. Tournier, J. De Physique. 35, C4-229 (1974).

25. R. E. Walstedt and L. R. Walker, Phys. Rev. B9, 4857 (1974).

26. A. A. Abrikosov, Soviet Phys. Uspekhi. 12, 168 (1969).

27. J. Kondo, Solid State Physics, edited by F. Seitz, D. Turnbull, and H. Ehrenreich, Vol.23, p. 183, (Academic Press, New York, 1969).

28. J. Friedel, Can. J. Phys. 34, 1190 (1956); Nuevo Cimento (Suppl.) 7, 287 (1958); Metallic Solid Solutions, edited by J.Friedel and A. Guinier, (Benjamin, New York, 1963).

29. P. W. Anderson, Phys. Rev. 124, 41 (1961).

30. L. L. Hirst, Phys. Kondens. Mat. 11, 281 (1970).

31. J. Kondo, Prog. Theor. Phys. (Kyoto) 28, 846 (1962).

32. K. Yosida and A. Okiji, Progr. Theor. Phys. (Kyoto) 34, 505 (1964).

33. D. J. Scalopino, Phys. Rev. Lett. 16, 937 (1966).

34. A. A. Abrikosov, Phys. 2, 5 (1965).

35. Y. Nagaoka, Phys. Rev. A 138, 1112 (1965).

36. H. Suhl and D. Wong, Phys. 3, 17 (1967).

37. H. Suhl, Phys. Rev. A 138, 515 (1965); Phys. 2, 39 (1965); Phys. Rev. 141, 483 (1966).

38. C. Zener, Phys. Rev. 81, 440 (1951).

39. H. Frohlich and F. R. N. Nabarro, Proc. Roy. Soc. A 175, 382 (1940).

40. J. H. Van Vleck, Rev. Mod. Phys. 34, 681 (1962).

41. C. Kittel, Quantum Theory of Solids, p. 360 (John Wiley and Sons, 1963).

42. J. E. Zimmerman and E. E. Hoare, J. Phys. Chem. Solid. 17, 52 (1960).

43. W. Marshall, Phys. Rev. 118, 1519 (1960).

44. M. W. Klein and L. Shen, Phys. Rev. B 5, 1174 (1972).

45. A. J. Heeger, A. P. Klein and P. Tu, Phys. Rev. Lett. 17, 803 (1966).

46. R. Caton, Ph.D. thesis, City College of the City University of New York, 1974 (unpublished).

47. C. M. Hurd and J. E. A. Alderson, Phys. Rev. B6, 1894 (1972).

48. P. L. Garbarino and C. S. Reynolds, Phys. Rev. B4, 167 (1971).

49. D. Shaltiel and J. H. Wernick, Phys, Rev. 136, A 245 (1964).

50. J. B. Haddad, Ph.D. thesis, City College of the City University of New York, 1974 (unpublished).

51. H. Zijlstra, Selected Topics in Solid State Physics, edited by E. P. Wohlforth, Vol. IX (John Wiley and sons Inc. New York 1967).

52. C. M. Hurd, J. Phys. Chem. Solid. 28, 1345 (1967).

53. F. W. Smith, Phys. Rev. B10, 2980 (1974).

54. C. M. Hurd, J. Phys. Chem. Solid. 30, 539 (1967).

55. B. Manhes, Ph. D. thesis, Grenoble, 1971 (unpublished).

56. E. Lagendijk, L. Niesen, and W. J. Huiskamp, Phys. Lett. 30A, 326 (1969).

57. P. Steiner, G. N. Beloserskij, D. Gumprecht, W. V. Zdrojewski, and S. Hufner, Solid State Commun. 13, 1507 (1973).

58. P. Steiner, G. N. Beloserskij, D. Gumprecht, W. V. Zdrojewski, and S. Hufner, Solid State Commun. 14, 157 (1974).

59. H. Claus, Phys. Rev. B5, 1134 (1971).

60. D. A. Smith. (to be pyblished).

61. V. Cannella and J. A. Mydosh, AIP Conf. Proc. No.18, Magnetism and Magnetic Materials-1973, edited by C. D. Graham, Jr. and J. J. Rhyne (AIP, New York, 1974) p. 651.

62. V. Cannella, in Amorphous Magnetism, edited by H. O. Hooper and A. M. degraff, p. 195 (Plenum Press, New York, 1974).